INSTITUTO SUPERIOR TÉCNICO
Universidade Técnica de Lisboa

Hydrodynamical and Ecological Modelling of the North Sea

Bartolomeu Deen Luís Bernardes

Dissertação para obtenção do Grau de Mestre em
Engenharia do Ambiente

Presidente:	Doutor Ramiro Joaquim de Jesus Neves
Orientador:	Doutor Ramiro Joaquim de Jesus Neves
Co-orientador:	Mestre Ana Sofia de Carvalho Saraiva
Vogais	Doutor Tiago Morais Delgado Domingos
	Doutor Aires José Pinto dos Santos

Outubro de 2007

Agradecimentos

Gostaria de agradecer ao Professor Ramiro Neves, na qualidade de orientador, por me ter dado a possibilidade de elaborar a tese num tema interessante e especialmente sobre uma região à qual tenho raízes familiares; ao seu entusiasmo e inspiração que foram particularmente relevantes ao longo destes meses.

À Sofia, co-orientadora, pelos conhecimentos aprofundados sobre o MOHID (e não só), que me proporcionou uma aprendizagem realmente forte ao longo do desenvolvimento da tese. Ao Luís, pelas mesmas razões.

A big "thank you" to all the CEFAS staff that helped me develop the work, particularly Sonja, Paul and David Mills.

A toda a equipa do MARETEC em geral.

Em particular, ao Guillaume que me deu a conhecer o MatLab (!) e me esclareceu uma montanha de dúvidas; à Ângela pela paciência que teve no código; ao Pedro Pina pelos conhecimentos em detecção remota; à Madalena por tantas sugestões dadas; ao Rodrigo, pelo zombo; ao David, pelo fora de jogo (!).

A todos os meus amigos que me apoiaram durante este último ano: aos de cá e aos ilhéus.

Gostaria de agradecer a minha família o apoio que me deram: aos meus pais, à Sara, ao Gastão e Christine, e ao Sebastião.

Abstract

The North Sea is one of the most important shelf seas in Europe as it provides important economical resources to adjacent countries. Using numerical models one can evaluate and predict changes to the system, link cause to effect and enable stakeholders of such resources (countries) to have powerful assessment tools at their disposal in order to manage it with the best approach. Phytoplankton abnormal growth can result in, among other, oxygen deficiency causing undesirable disturbance to the water quality of a given area, thus OSPAR requires a member state to reduce its nutrients discharge loads to 50% of 1985 levels. MOHID model uses a 2D hydrodynamical model to compute tides and a nested 3D ecological model to simulate parameters, such as physical, biological and chemical processes. Using the 2D hydrodynamical model, residual circulation and residence time was calculated in a specific region. The validation of the hydrodynamical model was done using tidal harmonic analysis that presented good results. The 3D ecological model simulates phytoplankton (flagellates) and zooplankton (mesozooplankton). Results show good agreement between the model, field data and satellite imagery. Transboundary nutrient transport fluxes were computed, giving strong confidence that nutrients are transported from the UK to the Dutch coast in an anticlockwise direction, following the circulation pattern. Other findings include phytoplankton growth limitation by light through "self shading", and not nutrient limitation. This alerts to the possibility that a reduction on nutrients will probably not influence the system and therefore, is a matter to be addressed in future works.

Keywords

North Sea, Modelling, Tidal Harmonic Analysis, Hydrodynamics, Eutrophication, Phytoplanktona

Resumo

O Mar do Norte é um dos mares mais importantes da Europa porque produz recursos económicos importantes aos países adjacentes. Ao utilizar modelos matemáticos, pode-se medir e prever mudanças no sistema, ligar a causa ao efeito e dispor às partes interessadas (países) uma poderosa ferramenta de avaliação para gerir o sistema da melhor maneira possível. O crescimento anormal do fitoplâncton pode resultar, entre outros efeitos, em baixos níveis de oxigénio, resultando num distúrbio não desejável da qualidade da água. Por este motivo, a OSPAR requer que os estados membros tenham de reduzir a concentração de nutrientes nas suas descargas a 50% (níveis de 1985). O MOHID foi aplicado no Mar do Norte, recorrendo a um modelo hidrodinâmico 2D com um sub modelo ecológico 3D encaixado. No modelo 2D hidrodinâmico, calculou-se a circulação residual e tempos de residência. Uma análise harmónica da maré foi efectuada, mostrando bons resultados. Quanto ao modelo 3D ecológico, este simula fitoplâncton (flagelados), zooplâncton (mesozooplâncton) e as propriedades relevantes. Os resultados mostram uma boa correlação entre o modelo e os dados de campo. Os nutrientes são transportados do Reino Unido para a costa da Holanda num padrão semelhante à circulação. Conclui-se também que a limitação do crescimento do fitoplâncton é devido à luz (por ensombramento do fitoplâncton) e não devido a limitação de nutrientes. Esta conclusão faz alertar para a possibilidade de que uma redução nos nutrientes provavelmente não irá influenciar o sistema, sendo por isso uma questão a ser endereçada em trabalhos futuros.

Palavras-chave

Mar do Norte, Modelação, Análise Harmónica da Maré, Hidrodinâmica, Eutrofização, Fitoplâncton

Table of contents

Index of Figures

Index of Tables

Abbreviations

BSH - Bundesamt für Seeschifffahrt und Hydrographie, Federal Maritime and Hydrographic Agency, Germany

CEFAS – Centre For Environment, Fisheries and Aquaculture Science, UK

ECMWF – European Centre for Medium-Range Weather Forecasts

GUI – Graphics User Interface

HDF - Hierarchical Data Format

ICG-EMO - Intersessional Correspondence Group on Eutrophication Modelling;

IOW - Institut für Ostseeforschung Warnemünde, Baltic Sea Research Institute Warnemünde, Germany

MOHID – Water modelling system

NCEP - National Centres for Environmental Prediction

OISST - NOAA Optimum Interpolation (OI) Sea Surface Temperature (SST)

OSPAR - Convention for the Protection of the Marine Environment of the North-East Atlantic;

OSPAR CP – OSPAR Common Procedure

RIKZ - Rijksinstituut voor Kust en Zee (RWS RIKZ), the Netherlands

ROFI – Regions Of Freshwater Influence

SPM – Suspended Particulate Matter

SST – Sea Surface Temperature

TBNT – Transboundary Nutrient Transport

WOA – World Ocean Atlas

1. Introduction

1.1. Objectives

The objective of this thesis is to study the hydrodynamic circulation of the North Sea, specially the movement of the different water bodies and in addition, to study the primary production, as well as the phosphorus and nitrogen cycles and its relation with the water quality using a mathematical model (MOHID).

1.2. Context

The subject for this thesis started off from the need to model the North Sea system and assess the OSPAR strategy to reduce eutrophication. In particular, to assess the measures currently underway by the OSPAR contracting parties to effectively reduce 50% of nutrient (phosphorus and nitrogen) input compared to 1985 levels (Skogen, 2004).

The evaluation of the current eutrophication status can be made using mathematical models, to predict the environmental consequences of nutrient reduction: its time lag between the actual reduction and the system response. One other useful outcome of model applications is the ability to know the fluxes of such nutrients between borders.

The North Sea is one of the most studied regions regarding the effect of eutrophication, with several countries and organizations producing knowledge on the matter. Portugal decided to take place in this international exercise of understanding its causes and determining its origin since the topic is closely connected to the Portuguese estuarine systems, mind the dimensions.

Another goal of this thesis is to validate the MOHID model in a bigger scale, using the vast amount of data available and compare it with existing models, facilitating this assessment.

1.3. Methods used

In this study we make use of the MOHID System and apply it to the North Sea, using a 2D hydrodynamical model to provide boundary conditions to a nested 3D ecological submodel. The nested model approach was used because the computation time is not feasible for a full 3D ecological model for the whole domain.

The thesis structure reflects this separation: a first part regarding the 2D hydrodynamical model, and the second part regarding the 3D ecological submodel.

The interpretation of the hydrodynamics of the 2D model consists of:

- computing the residual circulation: fluxes and velocities;
- calculating lagrangean tracers and residence times of the water in particular areas of the domain;
- Analysing harmonic components: on a point and on the whole domain.

For the 3D ecological submodel, the analysis consists of:

- Plotting the spatial evolution of the properties considered;
- Comparing timeseries results with station data;
- Processing satellite data and compare it with model results;
- Make use of fluxes between boxes to conclude upon the transboundary nutrient transport;
- Examine the limitation factors on the phytoplankton growth.

All the data used in this work was thoroughly subjected to pre-processing to fit the requisites of the MOHID modelling software. This includes converting formats (netcdf, hdf4, hdf5, timeseries, etc) and using/modifying some programs already written by MARETEC staff in several programming interfaces (MATLAB, FORTRAN, .NET)

2. The North Sea

The North Sea is a marginal sea of the North Atlantic situated on the Northwest European Shelf (Figure 1). It is bordered by several countries, namely, England, Norway, Denmark, Germany, the Netherlands, Belgium and France. It is connected to the Atlantic in the North, between England and Norway and the South between England and France/Belgium. To the east, between Norway/Sweden and Denmark it is connected to the Baltic Sea.

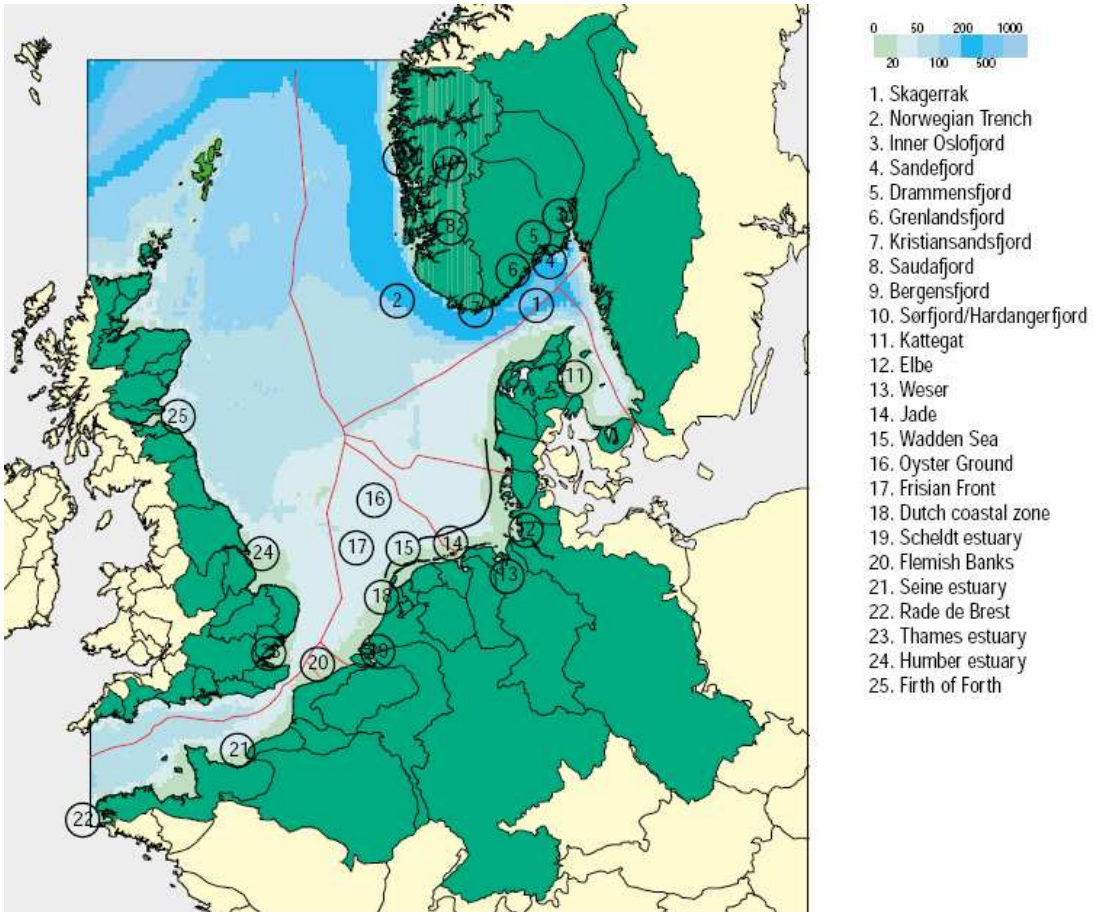

Figure 1: Map of the North Sea, showing some relevant points of interest and depth(blue scale)(OSPAR 2000)

Some global characteristics are listed in the following table below.

Length north-south	960 km
Width east-west	580 km
Surface area	750.000 km²
Volume	94.000 km³
Average depth	95 m
Maximum depth	700 m (Norway)
Annual river water input	300 km³
Drainage area	850.000 km² (184 million residents)
Average temperature in winter	6°C
Average temperature in summer	17°C
Salinity	34 to 35
Tidal range	0 to 8 m

Table 1: North Sea facts

The North Sea extends roughly 960km by 580km. The total surface area is approximately 750,000 km² and the total volume 94,000 km³. This represents less than 1/500 of the total water surface of the earth(OSPAR, 2000).

The bathymetry range from a shallow 50 meters on the southern part to 200 metres on the northern part. The Norwegian Trench has depths of up to 700 meters along the Scandinavian coast. Westerly winds prevail in the shelf causing a counter-clockwise current flow around the basin (Nunneri *et al*, 2007 after Lee, 1980). The tides have a big influence on the renewal rate of the water which is about three years (Sündermann *et al*, 2002).

The North Sea shelf area is a pre-historic continental drift depression, overlaid by sedimentary deposits a few kilometres deep originated from the surrounding land masses. During the ice age, several mountain glaciers spread over the North Sea, supplying sediments and causing large sea level changes. It also defined the present underwater topography. After the ice age, sea levels rose to those today, creating the circulation patterns and sediment dynamics seen today. In the shallower areas mainly sand and gravel deposits occur. Accumulated in the depression, there are deposits of fine-grained muddy sediments(OSPAR, 2000).

Along the coasts of the North Sea, there are a big variety of landscapes that formed from differences in geology and vertical tectonic movements. The northern coastlines suffered uplift due to the loss of the weight from the ice. Scotland and Norway display mountainous landscape with a few rocky islands, often dissected by deep fjords.

The English east coast is characterized by estuaries and sand and mud flats in areas such as the Wash. Along the English channel the coastline of southern England is dominated by low cliffs and flooded river valleys. Along the French coast, there are maritime plains and extensive estuaries, cliffs and the rocky shoreline of Bretagne. Moving along the shoreline northerly, there are mostly beaches and dunes with many

estuaries such as the Scheldt, Rhine, Meuse, Weser and Elbe. Along the Wadden Sea in the Netherlands, we find the tidal inlets and many flat islands.

The shallow tidal regions have a highly primary productivity that is enhanced by human supply of nutrients by the rivers. These areas are very important because they support a number of different ecological habitats, such as migratory birds and they are also a nursery for juvenile fish.

The river systems that discharge to the North Sea have a total catchment are of 850 000 km^2, resulting in an annual fresh water input of roughly 300 km^3 (OSPAR, 2000). About one third of the water is constituted by melt water from Norway and Sweden. Important rivers that discharge to the North Sea are: Elbe, Weser, Meuse, Scheldt, Seine, Thames and Humber. One important source of fresh water is the Baltic Sea, producing about 470 km^3 of fresh water a year. This additional water flow is a source of contaminants and nutrients to the North Sea(OSPAR, 2000).

The North Sea water is consisted by a mix of water from the North Atlantic and fresh water run-off. Heat exchange with the atmosphere and freshwater supplies strongly influences the temperature and salinity of different areas. The deeper waters of the North Sea consist of water of Atlantic origin, influenced by surface heat exchange and, in certain areas, slightly modified through mixing with less saline surface waters. The circulation and distribution of the different water masses is very important in supporting biological productivity, transport and concentration of living and non-living matter in the region(OSPAR, 2000 and Sündermann, 2002).

The surface temperatures of the North Sea show a year cycle with amplitudes ranging from 8º in the Wadden Sea to 2º in the northerly entrances. Long term variability of the surface temperature is closely correlated with the strength of the atmospheric circulation of the North Atlantic Oscillation (NAO).

Light transmission through the water column is mainly limited by suspended matter and plankton. Its spatial and temporal variability result in high variability of the light transmission(OSPAR, 2000).

In the winter months, the areas outside the Norwegian Trench are vertically well mixed. In the beginning of spring there is a thermocline development over large areas of the North Sea, as the solar input increases. It separates a less dense surface layer from the rest of the water column. The strength of this phenomenon depends on the heat input and the turbulence generated by the tidal systems and the atmospheric conditions (mainly the wind). In autumn, the storms and the seasonal cooling at the surface destroy the thermocline and mix the surface waters with the bottom layers. Shallow areas remain well mixed throughout the year because of strong tidal mixing. Along the Kattegat, Skagerrak and the Norwegian Trench there is a strong influence of the fresh water from the Baltic, and thus, due to the low salinity in their upper layers have a stable stratification all year round(OSPAR, 2000).

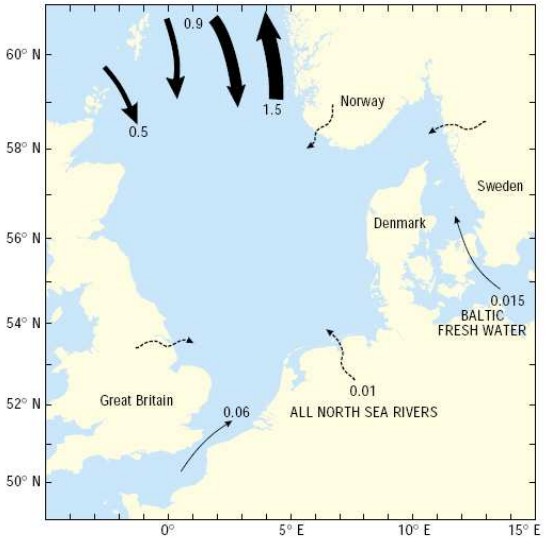

Figure 2: Long-term modelled mean (1955-98) influx and out flux of volume during winter (10^6 m^3/s) (OSPAR 2000)

On the North Sea lies is one of the most important fishing grounds in the world. Herring, plaice, haddock and cod are the main fish species caught for human consumption(Sündermann *et al*, 2002 and OSPAR, 2000).

The offshore oil and gas industry has become a major economic activity in the North Sea since the late 1960s. Between 1990–92 and 1996–98, the number of platforms increased from 300 to 475, and oil production almost doubled. The major oil developments have been in the northern parts of the North Sea in the United Kingdom and Norwegian sectors. Gas deposits are exploited mainly in the shallower southern regions in the United Kingdom, Dutch, and Danish sectors, as well as in Norwegian waters. There are several gas and oil production platforms in the Wadden Sea, with further exploration being subject to tight controls (OSPAR, 2000).

The North Sea contains some of the busiest shipping routes in the world. In 1996 about 270 000 ships entered the main 50 ports in the North Sea and Channel area. Daily, more than 400 ships pass through and 600 ships cross (including 200 ferries) the Strait of Dover. Most of Europe's largest ports are situated on North Sea coasts and rivers, namely Hamburg, Bremen, Amsterdam, Rotterdam, Antwerp, Le Havre, and London with Rotterdam/Europoort being the most important(OSPAR, 2000).

2.1. Anthropogenic Discharges

Land-based activities such as industry, households, traffic and agriculture may have an impact on the ecosystem of the Greater North Sea via riverine or atmospheric inputs of contaminants (Sündermann *et al*, 2002). Quantification has focused on the overall input of substances to the marine environment, and for substances other than nutrients only limited attention has been given to the contributions from different sources.

Substances of concern are nutrients, which may lead to eutrophication, and hazardous substances which could pose a risk to marine organisms and, via food from the sea, to human health. At the International Conferences on the Protection of the North Sea, commitments were made to reduce inputs of hazardous substances and nutrients into the North Sea by 50% between 1985 and 1995 and also to reduce by 70% inputs of dioxins, mercury, cadmium and lead.

Reduction of the inputs of phosphorus was achieved by improvement of urban waste water treatment plants and by the replacement of phosphorus by tensides as detergent in washing powders (Skogen *et al*, 2004). Limited reductions in the inputs of nitrogen were achieved through improvements in sewage treatment; in leaching of nitrate and in farm waste discharges. Little success has been reported in reducing inputs from diffuse sources, i.e. erosion and leaching of arable land (fertilisers), atmospheric deposition (nitrogen), runoff from roads (e.g. wear of tyres) and building materials(OSPAR 2000).

The Paris Commission adopted measures relating to the reduction of nutrient inputs in 1998 and 1999. The EC Urban Wastewater Treatment Directive (EC, 1991) regulates the required level of treatment of waste water (i.e. in general biological treatment). The deadline for implementing this Directive is 31 December 1998 to 31 December 2005, depending on the size of the population. In 1995 the portion of the population connected to sewerage treatment in different countries ranged from 80 – 98% (OSPAR, 2000).

Agricultural land sums more than 42% of the total land area in Europe, although the proportion of each country varies between less than 10% and more than 70%. There are substantial environmental impacts associated with agricultural activities and the main types of pollution are from nitrates, ammonia, methane, pesticides and run-off of silage and slurry (OSPAR, 2000).

2.2. Plankton and Eutrophication

OSPAR Committee defines Eutrophication as follows (OSPAR, 2003):

''Eutrophication'' means the enrichment of water by nutrients causing an accelerated growth of algae and higher forms of plant life to produce an undesirable disturbance to the balance of organisms present in the water and to the quality of the water concerned."

Figure 3: Phytoplankton bloom off the English Coast (SeaWiFS)

Algae growth, in this case, phytoplankton in temperate seas is frequently dependent on the spring development of water column stability, supplying enough sunlight for the rapid spring bloom. Many larval fish feed on this diet and its timing is a key factor for the survival of juvenile fish. Thus, the timing of the spring bloom takes an important part of the seasonal biological cycles of shelf seas (Sharples *et al* 2006).

For over the last 30 years, the North West continental shelf has experienced an increase eutrophication in the coastal waters: the percentage of riverine input of nitrogen and phosphorus into the shelf seas has increase from 20% and 15% in the 1950s to 52% nitrogen increase and 52% phosphorus increase in 1980 (Patsch *et al*, 1997). Since the oceanic inputs of nutrients do not appear to show an increase, the nutrient supply to these areas is governed by riverine input (Radach 1992), which continuously supply the Sourthern North Sea, that has the highest primary production (Skogen and Moll, 2005).

This situation can lead to problems such as toxic algal bloom (Proctor *et al*, 2003) and oxygen deficiency (Tett *et al* 2007), which cause an "undesirable disturbance".

The reduction of phosphorus input by 50% has been achieved by most countries, but no real reduction of nitrogen. The reduction of P has probably lead to a reduced primary production at some times in areas where phosphorus was the limiting nutrient (Skogen *et al*, 2004). Furthermore, the reduction of P has lead to an increase of imbalance between these two nutrients (Skogen *et al*, 2004), which can be the cause of the dominance of *Phaeocystis* (that is sustained by nitrogen excess) in the Southern bight of the North Sea (Lacroix *et al*, 2007).

Phytoplankton in the open North Sea is mainly dominated by pico- and nano-plankton. The algae in the pico and nano size ranges are effectively controlled by their microzooplankton grazers. Mesozooplankton show a much slower population response, and this lack of control allows for rapid biomass increases of the larger algae(OSPAR 2000). Diatoms and flagellates fluctuate along different annual cycles with particularly

large inter-annual fluctuations in summer dinoflagellate stocks. Nanoplankton population densities appear to have increased sharply at the end of the 1970s (OSPAR 2000).

The species modelled in this study is phytoplankton and mesozooplankton (hereafter named zooplankton).

2.3. Tide

The tide is a result of the gravitational forces between stellar bodies (mainly the moon and the sun) acting on the worlds Oceans. It's origin was one of the most studied field in the ancient times. Aristotle linked the tidal motions to the moon as early as the third century BC. Later, Newton in the 17th century explained how the tide works.

The gravitational force varies with the distance of the attaction body: the largest on the point's on the earth's surface closer to the sun(or the moon). The tides are a result of the balance between centrifugal and gravitational forces, which are determined by the angular velocity of the earth's rotation. These forces balance themselves near the earth's centre, but at the surface, the remaining force is significant to produce the tide. Its direction is outward and opposite to gravity at the point directly under the sun(or moon) and the point directly opposite. The variation of the gravitational field is minuscule, and not enough to produce the tide. It's horizontal component, which acts on the rest of the earth, is responsible for the tides as we know them(Parker *et al*, 1991). Figure 4 depicts this phenomenom for the moon.

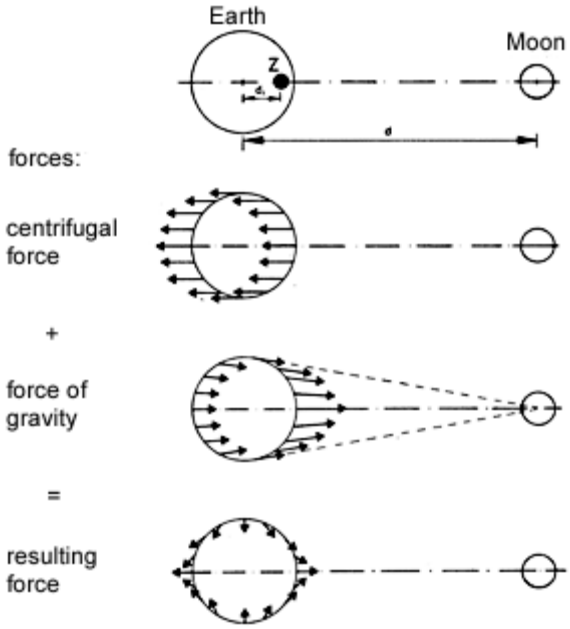

Figure 4: Tidal forces (from NOAA 1998)

The resulting gravitational potential of the moon and the sun, produces a long wave, with a period of 12h and 25 minutes, that is exactly half a lunar day. The propagation and amplitude throughout the Earth are influenced by friction, the rotation of

the Earth (the Coriolis effect) and the resonance determined by the shape and the depth of the ocean basins and coastal morphology (Luijendijk, 2001).

When the earth-sun-moon system is aligned, the forces of both systems are amplified. This enhances the tide, when the moon is full(spring tide) or new(neap tide). The following figure shows this effect.

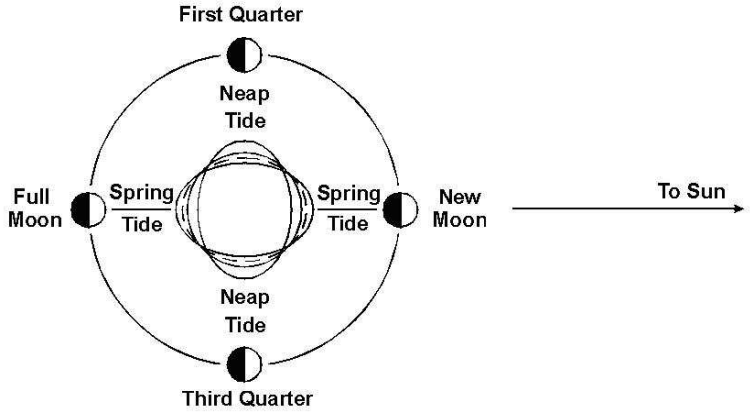

Figure 5: Spring/Neap tides (from NOAA 1998)

Spring/Neap tide occurs in cycles of 29.53 days, which is the sinodic month. When the sun is at its equinox relative to the earth (90º in the equator in spring and autumn) and the moon is in its spring cycle, the amplitude of the tide is the greatest. Also, when the moon is at its perigee (closest approach to the earth), the tide amplitude is the biggest.

Marginal seas or estuaries cannot produce a response to astronomical tidal forcing as they are too small and shallow. The tidal movement in these regions are determined by the tides of the deep ocean which enter and leave the region periodically at the connection points. The amplitudes and phases of these tides depend on the similarity with the tidal frequencies and amplitudes of the the tides in the deep ocean.

The North sea can be pictured as a bowl with a small opening in the south-west(English Channel) and a large opening in the North-West(Atlantic Ocean). Both these opening influence the tide in the North Sea. There is a distortion cause not only by the geometry(bathymetry) of the region but also the effect of the Coriolis force. This latter force is cause by the rotation of the earth, deflecting the tidal movement to the right in the Northern Hemisphere(to the left in the Sourthern hemisphere), causing a counterclockwise rotation. When the Coriolis force if of the same magnitude of the gravitational field, a geostrophical equilibrium is reached, resulting in a Kelvin wave. The tidal wave in the North Sea has caracteristics of such a wave. The wave propagated counterclockwise around the region, with a central point, called the amphidromic point, that doesn't not have tidal amplitude.

These tidal currents are the most energetic feature in the North Sea, mixing the entire water column in most of the Southern North Sea and English Channel. These represent 50% of the water transport in the Western North Sea.

2.3.1. Harmonic Analysis

Harmonic analysis is a method of signal demodulation, in which the user specifies which frequencies are to be examined. It uses the least-squares technique, originated from Lord Kelvin (1824 – 1907) in the year 1867.

The method enables the resolution from a water level time series of several hundred tidal components, of which 45 have astronomical origin and are identified with a specific frequency in the tidal potential. Each one corresponds to a relative astronomical motion between the earth, sun, moon and other celestial bodies. The remainder are shallow water components associated with bottom frictional phenomena, non-linear terms in the equations of motion and atmospheric effects. The usual harmonic components are dominated by diurnal and semidiurnal motions, followed by fortnightly, monthly, semi-annual and annual variability.

The harmonic analysis generates the amplitude and phase lags of a component that the user has specified through the frequency. One can reconstruct a water level timeseries using the harmonic component amplitude and phase data. This filters out any noise and atmospheric effects on water level timeseries. Based on the amplitudes and phases of such analysis, accurate comparisons can be made between observations and model results.

More information on this method can be found in Parker *et al* (1991) and Pawlowicz (2002).

3. Model description

This chapter describes the numerical model used to study this thesis' subject.

3.1. Overview

MOHID Water is a numerical model included in the MOHID Water Modelling System (Braunschweig *et al*, 2004a, Braunschweig *et al*, 2004b). It can be used to model water bodies, porous media flow and infiltration and watersheds. It allows the simulation of the main physical, chemical and biological processes that occur in the marine environment. It uses an object oriented programming philosophy and the FORTRAN 95 features. It is organized in modules (or classes) that connect each other in a way that is possible to transfer information from one to another.

To calculate each property the model is based on the concept of finite volume, where the equations are applied macroscopically at each control volume (each cell in the grid), using divergent flux, that assures the conservation in the transport of properties.

For the most part, there is the calculation of two types of properties:

- Hydrodynamical: velocity, water level, water fluxes and turbulent viscosity;
- Water Properties: salinity, temperature, density, nutrients, suspended matter, phytoplankton, zooplankton, etc.

MOHID System has a GUI that simplifies the use of the system. It is divided into three different parts:

- Pre-processing: data acquisition and feeding;
- Execution: the calculation step;
- Post-processing: allows the exploration and interpretation of the results.

The model results can be viewed in two different formats, depending on the type of study that is being developed:

- Timeseries of values of specific cells
- Matrix like form, using Hierarchical Data Format (HDF v5) developed by the National Center of Supercomputing Applications (NCSA).

The matrix like output (HDF5) can be used by MatLab for data processing and viewing, as well as the PostProcessor tool. This feature was created and developed during this thesis preparation, resulting in the development of alternate and flexible tools for post-processing of the model's data.

The following paragraphs briefly describe the characteristics of each MOHID module used in the hydrodynamic and ecological modelling of the North Sea. Further detailed descriptions of the structure can be found in Annex II, Leitão(2003), Braunschweig(2004a) or http://www.mohid.com.

3.2. History

Starting back at 1985, one of the most recent versions of MOHID is MOHID Water. In the philosophy of the software, there has always been a continuous effort of implementing new features. These improvements and tweaks were made available on a regular basis and were used in the framework of many research and engineering projects. The name, MOHID (Portuguese abbreviation for "MOdelo HIDrodinâmico"), was derived from one of the first versions, that was, in the beginning, a two dimensional tidal model written in FORTRAN 77 (Neves, 1985).

Traditionally, it was a hydrodynamical model, used to study estuaries and coastal areas using a classic finite-differences approach. Further developments, included the conversion to 3D and addition of baroclinic effects (Santos, 1995), and full discretization to finite volumes approach to allow the use of generic vertical coordinates (Martins, 2000). Previous versions of the model have been applied in numerous studies and integrating a large variety of processes and scales.

The following items shows the recent applications of MOHID Water modelling to various applications:

- Estuaries: Tagus, Portugal (Portela, 1996; Pina 2001; Braunschweig *et al*., 2003; INAG/Maretec, 2003; Fernandes, L., 2005; Saraiva *et al*., 2007); Guadiana , Portugal (Cunha *et al*., 2000); Douro, Portugal (Pina *et al*., 2003); Sado, Portugal (Martins *et al*., 2001); Westerschelde, The Netherlands (Cancino and Neves, 1999); Gironde, France (Cancino and Neves, 1999); Carlingford, Ireland (Leitão, 1997);
- Coastal lagoons: Ria de Aveiro (Leitão, 2003; Trancoso *et al*, 2005); Ria Formosa (Silva *et al*, 2002);
- Coastal systems: Estoril Coast (Fernandes, R. *et al*, 2005), Ría de Pontevedra (Villarreal *et al*., 2002)
- Ocean: Algarve coastal circulation (Leitão, 2007); Mediterranean outflow (Riflet, 2007); Portuguese coastal current (Coelho, 2002); Slope current along the European Atlantic shelf break(Neves *et al*., 1998); Operational modelling of the Atlantic (Riftlet, 2007);
- Reservoirs: Roxo, Monte Novo and Alqueva reservoirs (Braunschweig, 2001);

Since the model was made available on the internet (http://www.mohid.com) there was a substantial increase of users. The support is maintained by an online forum and wiki. The model allowed the development and coupling of a transport model, including cohesive sediment transport (Cancino and Neves, 1999). This development allowed the coupling of several other modules, including a water quality module (Portela,

1996, Miranda, 1999, Pina, 2001). This step opened new frontiers for model applications and transformed it into a fully integrated tool ready to be applied in almost every aquatic system. Starting in 1998, the model programming was reorganized, writing it in ANSI FORTRAN 95. This provided the programmers with several new features that include the ability to produce object oriented programming (although it is not an object oriented programming language). This approach and philosophy, made MOHID development relatively ease to new users and programmers.

New developments in parallelised computing are being implemented in the MOHID system in order to enhance its capabilities and be in line with the technology development.

3.3. Hydrodynamics

MOHID solves the three-dimensional primitive equations in Cartesian coordinates for incompressible flows. Given its Boussinesq approximation, hydrostatic equilibrium is assumed. MOHID uses a general vertical coordinate.

Mass and momentum evolution equations are:

$$\frac{\partial u_i}{\partial x_i} = 0 \qquad \textbf{(1)}$$

$$\frac{\partial u_1}{\partial t} + \frac{\partial (u_j u_1)}{\partial x_j} = -fu_2 - g\frac{\rho_\eta}{\rho_0}\frac{\partial \eta}{\partial x_1} - \frac{1}{\rho_0}\frac{\partial p_s}{\partial x_1} - \frac{g}{\rho_0}\int_z^\eta \frac{\partial \rho'}{\partial x_1} dx_3 + \frac{\partial}{\partial x_j}\left(A_j \frac{\partial u_1}{\partial x_j}\right) \qquad \textbf{(2)}$$

$$\frac{\partial u_2}{\partial t} + \frac{\partial (u_j u_2)}{\partial x_j} = fu_1 - g\frac{\rho_\eta}{\rho_0}\frac{\partial \eta}{\partial x_2} - \frac{1}{\rho_0}\frac{\partial p_s}{\partial x_2} - \frac{g}{\rho_0}\int_z^\eta \frac{\partial \rho'}{\partial x_2} dx_3 + \frac{\partial}{\partial x_j}\left(A_j \frac{\partial u_2}{\partial x_j}\right) \qquad \textbf{(3)}$$

$$\frac{\partial p}{\partial x_3} = -\rho g \qquad \textbf{(4)}$$

Where u_i are the velocity vector components in Cartesian x_i directions positive to the east, to north and upward, η is the free surface elevation, f is the Coriolis parameter, A_j the turbulent viscosity and p_s is the atmospheric pressure. ρ is density and ρ' its anomaly. Density is computed depending on salt, temperature and pressure, by the UNESCO equation of state (UNESCO, 1981).The model uses an ADI (Alternate Direction Implicit) time discretization scheme which minimizes stability restrictions, and is defined in an Arakawa-C type grid. Turbulence is computed through a set of available models:

- Horizontal turbulence - Constant, Smagorinsky (1963), Proportional to depth and to the square of velocity;
- Vertical turbulence – Constant, Nihoul (1984), Leendertse and Liu (1978), Backhaus and Hainbucher (1987), Pacanowski and Philander (1981), and GOTM (Burchard *et al*, 1999) – http://www.gotm.net, a turbulence models library

coupled with MOHID, including a k-ε model and Mellor-Yamada second order turbulent closure model (Mellor and Yamada, 1982).

Momentum, mass and heat transport is computed using a generic 3D advection-diffusion library including various advection schemes namely: first, second and third order upwind, centred differences and TVD (Total Variation Diminishing). Advection is solved in the three dimensions as a one-dimensional case and various time discretizations can be combined: explicit, semi-implicit or fully implicit.

3.4. Transport

Transport phenomena in the water column for a given property (P), can be described by the 3D advection-diffusion differential equation:

$$\frac{dP}{dt} = \frac{\partial P}{\partial t} + u_j \frac{\partial P}{\partial x_j} = \frac{\partial}{\partial x_j}\left(k_\Theta \frac{\partial P}{xj} \right) + (Sources - Sinks) \quad \textbf{(5)}$$

P is the concentration (ML^{-3}), j is the index for the correspondent Cartesian axis (x_1, x_2, x_3) or (x,y,z), K_Θ is the turbulent mass diffusion coefficient (horizontal/vertical). Sources and sinks related to reaction processes taken place inside the assumed control volume, which undertakes local production and destruction terms.

Particulate properties transport is governed by a 3D advection-diffusion equation where the vertical advection includes the particle settling velocity.

$$u_Z = u_{Z'} + w_S \quad \textbf{(6)}$$

Where u_z is the overall vertical velocity of the particulate property, $u_{z'}$ is the vertical current velocity, and w_s is the property's settling velocity. This methodology enables to compute particulate properties transport, like particulate contaminants or particulate organic matter, likewise and dependent of cohesive sediments.

3.5. Boundary Conditions

The interpretation of transport phenomena through a numerical model requires that appropriate boundary conditions are provided. These boundary conditions can be provided at the surface and bottom of the domain and on the lateral boundaries, and can be closed, open or mobile. Imposed values, inwards-outwards fluxes, decaying laws can be imposed depending in the type of boundary. In the water column, any flux between land and water, such as a river or an effluent, is computed as a discharge. Discharges can contain hydrodynamic properties (e.g. momentum), or water properties (e.g. temperature, salinity, suspended particulate matter, pollutant loading, nutrients, phytoplankton).

The open boundary can correspond, for example, to the oceanic boundary. Tide is imposed at the open boundary, where water level is normally imposed after being computed through tidal harmonic components. For an open boundary, a property can be relaxated from each dataset/property boundary condition within a number of cells from the boundary into the domain. Relaxation coefficients values increase progressively from boundary to domain interior, providing a larger weight for the model defined solution in the interior and a smaller weight for this solution at the boundary. This scheme is based on Martinsen and Engedahl (1987).

Open boundary conditions is a "science" within hydrodynamic and transport modelling. An extensive overview on how this type of boundaries is handled in MOHID Water can be found in Leitão (2003).

3.6. Lagrangean Tracers

The contaminants in the water column can be simulated through lagrangian tracers approach (Leitão, 1996) instead of a eulerian approach:

$$\frac{dx_i}{dt} = u_i(x_i, t) \quad \textbf{(7)}$$

Where *u* stands for the mean velocity and *x* for the particle position. The velocity at any point of space is calculated using a linear interpolation between the points of the hydrodynamic model grid. Turbulent transport is responsible for dispersion. The effect of eddies over particles depends on the ratio between eddies and particle size. Eddies bigger than the particles make them move at random. Eddies smaller than the particles cause entrainment of matter into the particle, increasing its volume and mass according to the environment concentration. The random movement is calculated following the procedure of Allen (1982). The random displacement is calculated using the mixing length and the standard deviation of the turbulent velocity component, as given by the turbulence closure of the hydrodynamic model. Particles retain that velocity during the necessary time to perform the random movement, which is dependent on the local turbulent mixing length (Leitão, 1996).

3.7. Ecological Model

For this study, a specific MOHID module named Water Quality was used to model the primary production in the North Sea. Figure 6 shows the relations of the properties and modelled species.

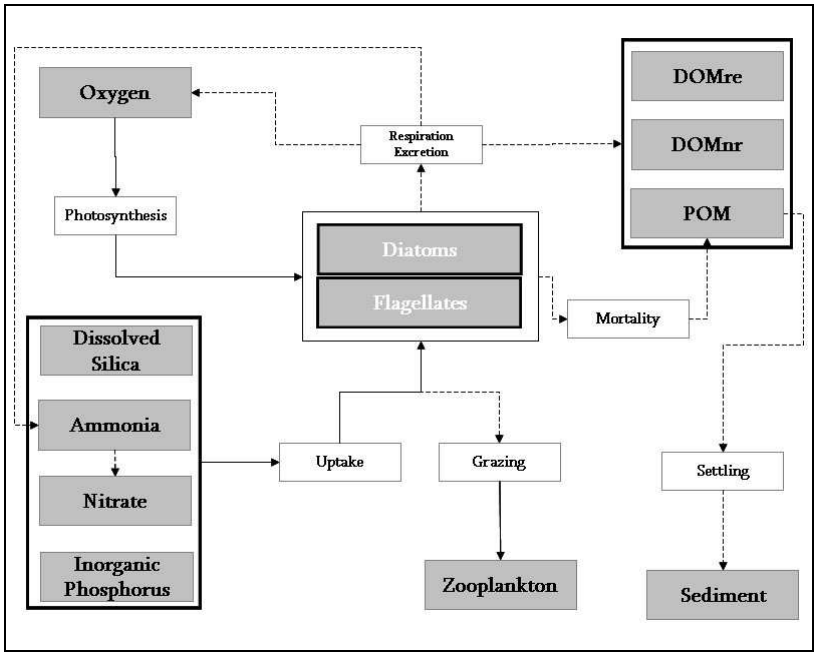

Figure 6: MOHID Water Quality Module

The model Water Quality is adapted from EPA (1985) and belongs to the category of ecosystem simulations models i.e. sets of conservation equations describing as adequately as possible the working and the interrelationships of real ecosystem components. The pelagic and benthic biogeochemical processes are implemented in the form of sink and sources terms of the transport model. The benthic ecological processes include mineralization of organic matter and oxygen depletion.

The Water Quality module communicates with the Water Properties module. This latter module coordinates the evolution of the water properties in the water column, using a eulerian approach. This coordination includes the transport due to advective and diffuse fluxes, water discharges from rivers or anthropogenic sources, exchange with the bottom (sediment fluxes) and the surface (heat fluxes and oxygen fluxes), sedimentation of particulated matter and the internal sinks and sources (water quality). The model considers 18 properties, including nutrients and organic matter (nitrogen, phosphorus and silica biogeochemical cycles), oxygen and organisms. It enables the user to choose between the simulation of one group of phytoplankton or two groups – flagellates and diatoms. The same type of option is made for secondary producers: one generic group of zooplankton or two groups – microzooplankton and mesozooplankton. The model is also able to simulate heterotrophic bacteria in the water column.

In this study, just one group of primary producers and one of secondary producers was chosen: phytoplankton (flagellates) and zooplankton (corresponding to mesozooplankton). Since the as the diatoms were not included, the silica cycle was left out of the model. Many of the equations are written as dependent on a regulating factor, which contains the functional response of the organism to some environmental parameters such as light, nutrients or temperature. When growth is a function of many

resources, there is a large range of functional forms that might express the joint dependence. To control the various possibilities, it is common to think of separate resources as limiting factors reducing some theoretical maximum growth rate - factors that can be determined separately and the combined by a small number of ways. Each growth limitation factor can range from a value of 0 to 1. A value of 1 means the factor does not limit growth (i.e. is at optimum intensity, nutrients are available in excess, etc) and a value of 0 means the factor is so severely limiting that growth is inhibit entirely. The limiting factors for the phytoplankton growth results are briefly presented in the ecological model section of this thesis.

For further reference, Annex II has more detailed information on the model's technical description (MARETEC/IST, 2003 and 2006).

4. 2D Model

This chapter describes the 2D model used to simulate the hydrodynamics of the domain area. Its results are later used by the 3D submodel.

This domain spans from latitudes 48ºN to 64ºN and longitudes 12ºW to 13ºE, and includes tidal, wind forcing and river discharges. The domain span was chosen in order to include the wider North Sea: from the North of France, half way to the North of Norway, including the British Isles and Ireland and to the west to the entrance of the Baltic Sea. The resulting hydrodynamic data was used for the harmonic analysis and for the lagrangean tracers.

4.1. Model Setup

This section describes how the model was setup for the 2D application.

4.1.1. Grid and Bathymetry

To study the hydrodynamics (transient circulation, residual circulation and residence time), this application uses a bathymetry that spans from latitudes 48ºN to 64ºN and longitudes 12ºW to 13ºE (about 1800km by 1900km in the centre of the domain). It spans 436 cells in longitude and 250 cells in latitude. The bathymetry data used to run the model was provided by CEFAS and has an initial 0.055º longitude and 0.033 º latitude resolutions (Figure 7). It uses an irregular grid with resolution ranging from 0.1º (11km) at the borders to 0.04º(4.5km) at the centre of the domain (Netherlands/Belgium/UK region)(Figure 8).

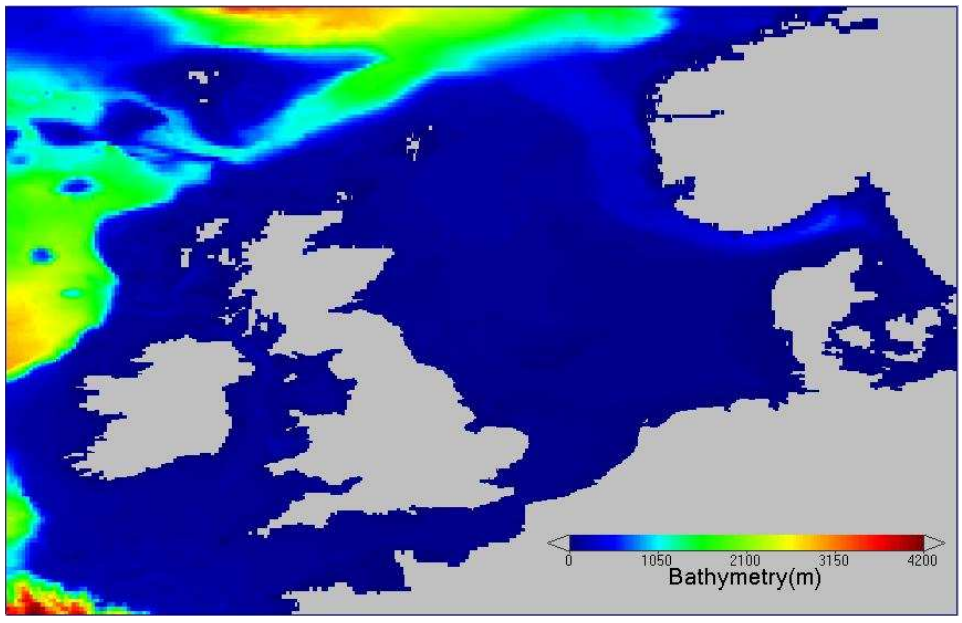

Figure 7: Bathymetry of the North Sea provided by CEFAS

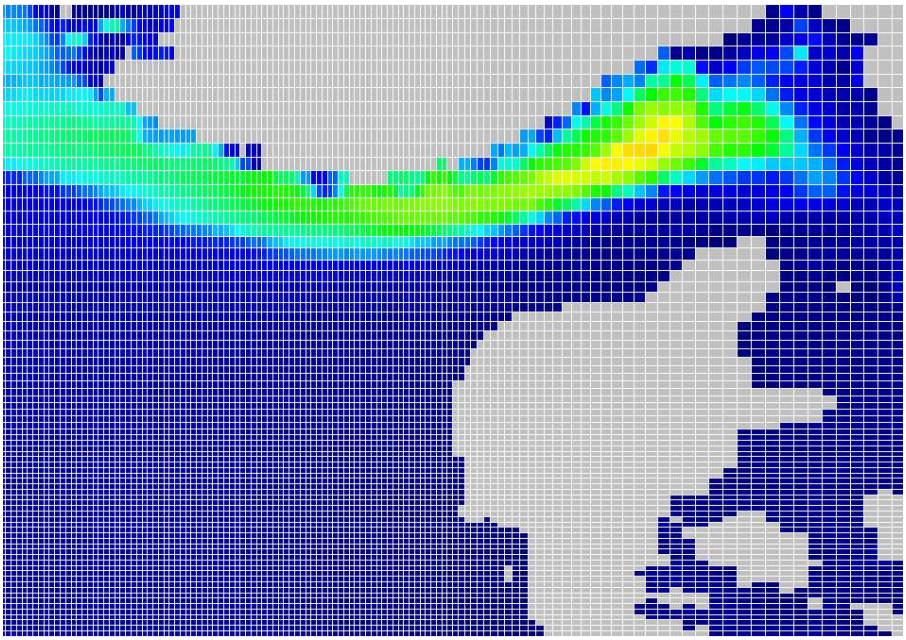

Figure 8: Irregular grid at Denmark/Norway region. Higher resolution at the bottom left.

The bathymetry was compiled by Joanna Staneva (CEFAS), who applied integration and smoothing routines, using different data sources such as ETOPO 2,DYNOCS (North Sea),CEFAS - English Channel, CEFAS - Irish sea, RIKZ Wadden Sea (Dutch part), IOW Belt Sea, IOW Baltic Sea, BHS kusten (German Bight). The institutes that provided the data are CEFAS, RIKZ, IOW and BSH. All the datasets used in this model, such as the bathymetry and wind field were interpolated to this grid.

4.1.2. Time span and spin up run

The model is run for one year in this from 1999-12-26 to 2000-12-31. It includes a spinup run for 5 days (from 1999-12-26 to 2000-01-01) and then runs 3 months at a time, all with a timestep of 60s.

4.1.3. Tidal Forcing

The tide was forced in the boundary of the domain using the FES2004 global solution (Lyard *et al*, 2006). The resulting input file for the model has 168 tidal gauges dispersed around the boundaries of the domain, inputting 11 harmonic components to the model (M2, S2, K2, N2, K1, O1, P1, Q1, Ssa, Mm, Mf). The Baltic sea boundary is also defined as an open boundary with tidal gauges.

4.1.4. River Discharges

The river discharges) from 1977 to 2006, were compiled by CEFAS using a number of different sources (Annex 1.1). 152 river discharges were imposed, with daily flow means (in m^3/s). Many discharges have also nutrient data which was used in the ecological model (3D submodel). Because showing 152 discharges is not feasible, annex 1.5 shows the locations of riverine discharges in the 3D model.

4.1.5. Meteorology

The meteorology data used was retrieved from the ECMWF ERA-40 reanalysis data server. It includes four times daily surface data for wind forcing(X velocity and Y velocity at 10m) with a resolution of 2.5 º. This dataset was interpolated to the model grid using specific routines.

4.2. Results and Discussion

4.2.1. Transient Circulation

To describe the transient circulation of the North Sea, the model was run using the grid presented above and forced with tide, river discharges and wind. The following figure, presents the flood and ebb conditions in the region.

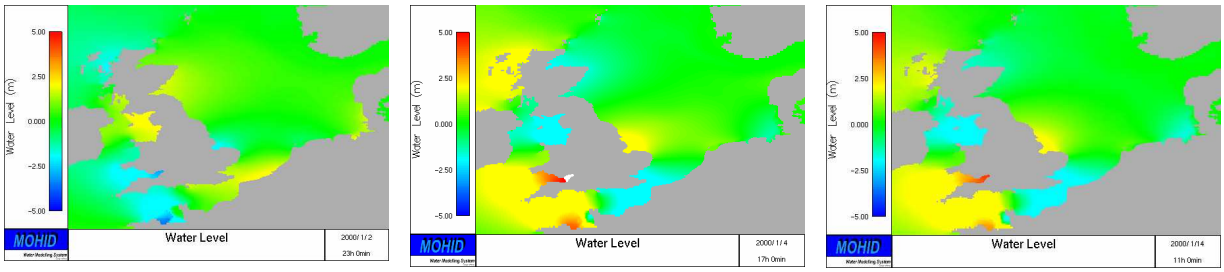

Figure 9: Water level in the North sea (1Jan 23h, 4Jan 17h and14Jan 11h)

In the region of Bretagne/Normandy and Wales, it is particularly interesting the fact that the tidal amplitudes are higher, ranging from -6 to +6 m from ebb to flood conditions. It is possible to conclude from the results that the tide reaches the Netherlands with an age of at least 2 days, after circulating clockwise around the British Isles. The tide appears not to enter the North Sea by the English Channel. Figure 10 shows the velocity modulus (in colour) and the velocity vector. During ebb/flood cycles the velocity gradient is high in the English Channel with velocities reaching 1.5 m/s and even higher in the Irish seas, around Wales.

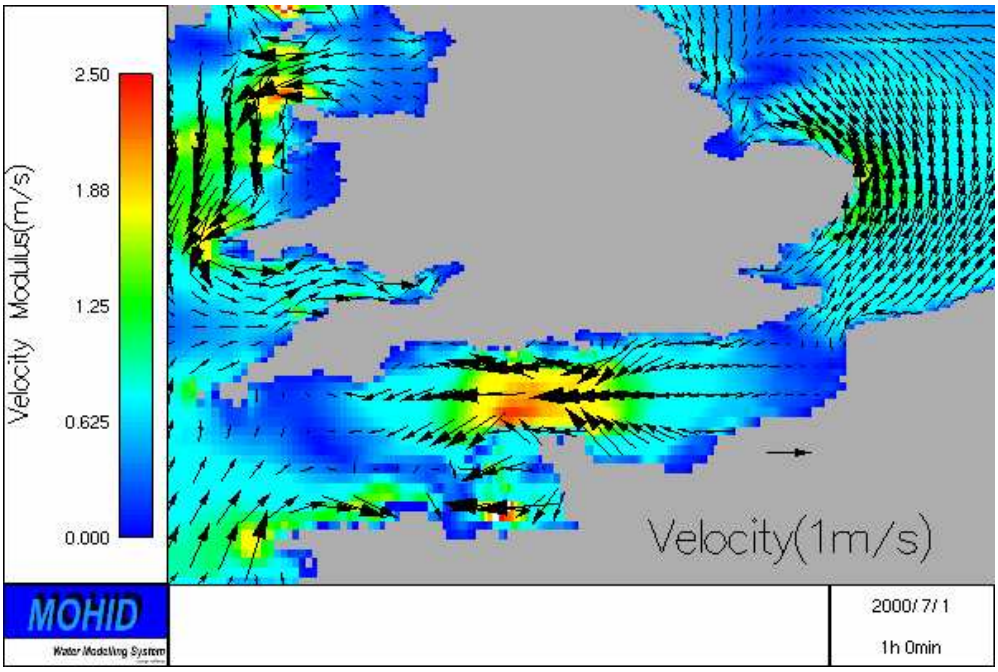

Figure 10: Instantaneous Velocity field

4.2.2. Residual circulation

The transient circulation gives information about the instantaneous flow, but to better understand the transport processes inside the North Sea, the model is able to compute the residual circulation. The residual circulation is the average flow, giving the idea of the preferential transport of any property discharges in the domain. To obtain the residual velocity, the model was run over a period of time (3 months), much more than the time periods associated to the variability of the transient flow.

The residual circulation can be defined in several ways:

- As the average of the transient water flux per unit of length – residual specific flux(m2/s)
- As the residual specific flux divided by the average depth of the water column, which is also a velocity (m/s)

The residual flux gives a picture of the residual movement of the water volume, but it is difficult to visualise in situation that include both deep and shallow waters, because the adequate scale is a function of depth.

Figure 11 shows the residual velocity derived from residual flux at the area of interest of the North Sea. In the Skagerrak region, where the depths reach over 500m, the water flows in the direction east-west near the coast, but it flows in the opposite direction some 50km southerly. In the northern boundary, the residual flux is much higher than in the central-southern part of the North Sea. Also, in the Irish seas, as picture in the previous point, the residual flux is much higher than in the rest of the North Sea.

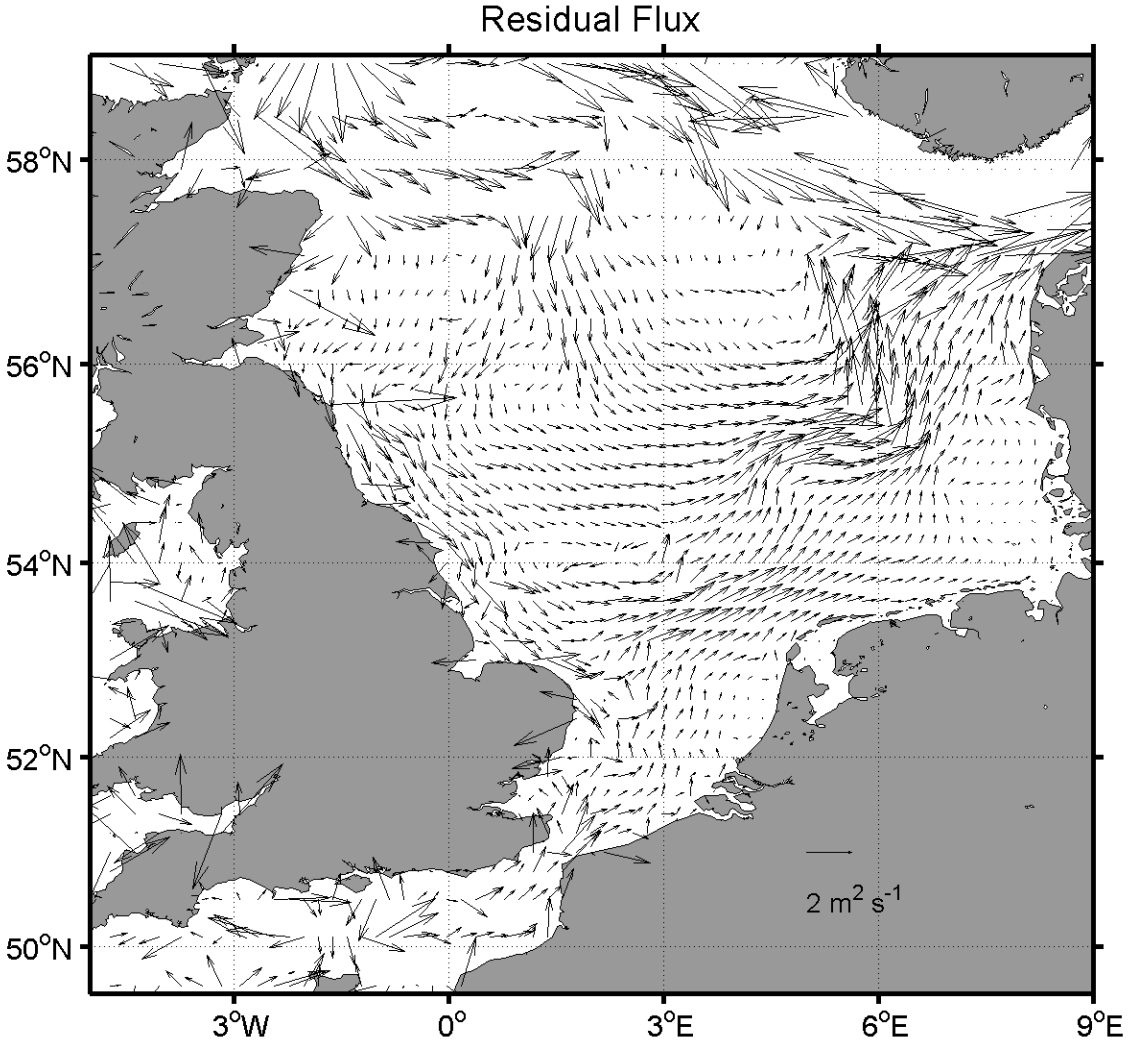

Figure 11: Residual flux in the North Sea

The following figure depicts the residual velocity in the North Sea. It is possible to deduce that the circulation in the North Sea has a counter clockwise direction. The water enters the shelf in the northern boarder, and circulates southerly, from the UK to the Netherlands, Germany and Denmark. Then it leaves the shelf on the Norwegian trench. Moreover, the water flux passing through the Straight of Dover is significant, although the tidal influence of the English Channel in the North Sea is small.

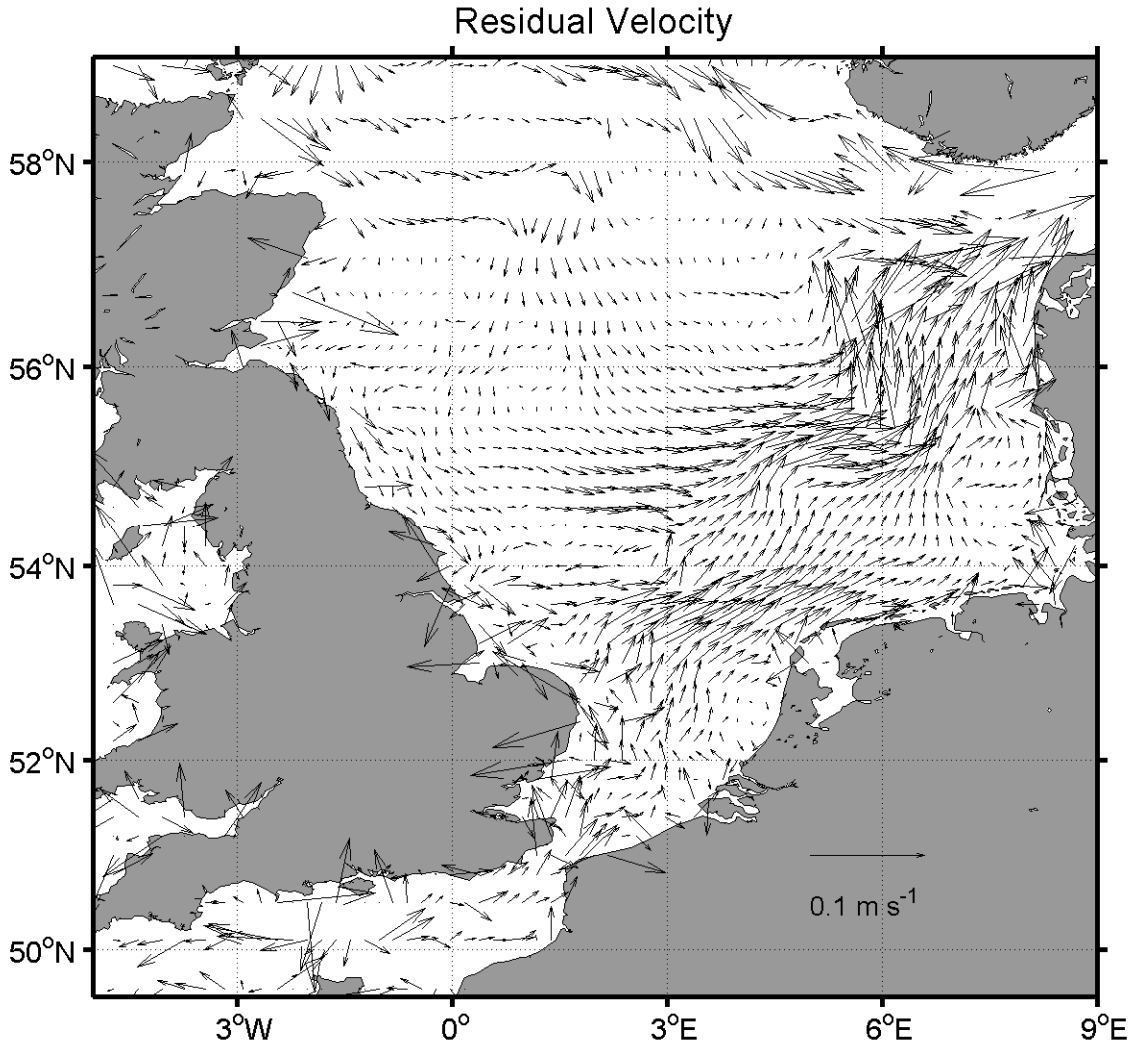

Figure 12: Residual Velocity

4.2.3. Tidal Harmonic Analysis

The harmonic analysis is an important part of model validation, as it can say much about the hydrodynamical precision of the model.

For the comparison of the model results with "measured" sea levels, an analysis is made with data from several tidal gauges from around the North Sea (Figure 13). The data was retrieved from the XTIDE harmonic component database (XTIDE, 2004), using the interface from T_TIDE (Pawlowicz, 2002). This database is one of the world's references in harmonic component as many national hydrography authorities use it for official recording (for e.g. RIKZ in the Netherlands).

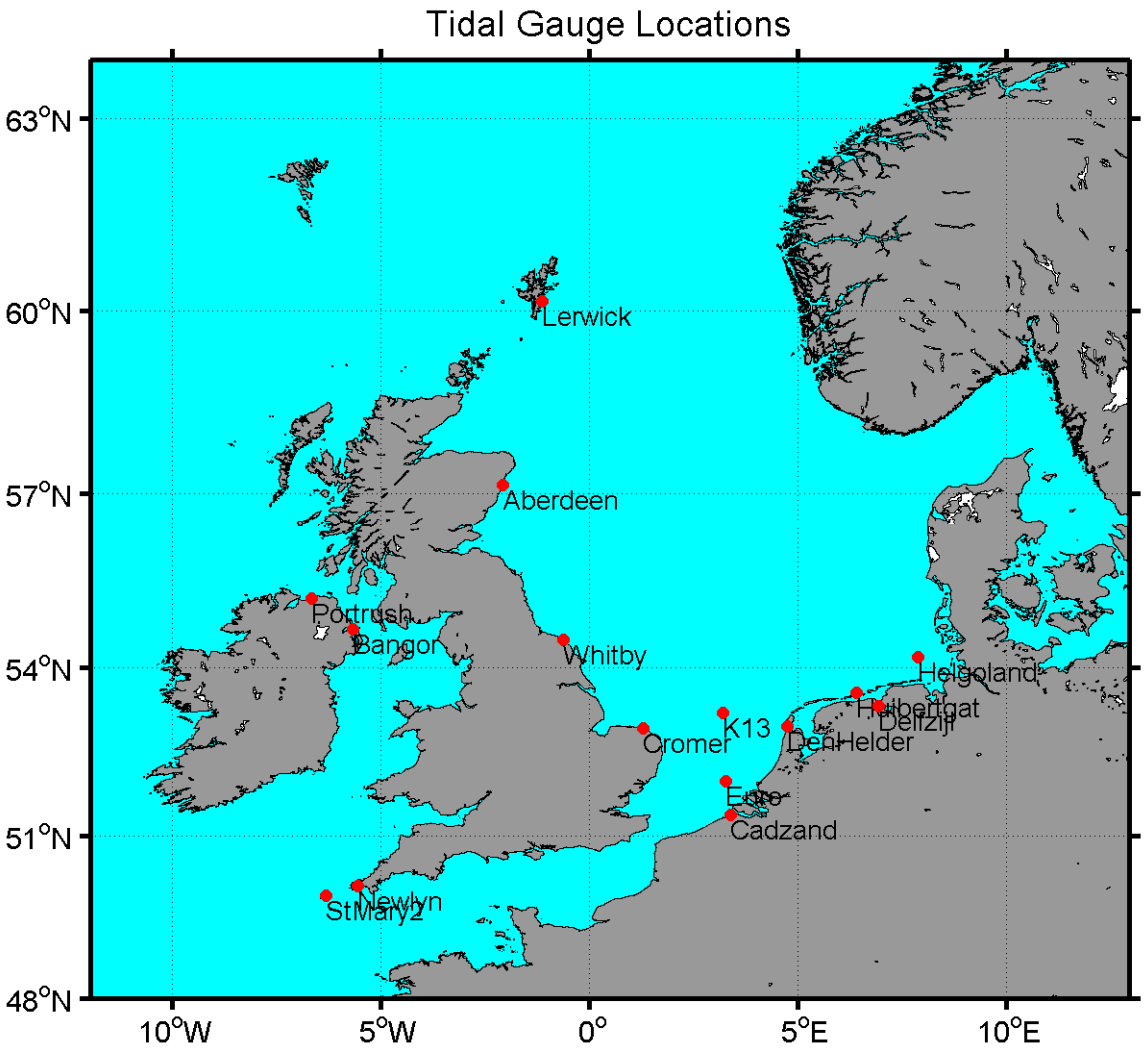

Figure 13: Map of the analysed tidal gauges

Timeseries analysis

In order to compare the model's result with the XTIDE database, which has only tidal data, one has to remove the non-tidal interactions from the model's timeseries to be able to compare solely the tide. This procedure is done by performing a harmonic analysis on the model's timeseries, and then reconstruct it based on the resulting harmonic components. This was computed with the T_Tide package (Pawlowicz 2002; Foreman, 1977) using MatLab. The analysis can be made by comparing the timeseries (statistical analysis) and by comparing the harmonic components (harmonic analysis).

For some of the gauges, a plot was made with the model's and the XTIDE's timeseries (Figure 14, Figure 15, Figure 16 and Figure 17 shows this for a 5 day period). The tidal simulation of the UK gauges is reasonably accurate, but in the case of the Netherlands and German tidal gauges, although the timing of the tide is accurate, the simulated water level is underestimated. The following figures show these differences.

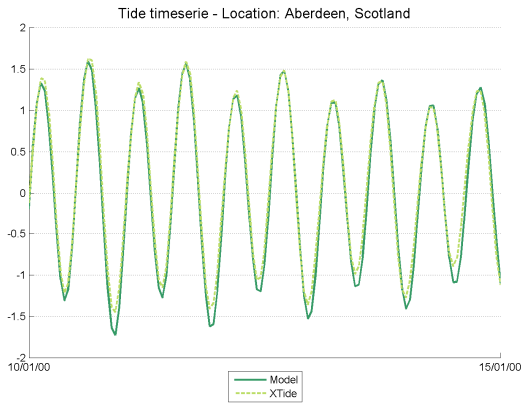

Figure 14: Aberdeen tidal gauge timeseries

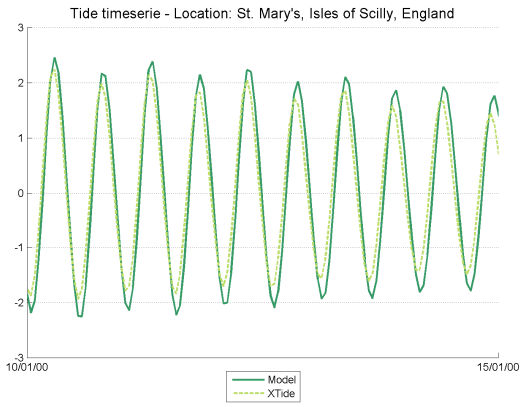

Figure 15: St. Mary tidal gauge timeseries

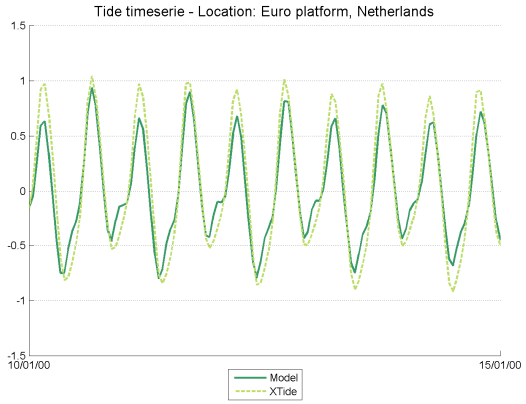

Figure 16: Euro platform tidal gauge timeseries

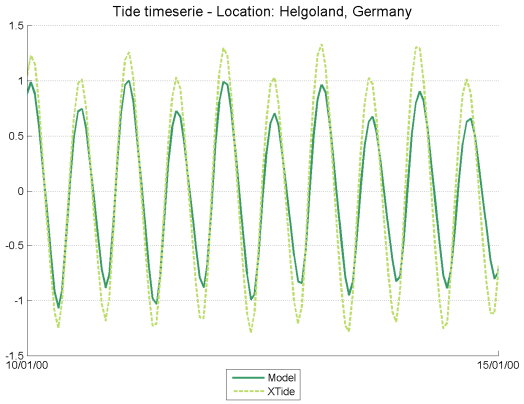

Figure 17: Helgoland tidal gauge timeseries

From the resulting two timeseries, a statistic analysis was made using several descriptors. The descriptors are based on Chambel-Leitão (2007) from Evans (2003):

- Correlation coefficient: also known as the Pearson product-moment correlation coefficient;
- Model Efficiency: Nash-Sutcliffe coefficient;
- RMSE: Root Mean Square Root;
- Bias: Mean differences between timeseries, in metres.

The following figure (Figure 18) shows the mean and standard deviation (error bars) of the descriptors, for all 15 tidal gauges analysed (map from Figure 13). The model generally agrees with the observations. It presents a good correlation coefficient (90-99%), indicating that there is a linear correspondence between the two timeseries (Figure 18). From the results (including Figure 19), it is possible to conclude that the

accuracy of the model's timeseries decreases when a particular tidal gauge is further away from the tidal forcing on the Atlantic boundaries.

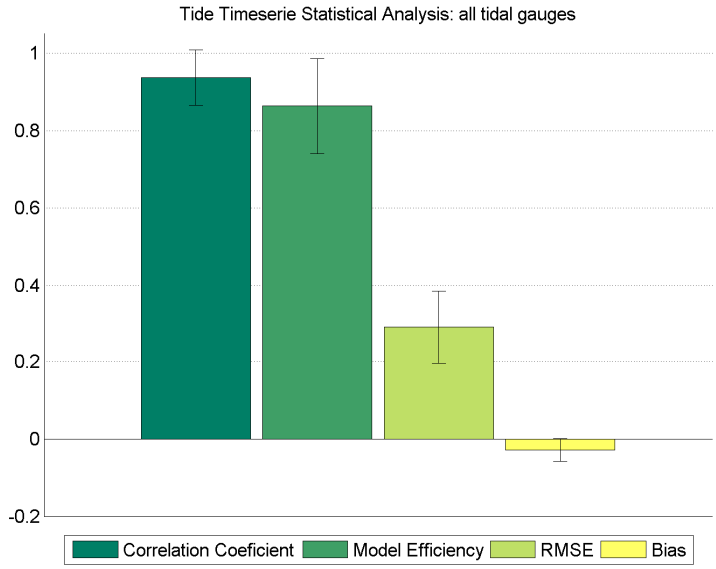

Figure 18: Model vs XTIDE timeseries statistical analysis for all locations [adim], except for Bias[m] (error bars are standard deviation)

The following figure shows the statistical descriptors for the selected tidal gauges. The bias indicates that is a difference between the amplitudes of the timeseries, which is more significant on the UK coast, as Figure 19 demonstrates. Furthermore, the RMSE increases as the tidal gauge is farther away from the forcing boundary.

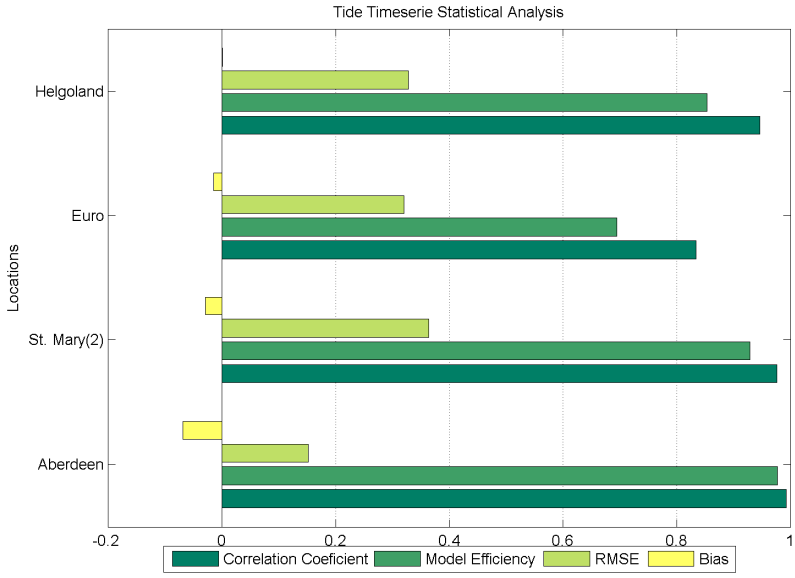

Figure 19: Model vs XTIDE timeseries statistical analysis for the selected locations [adim], except for Bias[m]

For the selected gauges, a comparison between the model's harmonic components and the XTIDE database's is done. Figure 20, Figure 21, Figure 22 and Figure 23, show the 8 main harmonic components, based on the model's amplitude. The phase graph (bottom of each figure) can sometimes be misleading: a phase of 360º is equal to 0º. It is also scaled 0 to 400 to account for the error bars. When the error is taken into account, the differences between the model and the XTIDE database are quite satisfactory for most tidal gauges: each lies on the others' error margin and vice-versa. From the results it is possible to conclude that there are some phase differences on the tidal gauges near the Dutch and German coasts, which can explain the inferior performance of these gauges (Figure 19). The bathymetry resolution can be blamed for these discrepancies, as discussed later, along with the spatial analysis.

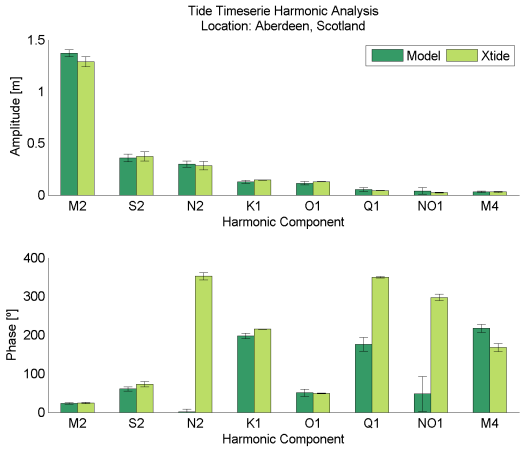

Figure 20: Aberdeen tidal gauge harmonic analysis

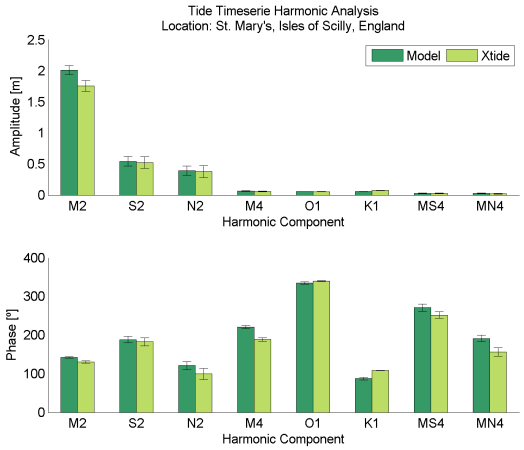

Figure 21: St. Mary tidal gauge harmonic analysis

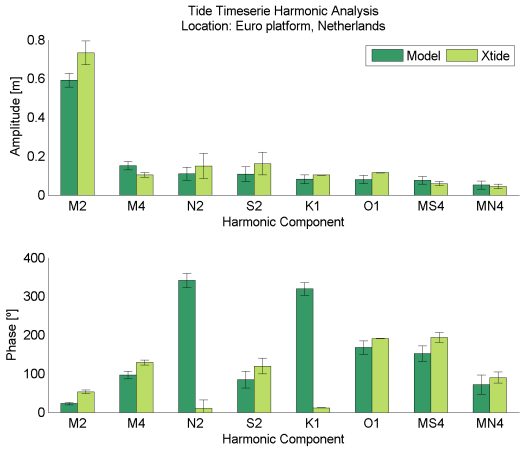

Figure 22: Euro platform tidal gauge harmonic analysis

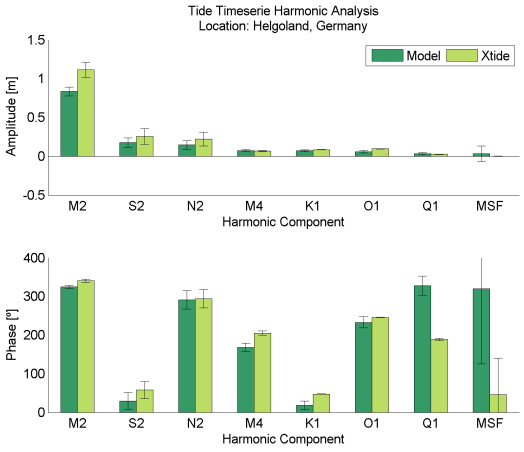

Figure 23: Helgoland tidal gauge harmonic analysis

Spatial analysis

A wider outlook of the whole North Sea can be obtained if the harmonic components for each cell in the model grid are computed. This outputs two maps, one for the amplitude and one for the phase, for each harmonic component, for the entire grid. The computation was done using MatLab and the T_Tide package (R. Pawlowicz 2002; M.G.G. Foreman, 1977). The following figures show the amplitude and phase for the harmonic components M2, S2, N2 and M4, which are the most relevant in the domain.

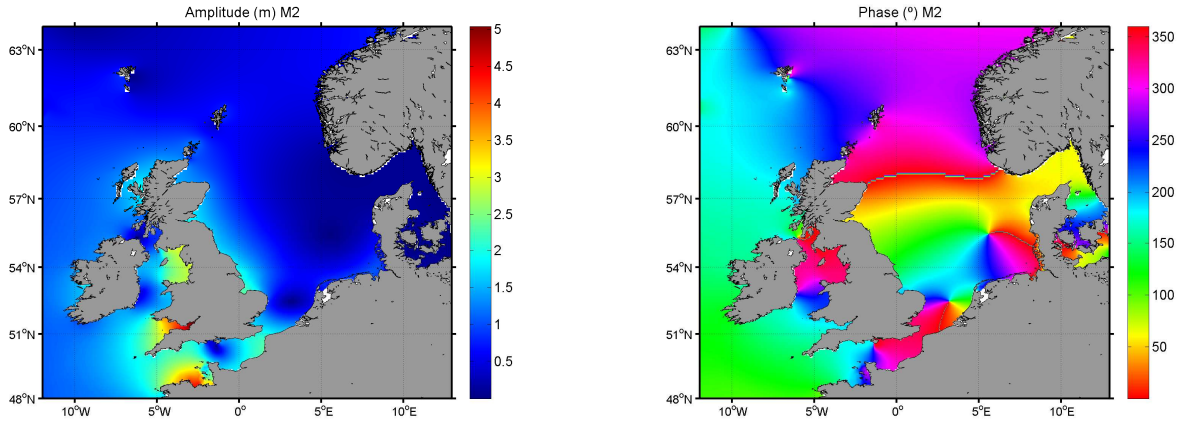

Figure 24: M2 tidal harmonic component: amplitude(metres) and phase(degrees)

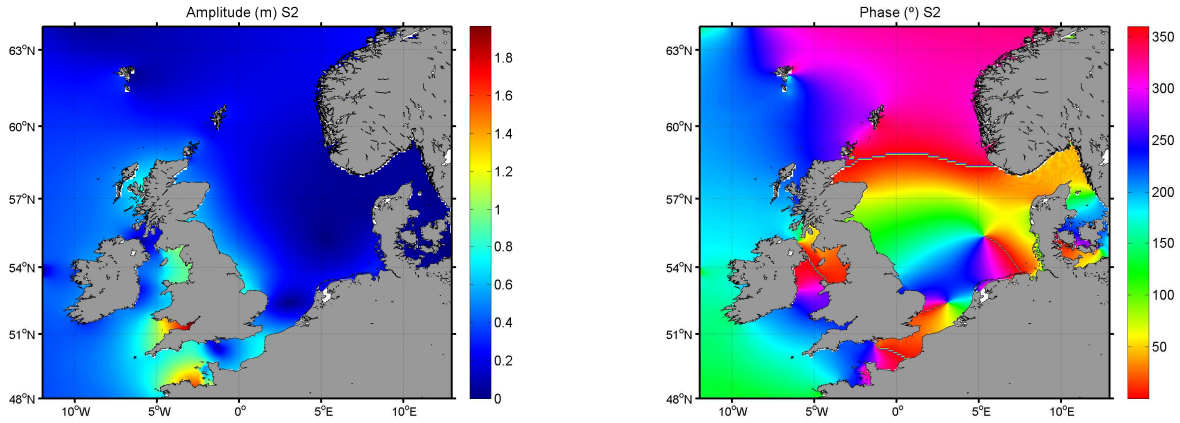

Figure 25: S2 tidal harmonic component: amplitude(metres) and phase(degrees)

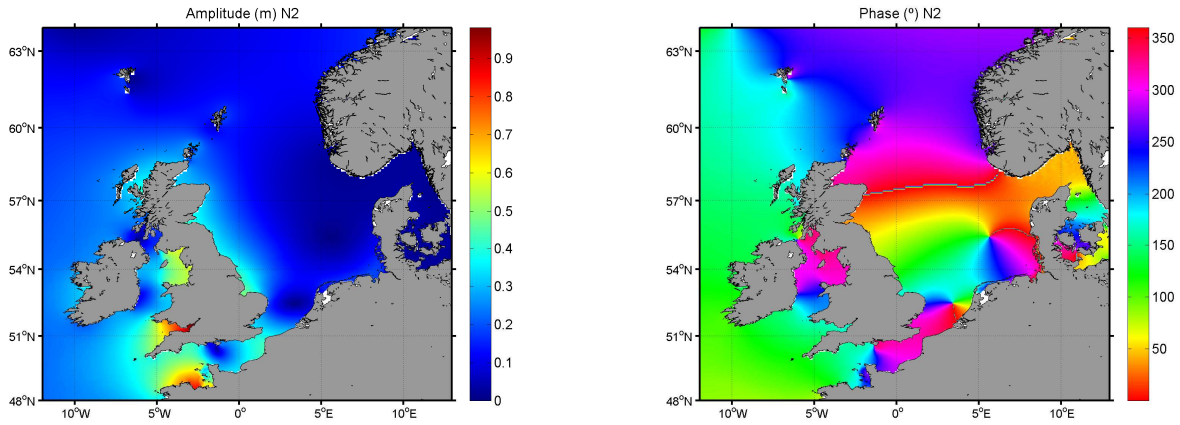

Figure 26: N2 tidal harmonic component: amplitude(metres) and phase(degrees)

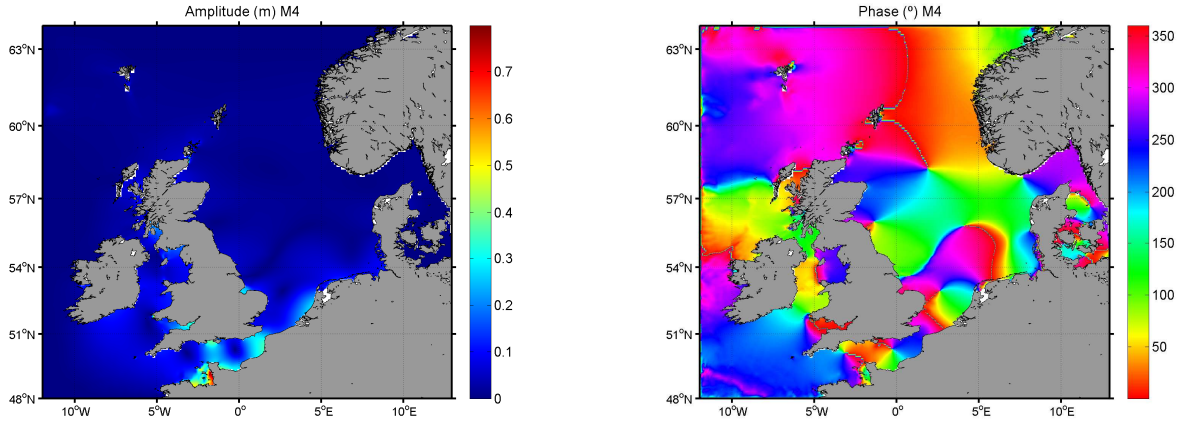

Figure 27: M4 tidal harmonic component: amplitude(metres) and phase(degrees)

Comparing the MOHID model's results with other published materials, for example Davies(1986), Helleiner(1997) and Anderson(2006), we can observe that there is visual correspondence in amplitude and phase for a variety of components(for e.g.M2 and M4). In order to check if the model is not generating fake tides, the model can be compared to the forcing dataset, which is from FES2004. If it agrees, it shows that the model is correctly simulating the tide along the domain with the forcing based on the boundary conditions.

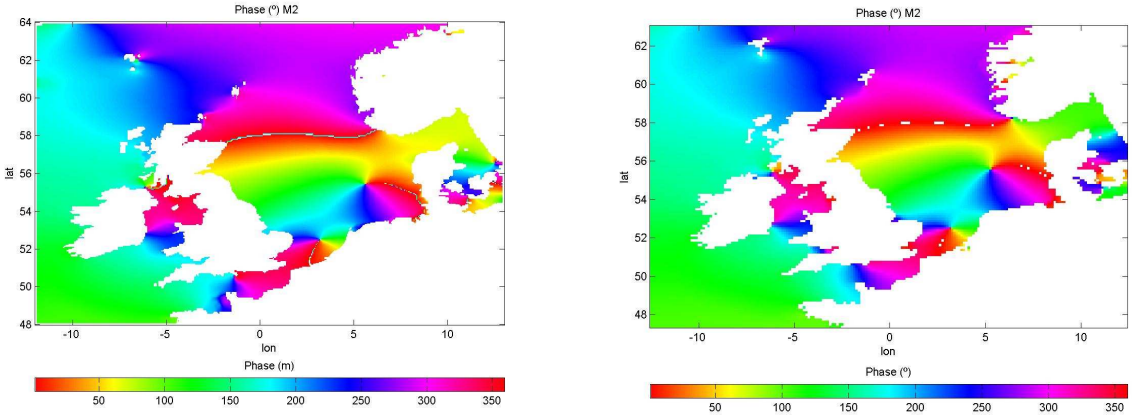

Figure 28: Comparison of M2 Tidal component phase between the model (left, same as Figure 24) and FES2004 solution (right)

Comparing the phase results with the FES2004 global solution (Figure 28), these generally agree between themselves. However, there are some differences, mainly in shallow water areas, where the harmonic components interact with the bottom and generate non-linear harmonic components.

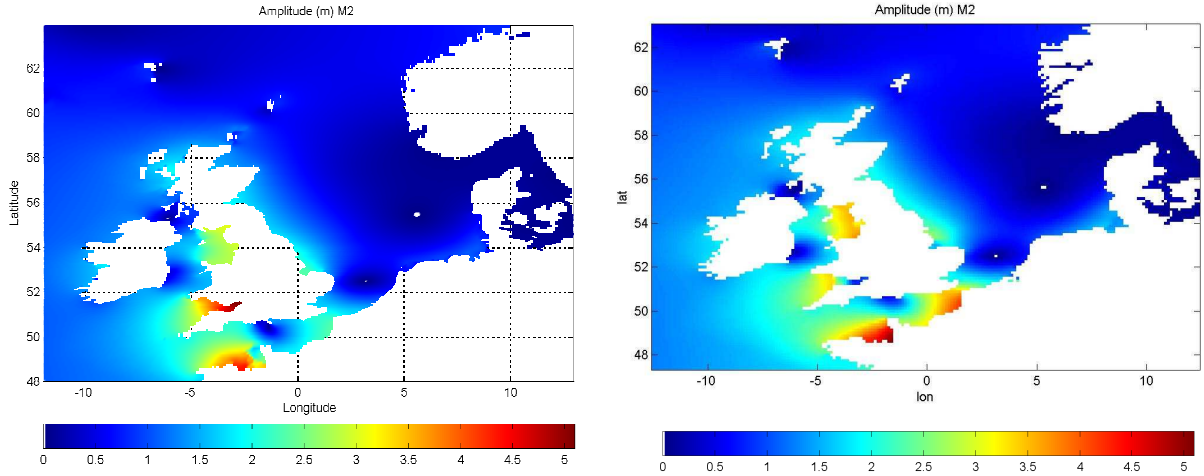

Figure 29: Comparison of M2 Tidal component amplitude between the model (left, same as Figure 24) and FES2004 solution (right)

Analysing Figure 29, we can see some discrepancies in the Bretagne/Normandy and in Wales: the model M2 component has distinctively different shapes. In these locations, the tidal amplitude range from -6 to +6m in spring tide. For that reason, the bathymetry used in the simulation can have significant errors (T. Letellier, 2004) because it is difficult to accurately determine the depths without having tidal influence in the measurements. Thus, there are significant differences between the model and the FES2004 solution for the M2 tidal component. That is the reason for using a wide scale model for giving the tidal signal to a nested model, ruling out the errors of the FES2004 as presented above.s

Amphidromic Points

One interesting fact about the North Sea is that there are three separate amphidromic points, i.e., points that show no tidal amplitude and for which the tide circulates around them. Figure 30 shows the points where this phenomenon occurs. The location of the amphidromic points in the model is accurate if we compare the model's amplitudes of the main harmonic components in the region (M2 (Figure 24) for e.g.).

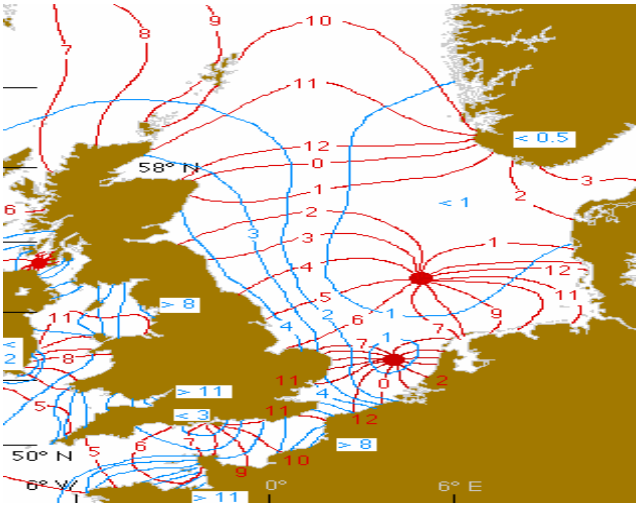

Figure 30: Amphidromic points in the North Sea are shown in red dots (M. Tomczak 1996)

4.2.4. Residence Time

Residence time is an important indicator for understanding the study region. This is particularly important in the case of algal blooms. Regions which have very short residence times are expected to have much lower algal blooms than regions with higher residence times. In this case, the problematic region is the UK/Netherlands/Belgium region (Mills *et al*, 2007) which will be specifically studied in the 3D model.

There are several ways to define residence time, which depend a lot on the data available to compute it and the concept of residence time itself. The use of a numerical model allows the most detailed calculation. In this case, the residence time is defined as the time required by water to leave a region and is computed using lagrangean tracers, which are used to label the water and to monitor its location and movements. The lagrangean module in MOHID is used to compute the tracers. Different regions inside the domain are identified by boxes, which are uniformly filled with lagrangean tracers. 10 boxes were considered, each one filled with a variable number of particles, each one with fixed volume (6.18E+08 m^3). The total amount of tracers and their initial distribution in each box are calculated so that the total volume of the tracers inside the box matches its water volume. The boxes have geometries similar to the countries water borders. The locations of the lagrangean tracers are monitored in time and their residence time inside each part of the region and the time required to leave the region are computed.

The following steps were used to compute the residence time:

- Computation of the hydrodynamics of the domain;
- Division of the domain into boxes, filled with lagrangean tracers with properties such as volume, spatial coordinated and the number of the box where it was released;
- Calculation of the residence time as the fraction between each box's particle volume and its total volume.

The following figure shows the initial distribution of the lagrangean tracers in the domain. Box 0(zero) is referred as the box that does not have particles inside. Box 3 is small, referring to the Belgium national waters. UK has two boxes (9 and 1). The Baltic Sea is box 8. Norway has two boxes: 7 and 10, because of the depth of the Norwegian trench.

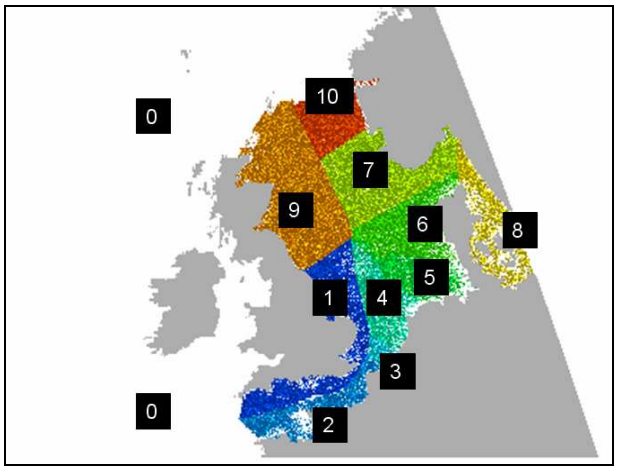

Figure 31: Box setup showing the 10 boxes and initial distribution

The total volume of tracers in the domain (all the boxes) is equal to the total volume of the domain at the beginning of the simulation. It is important to keep in mind that the total volume of the domain varies with time due to the tide and wind forced oscillations. Figure 32 shows exactly that phenomenon.

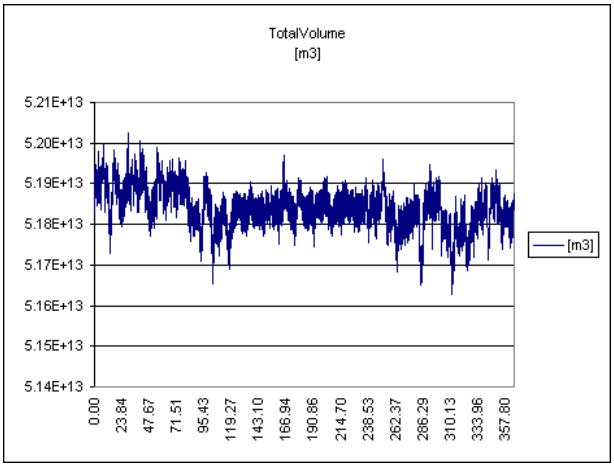

Figure 32: Total Volume of water inside the domain during simulation time(1year)

To evaluate the residence time inside the domain, the model was run for 1 year. Figure 33 shows the lagrangean tracer positions after 30 days. Most notably, the particle exchange between the Baltic Sea and the North Sea is very quick. As discussed in the previous section (Residual Velocity), it can be seen that the water leaves the domain following the Norwegian trench (green and red particles).

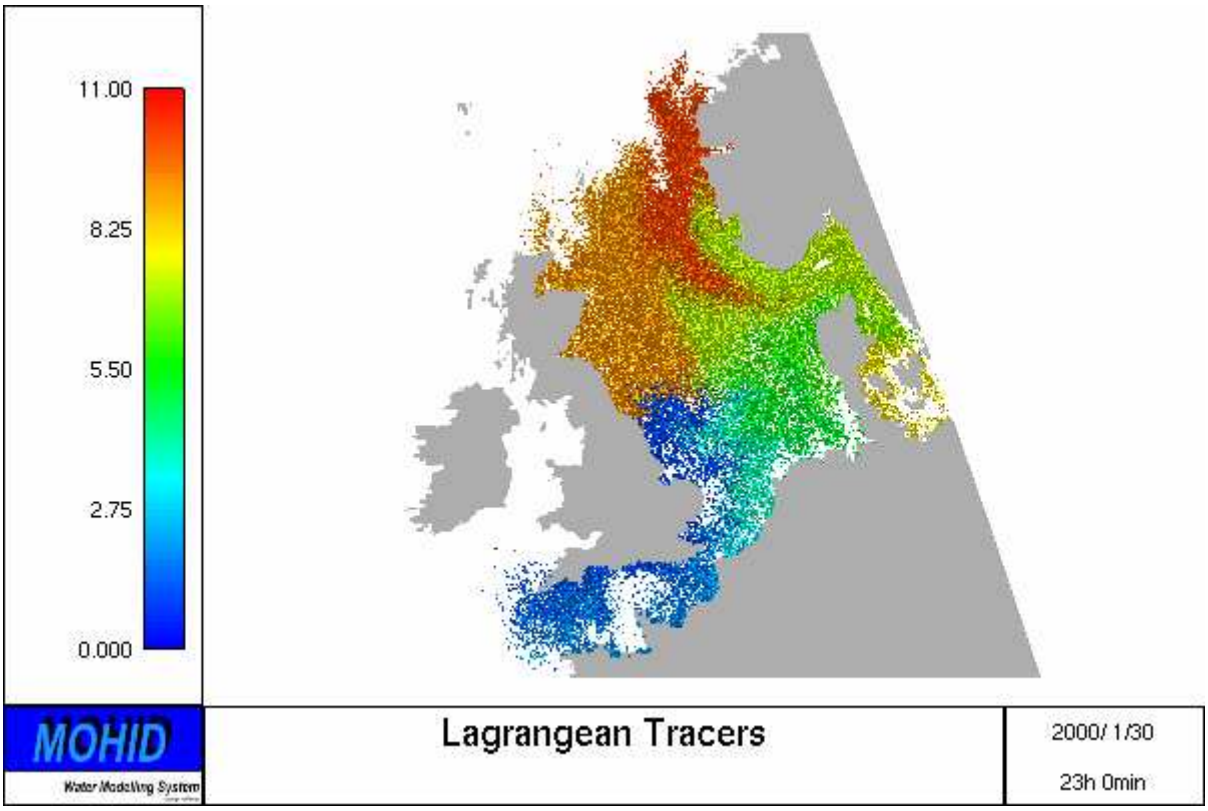

Figure 33: Distribution of the lagrangean tracers after 1 month

After 6 months (Figure 34), the particles are well mixes inside the domain, and there was a significant spread of red particles (box 10) to the north along the Norwegian coast. The particles found inside the Baltic Sea come from the boxes next to it and it appears to be well mixed.

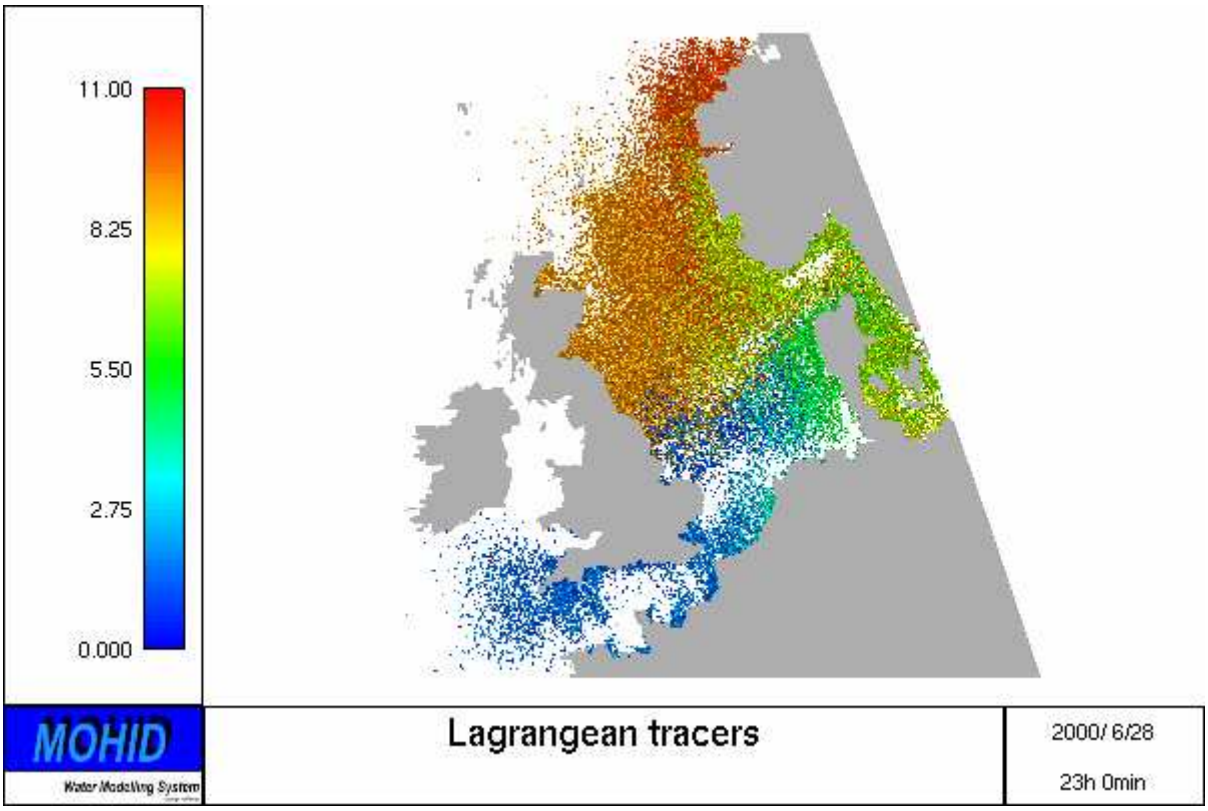

Figure 34: Distribution of the lagrangean tracers after 6 months

Figure 35 depicts the particle positions after 1 year. We can see that the particles belonging to bluish boxes(1,2,3) are all spread over the Netherlands, German and Danish coasts. The particles that were inside the English Channel have travelled westerly around the UK to the Irish Sea. The outflow of particles occurs northerly along the Norwegian coast.

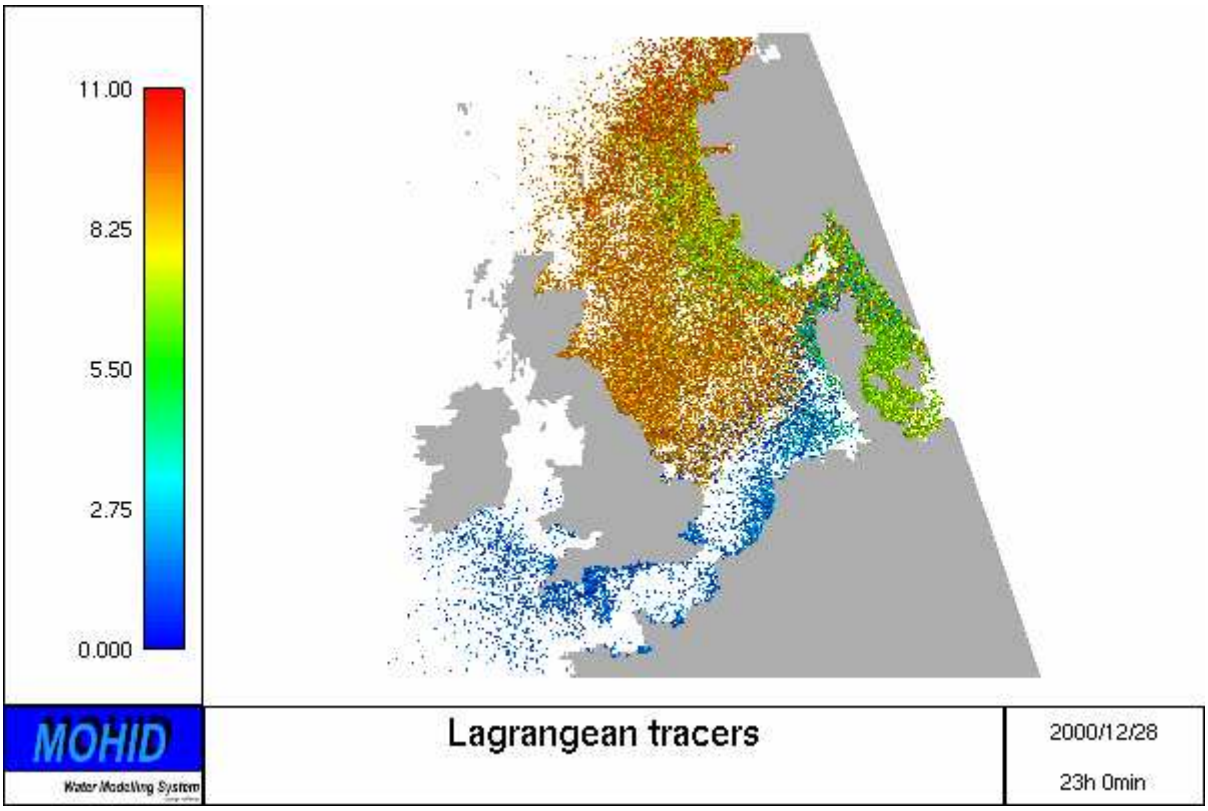

Figure 35: Distribution of the lagrangean tracers after 1 year

The evolution of the fraction of the tracers inside the domain (volume of all tracers inside the domain divided by the total volume of water in the domain in the same instant) is shown in Figure 36. After 1 year of simulation, about 75% of the initial volume remains inside the domain, which is a relatively long residence time.

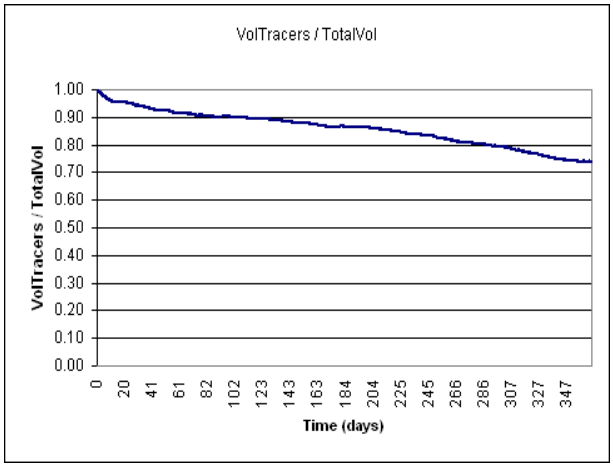

Figure 36: Evolution of the ratio between the volume of lagrangean tracers inside the boxes and the total volume as a function of the time.

Figure 37 shows the fraction of tracers of a box inside its own box (volume of tracers from a box divided by the total volume of water of the box in the same instant). Because each particle leaves its own box in a relatively quick manner (about 20% remain in the same box after 1 year), we can conclude that the domain is horizontally well mixed.

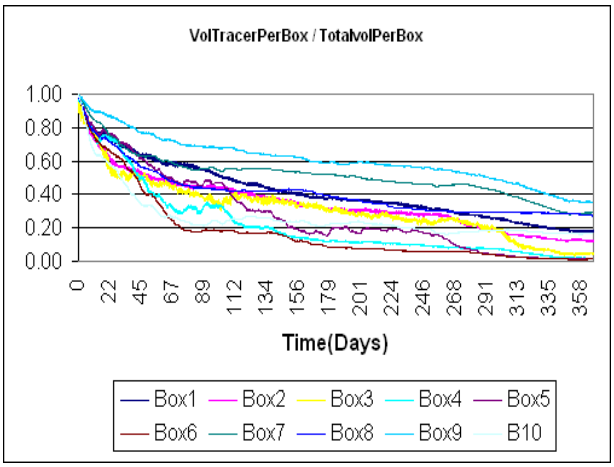

Figure 37: Evolution of the ratio between the volume of lagrangean tracers inside each and the total volume in each box as a function of the time.

The knowledge of the exchange of water among boxes can be more important than the knowledge of the residence time of the water in the whole domain. With the methodology used, it is possible to track the path of water masses in time. This tracking allows calculation of the residence time in each box and analyses the origin of the water in a given box at each time instant. The exchanges among regions are presented in the following figure (Figure 38). The use of "pie charts" represents the contribution of other boxes in the specific box. The bluish part of the pie chart represents new water that was not inside the domain, that is, water from water discharges or the open sea, either the Atlantic or Baltic. The white areas are land masses.

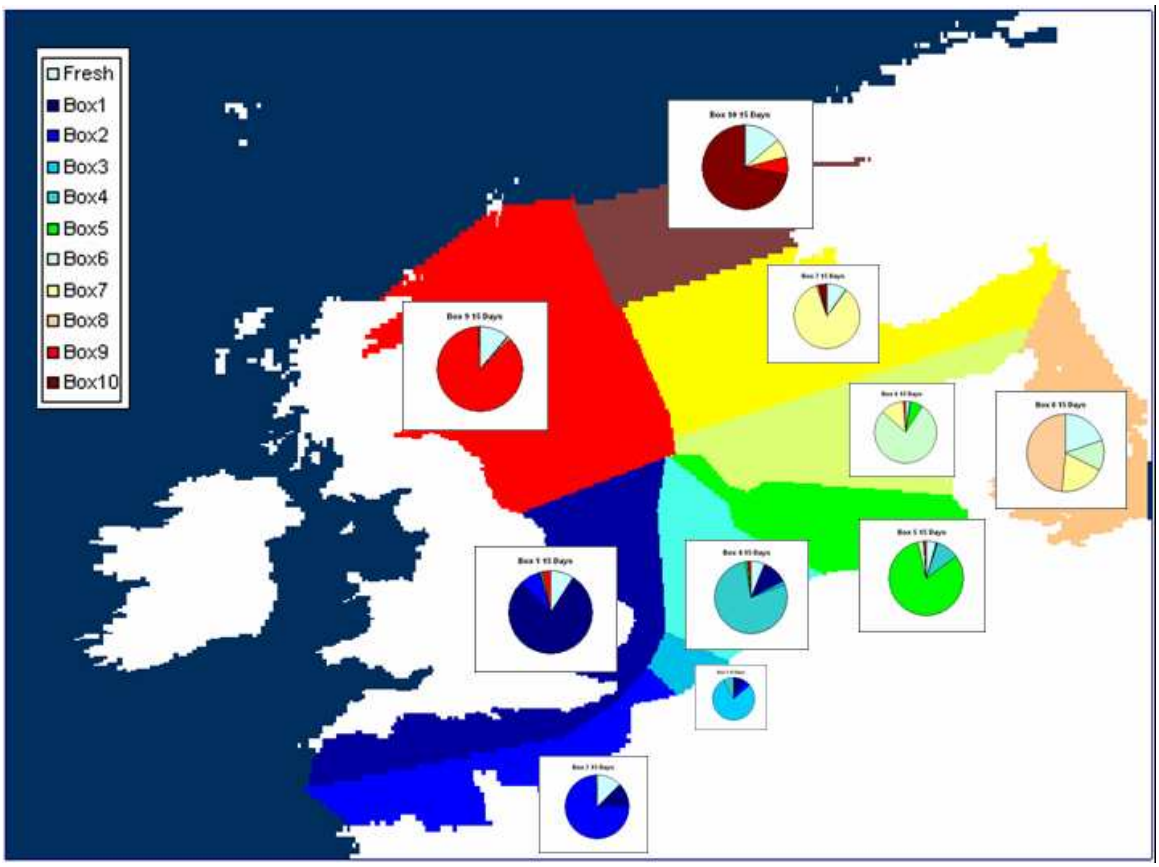

Figure 38: Water exchange among boxes (results integrated over 15 days).

Figure 38 enables one to extract some interesting conclusions from the circulation and residence time of water bodies in the North Sea. After 15 days, box 9, along the northern part of the UK does not have an influence on the southerly boxes; it only has an influence on box 10, along the Norwegian coast. In contrast, box 1, on the southern part of the UK has a major influence on the neighbouring boxes. This can be more evidently seen on Figure 39. Box 2 on the French coast has an influence on box 3(Belgium coast) but almost none beyond there (Netherlands and German boxes). Box 7(southern Norwegian box) has a strong influence on all boxes of the northeast corner of the domain, because of the currents flowing in the direction west-east along the Norwegian trench. After 150 days (Figure 39), box 9, on the northern part of the UK, has as influence on all the other boxes except for the English Channel boxes and the Baltic sea. This happens as the overall long-time circulation is counter clockwise on the North Sea (Figure 12), "delivering" the boxes' particles to the other boxes along this pattern of circulation. Even after 150 days (Figure 39) the French box almost does not contain particles from the neighbouring boxes, except for the no 1 box and fresh water. This shows that there is a small flux of water from the English Channel to the North Sea, but an opposite flow does not occur.

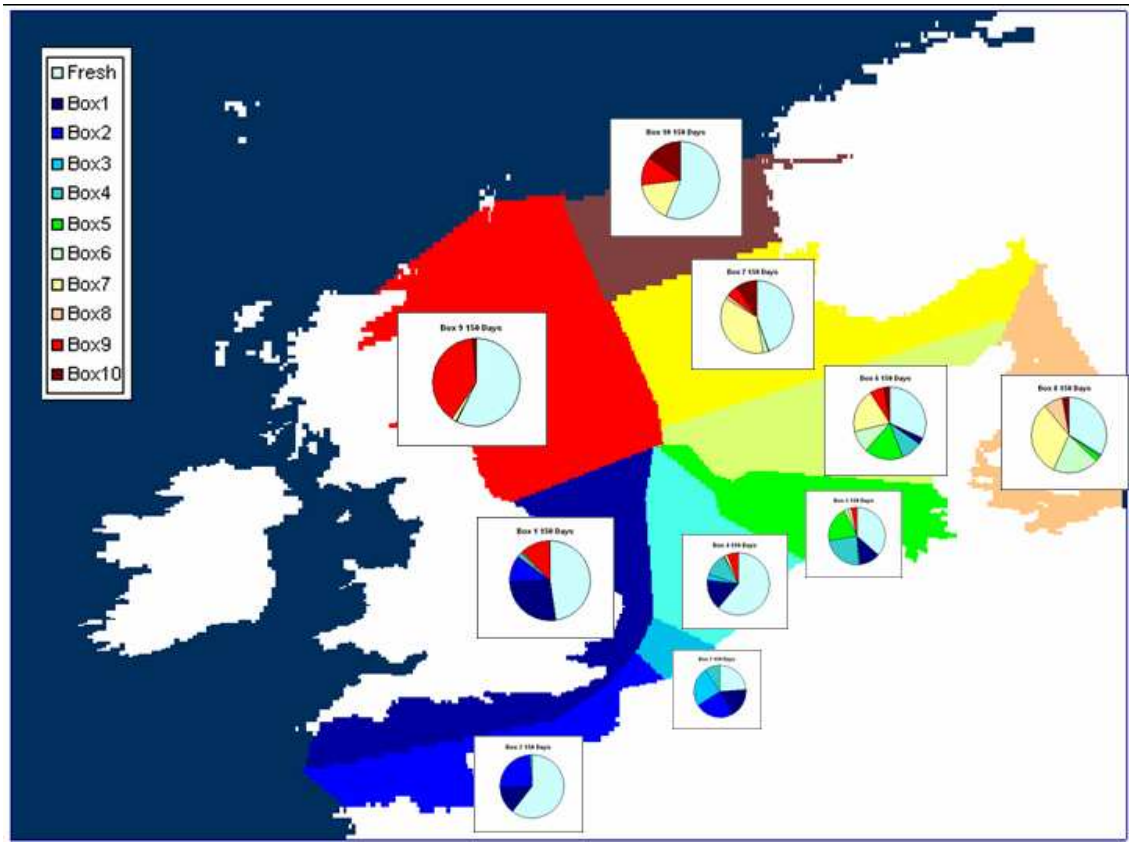

Figure 39: Water exchange among boxes (results integrated over 150 days).

From the Figure 38 and Figure 39 it is possible to conclude that the mixing of water bodies happens quite fast and the important water masses (the ones that feed more particles to the neighbouring boxes) are the UK boxes on the southern North Sea and the Norwegian boxes on the northern North Sea.

5. 3D Model

This chapter describes the ecological submodel, which is a 3D baroclinic submodel coupled to the 2D barotropic model (described previously).

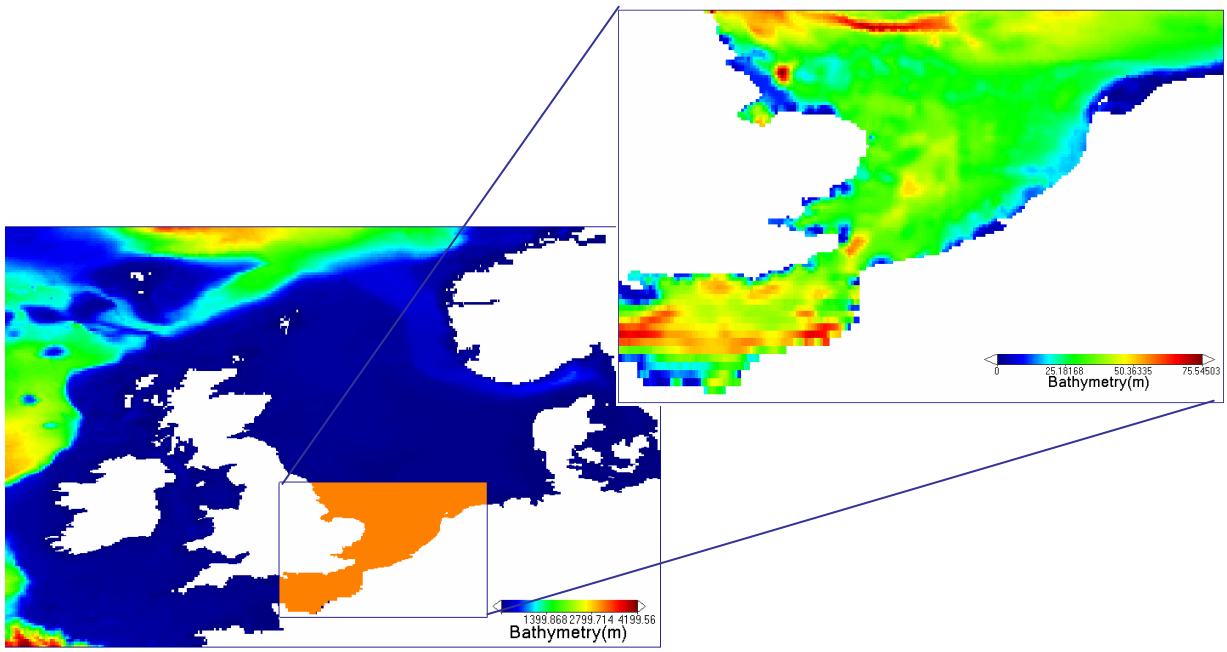

Figure 40: Coupling between the 2D hydrodynamical and 3D ecological model

In this submodel we use an ecological module that simulates the primary production in domain area. This domain spans from latitudes 49ºN to 54ºN and longitudes 1.5ºW to 6.5ºE.

5.1. Model Setup

5.1.1. Grid and Bathymetry

To study the primary production evolution on the domain, we use the same irregular grid as the father model (2D Model) with resolutions ranging from 0.1º at the southern boundary to 0.04º in the centre of the domain(roughly 4km). The domain was chosen to include some of the target areas for the OSPAR ICG-EMO Workshop (Mills *et al*, 2007), as shown in the next figure. The domain is a result from the 2D application.

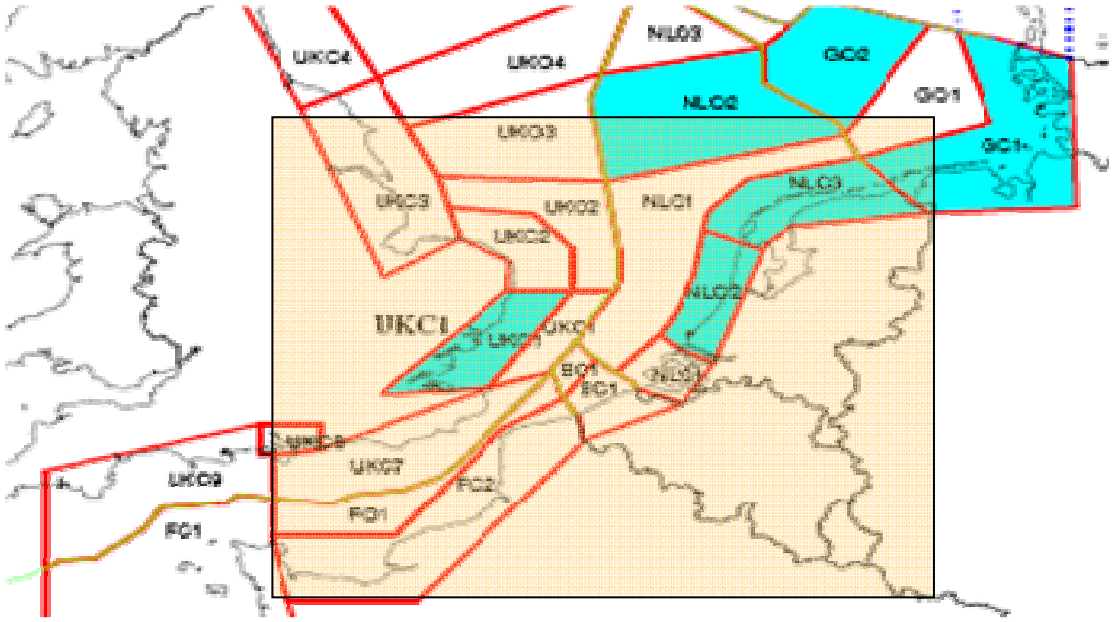

Figure 41: domain coverage (in orange) vs OSPAR target areas(in blue)

The bathymetry used in this model is exactly the same as the 2D model, but, as its domain is smaller it was cropped to the concerning region. Its depth varies from the shallow 5m in the Wadden Sea to about 75m in the northern part, south of the Dogger Bank. The following figures depict the bathymetry and the resulting grid which is 196x106 cells.

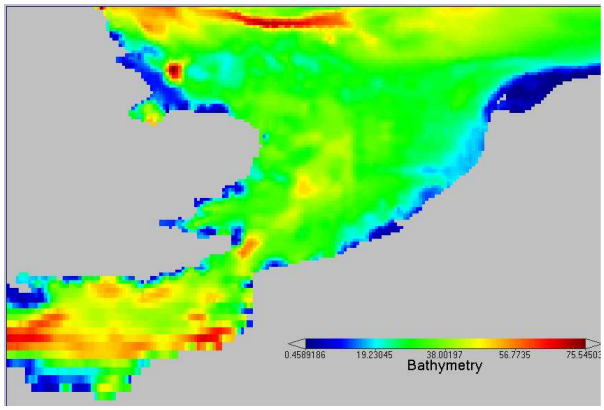

Figure 42: bathymetry of the 3D model

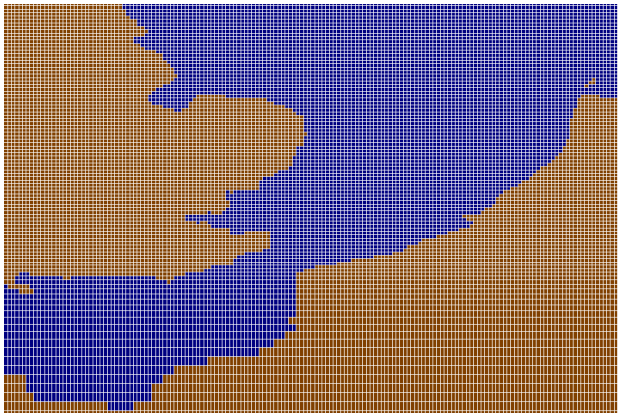

Figure 43: Irregular grid used in the 3D model

5.1.2. Vertical discretization

For the Z coordinate, there are 10 Cartesian layers (fixed along the bathymetry) with different thicknesses. The layer thickness and depth are represented on the following figure and table (Figure 42 and Table 2).

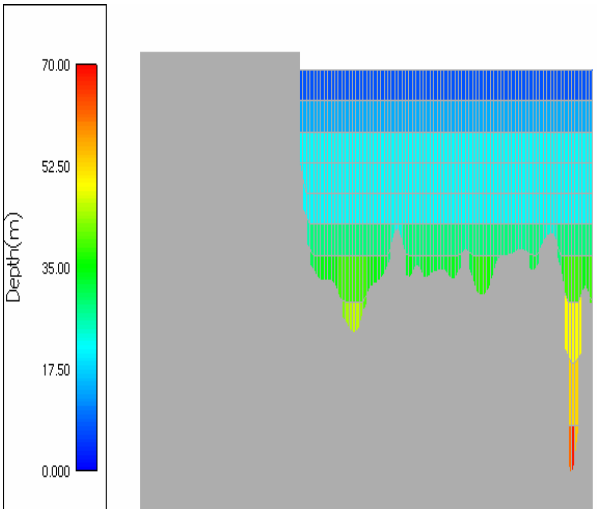

Figure 44: 3D layer representation

Layer Number	Depth(m)	Thickness(m)
10	0	5
9	5	5
8	10	5
7	15	5
6	20	5
5	25	5
4	32.5	7.5
3	42.5	10
2	52.5	10
1	82.5	30

Table 2 Vertical Coordinate cell definition

5.1.3. Time span and spin up run

The model's hydrodynamical properties have a spin up of 15 days. Before running the standard run (from 1 Jan 1998 to 31 Dec 1998), the model has been run for one year (1998 as well) in order to stabilize the ecological properties. 1998 was chosen because of the data availability at the time that it was setup (meteorology, satellite imagery and station data).

5.1.4. Model coupling

The 3D ecological model is coupled to the 2D hydrodynamical model in such a way that there is a flow of information (namely the hydrodynamical features: water level and velocities) to the sub model's boundary conditions. This was done to have realistic and feasible hydrodynamical boundary conditions for the submodel to run accurately.

5.1.5. Meteorology

The meteorology data for the model application was retrieved from the ECMWF ERA-40 reanalysis dataset with the time span of the model and a resolution of 2.5º global grid. It consists of four time daily surface data of the following datasets:

- 2m temperature
- Wind velocity X
- Wind velocity Y
- Cloud cover
- Relative humidity

The Solar Radiation data was retrieved from NCEP/NCAR 40-year reanalysis (Kalnay, 1996) because the ECMWF ERA40 dataset had some inconsistencies. If the

model used the ERA 40, it would have a lower than expected model temperature. This problem is discussed more ahead. All the datasets were interpolated to the model grid in order to be used by the model.

5.1.6. River Discharges

The river discharges data used is the same as the 2D model with the addition of riverine nutrient data. In this case, there are 29 river discharges with daily flow and nutrients from 1977 to 2006. The river discharge locations are in the Annex 1.6 and the data sources that originated them are specified in Annex 1.1. For the temperature, salinity, phytoplankton, zooplankton, dissolved oxygen and sediments a monthly reference was used, based on the Wissenkerke station (Oosterscheld, Netherlands) (Annex 1.3). Only 4 nutrients (nitrate and nitrite, ammonia, phosphate and silica) were available at some discharges, so, to construct the full set of nutrients and properties, a table of correspondence between the available nutrients and the full set of nutrients used by the model is used (Annex 1.2). The main river discharges are configured in such a way that it is discharged into a channel before entering the coastal area (Figure 45). This is done in order to accurately simulate the dilution process in an estuary before the discharge enters the sea. Each channel has a 1x20x2 cell dimension (roughly 4km by 60km by 10 m in depth).

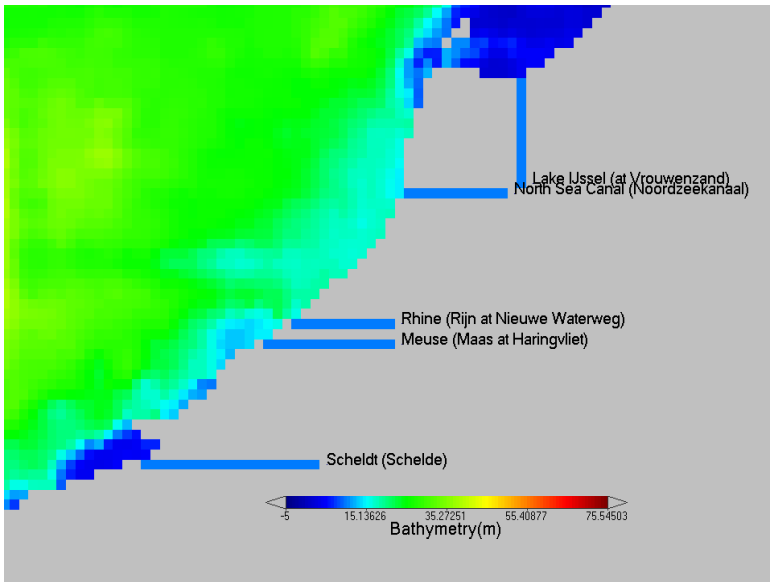

Figure 45: River discharge setup

To have an idea of which discharges are the most important the statistical means of the 29 rivers is represented in annex 1.4. The Rhine, Meuse, Seine, Lake Ijssel and Humber are the most important rivers by flow, these ranging from 1400m^3/s to 300m^3/s. Thames, Humber and Seine have the highest concentrations of Nitrate. Humber and Thames lead in Phosphate levels. Figure 46 represents the timeseries of flow (in m^3/s) of some of the main rivers discharging in the model's domain.

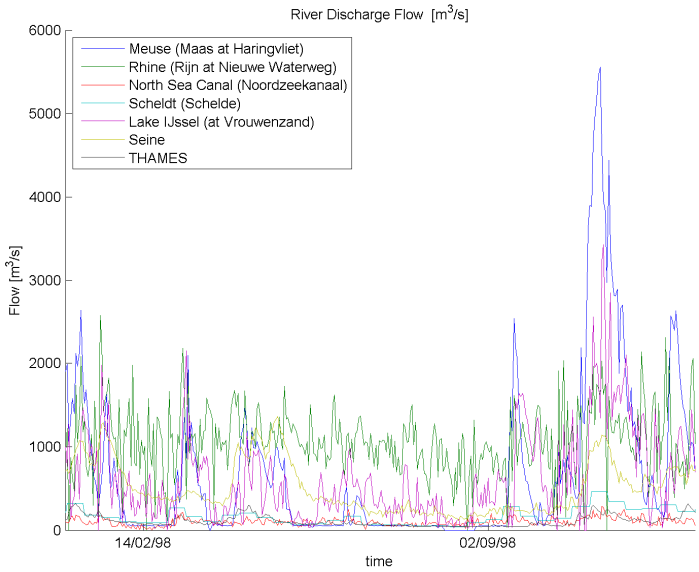

Figure 46: Main River flow, year evolution

5.1.7. Initial and boundary conditions

The initial condition is the property dataset field at the model start-up time. For phytoplankton, zooplankton and cohesive sediment, the initial and boundary conditions are constant along the domain, at respectively 0.01 mg C/l, 0.0025 mg C / l and 0.01 mg C/l. For the boundary conditions, the model performs a relaxation from each dataset/property field within 10 cells from the boundary into the domain, as described in the model description section. Figure 47 represents this phenomenon for the model domain:

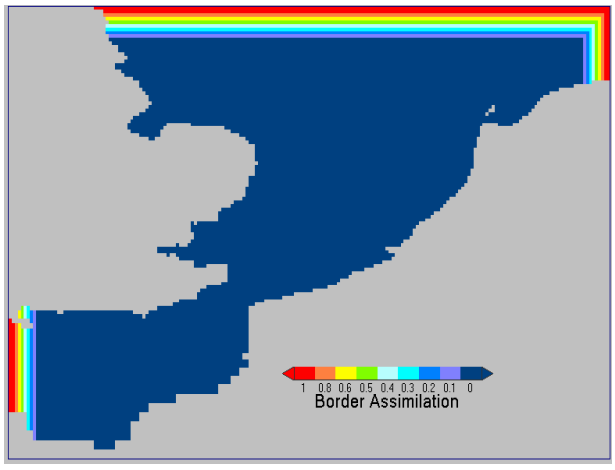

Figure 47: data assimilation zones

Temperature and Salinity

The temperature field was retrieved from the OISSTv2 (Reynolds *et al*, 2002) dataset which has 7 day mean sea surface temperature in a global 1 degree grid. For the salinity, the data was retrieved from the Levitus World Ocean Atlas 1994. It consists of long term monthly means, derived from data for years 1900 - 1992. Its data has a

resolution of 0.25 º latitude and longitude in a global grid and 33 standard depths (levels). Both datasets ware interpolated to match the model grid in latitude and longitude coordinates and also in depth.

Nutrients

For all nutrients, the model was spun up for 1 year. This was done in order to stabilize the model. The nutrient data input was retrieved from the World Ocean Atlas 2005. It consists of long term monthly means derived from data for years 1900 - 1992, retrieved from various sources, for Nitrate, Inorganic Phosphate, and Dissolved Oxygen. It has a global resolution of 1º and 14 standard depths for the Nutrients and 24 standard depths for the Oxygen. The nutrients that are not included in the World Ocean Atlas dataset and are used by the model were obtained by correspondence in respect to the Nutrient Equivalency table (Annex 1.2).

5.2. Model Results and Discussion

In order to assess the model's performance, some comparisons are made for several properties, between the model and field data:

- station data analysis(from RIKZ waterbase site), for several properties(phytoplankton, nutrients and temperature)
- satellite imagery spatial analysis(from SeaWIFS sensor): for chlorophyll/phytoplankton comparison.

Chlorophyll-carbon conversion

Because most field data is in ug chlorophyll/ L of chlorophyll and the model's results are in mg C/L, a conversion has to be made in order to present de data in the same units. This is made by multiplying the phytoplankton concentration (which is in mg Carbon/l) by a factor (ug carbon / in ug chlorophyll) that ranges from 20 to 50 in some references, but also 30 to 90. Figure 48 represents the enormous variability that this factor can have in presenting and interpreting the results.

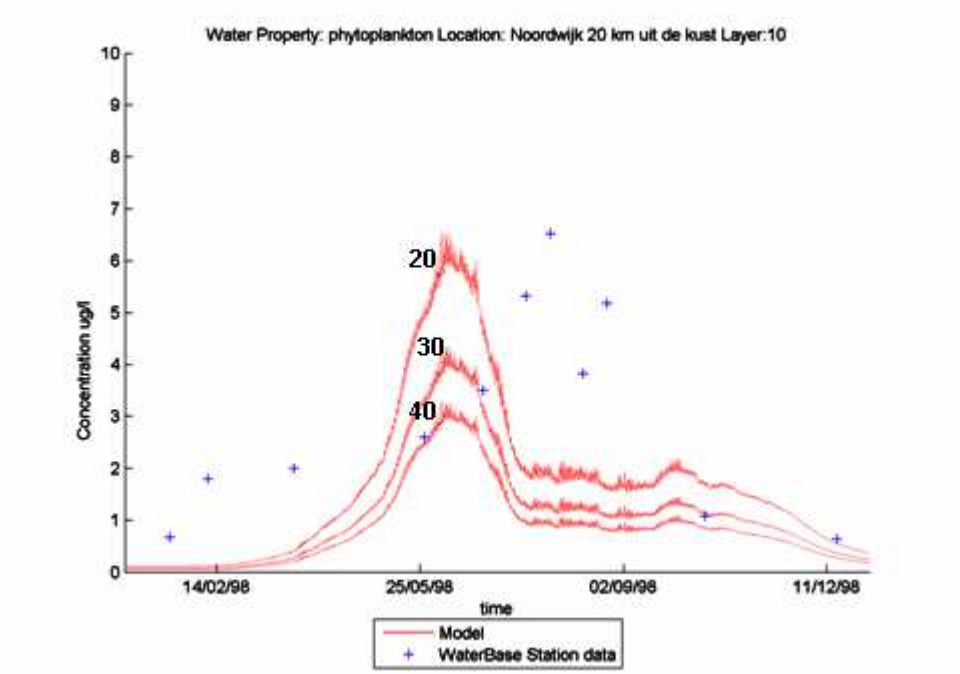

Figure 48: Different chlorophyll-carbon factor in a station at Noordwijk 20km

All the phytoplankton-related results are presented with a factor of **20** ug chlorophyll/mg carbon. The use of such a factor can have a significant effect on the interpretation of the results. The factor can vary in time, space and even for each species. For that reason, the assessment of chlorophyll results has to be cautious on the analysis of the magnitude, evaluating the pattern and variability throughout the year.

5.2.1. Spatial analysis

The following images depict a synoptic view over the domain area at surface depth (0-5 m). An instant in the winter (February 1st 1998) and the summer (July 1st 1998) was selected for this purpose.

Residual Circulation

As presented in the 2D Model chapter, the residual circulation is also presented here (velocity), to assess and support the box model fluxes conclusions to be carried out later.

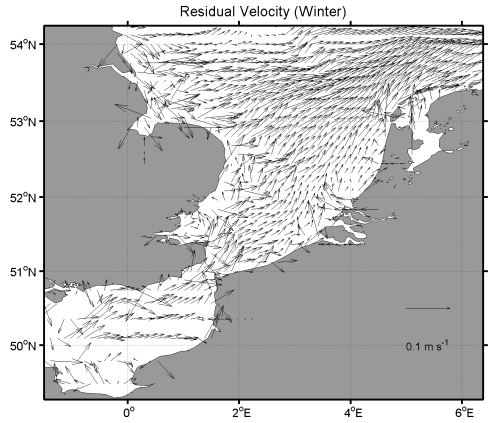

Figure 49: Residual Velocity in winter(Feb)

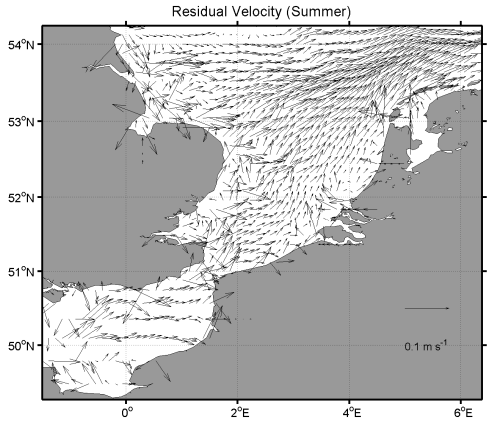

Figure 50: Residual Velocity in summer(Jun)

Temperature

The temperature evolution shows a normal yearly cycle. From the model's results a daily succession is visible in shallow water areas as for example the Wadden Sea, during spring/summer.

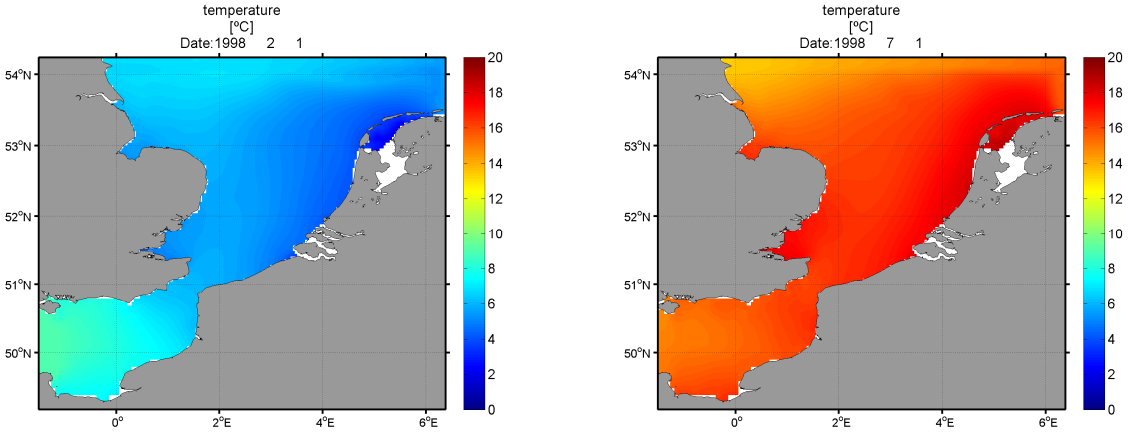

Figure 51: Temperature in Winter(1Feb) and Summer(1Jul)

When the model was first run, while evaluating the temperature results against station data and SST datasets, it seemed to have a discrepancy: it was about 2ºC lower than the reality. Figure 52 shows this situation.

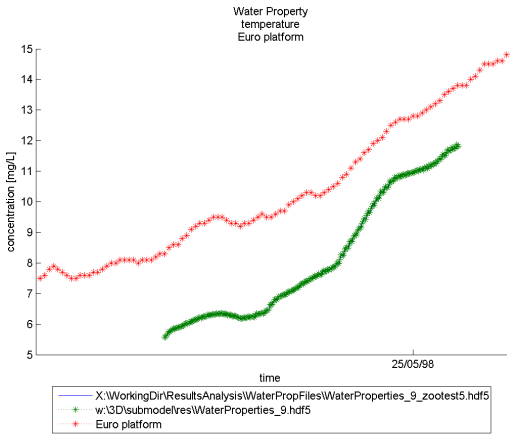

Figure 52: SST, red is station data, green is modelled

A series of tests were carried out which included, for e.g. changing the river setup, verifying the vertical turbulence scheme, etc. Finally, while carrying the last test specifically on the solar radiation, and testing a new dataset (NCEP/NCAR 40-year reanalysis, Surface, Downward solar radiation flux) instead of ECMWF ERA40 (Downward Surface Solar Radiation), the temperature timeseries were correct (as in Figure 72). The following figure (Figure 53) shows the difference between the two solar radiation datasets: about 100W/m^2.

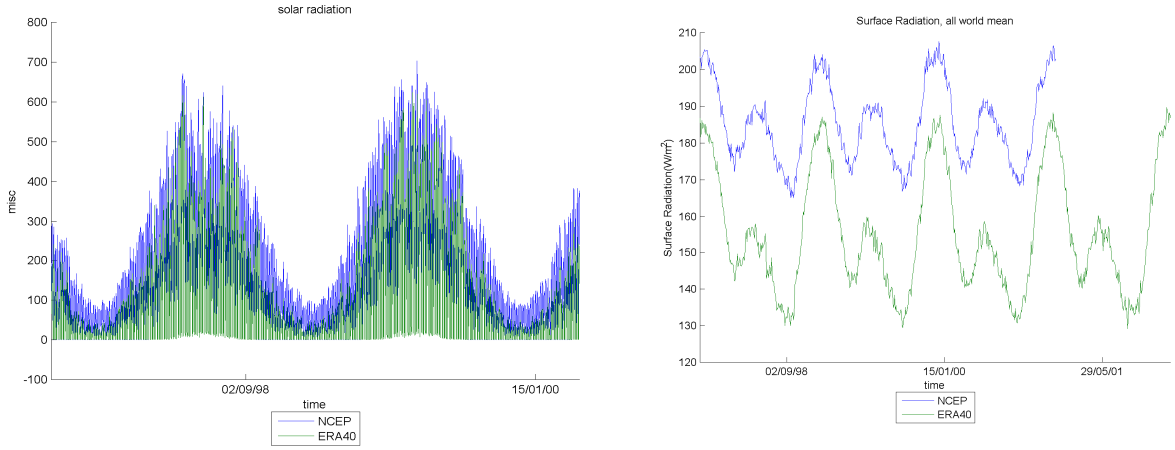

Figure 53: Solar radiation differences between NCEP40 and ERA40 (space averaged timeseries for the North Sea domain, and the whole world)

While carrying out the tests, several of these test's setups were implemented and many improvements were made. Moreover, the temperature boundary conditions and initial values were changed from the WOA05 climatology (which has 3D data) to OISSTv2 7 day means (which has only surface data). This was not relevant to the problem, as the temperature timeseries remained the same but this change probably deprecates the model from simulating thermal stratification, because the latter dataset has only surface data (as later explained).

To ensure that the temperature was correct, not only at the stations were data exists, the model's results were compared to the existing SST dataset (OISSTv2), which

is an interpolation of satellite data. If the results were different from the dataset which the model is forced from, it would indicate that the problem was intrinsic to the model, but, fortunately this was not the case. Figure 54 shows the SST differences between the model and OISSTv2: the red region is a shallow water area, which the field data (OISSTv2) cannot reveal because of its grid resolution (1º) and for it's a shallow water area, it is more sensible to meteorological variability (day/night cycles, air temperature and wind).

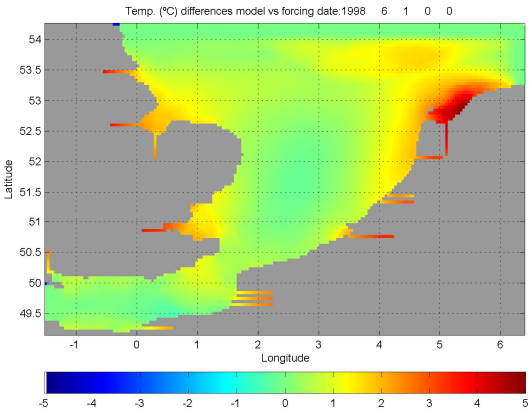

Figure 54: SST differences between model and OISSTv2

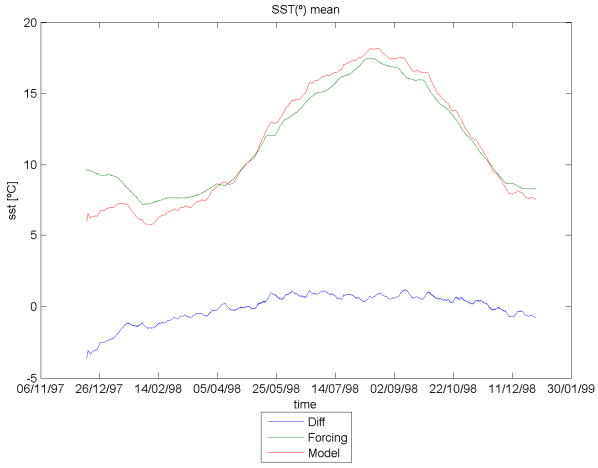

Figure 55: Space averaged time plot of the model(green), OISSTv2(red) and the differences between these two(blue)

Salinity

Figure 56 illustrates the regions of fresh water influence (ROFI), particularly the differences on the plumes from the Rhine and Scheldt rivers between winter and summer due to the riverine flows variability (shown in Figure 46).

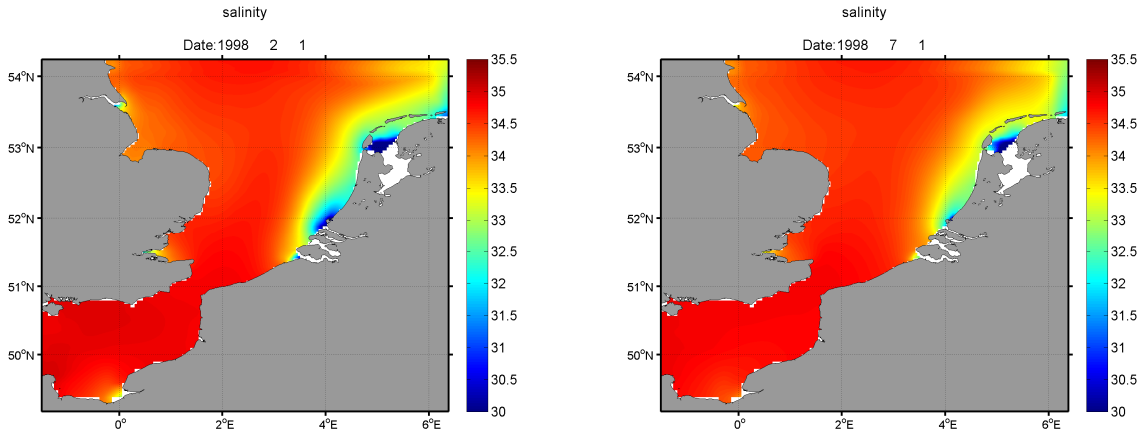

Figure 56: Salinity in Winter(1Feb) and Summer(1Jul)

Stratification

Since the model's sea temperature is forced using a dataset which has only sea surface data (resulting in a forcing with no vertical gradients), the model's capability to reproduce thermal stratification is severely reduced. But, as show by several authors (Pingree, 1978; Pohlmann, 1996; van Haren, 2004; Beusekom, 2007), the model's geography coverage usually has no thermal stratification: the tidal forces are sufficient to destroy the generation of stratification. This was one of the facts that lead us to choose the OISST temperature as an alternative for the World Ocean Atlas (WOA05) forcing (which has 3D temperature). Even so, to investigate if the model is ever stratified, the following figures depict a depth-time evolution at specific points were there are stations (merely for the location coordinates rather than its data). Analysing the difference between bottom and surface temperature (Figure 57), the conclusion is that the domain area is only thermal stratified during short periods of time in the summer, at the expected sites.

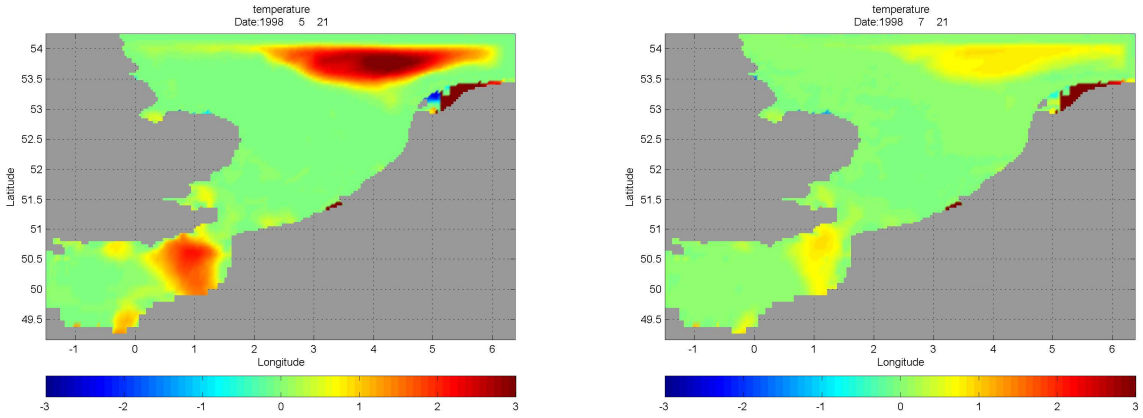

Figure 57: surface minus bottom temperature differences

The following images depict the depth-time profile of temperature, salinity and density at the Euro platform station. Blue parts at the bottom of the graph are the layers below the bottom. It does not appear to have any stratification all year round.

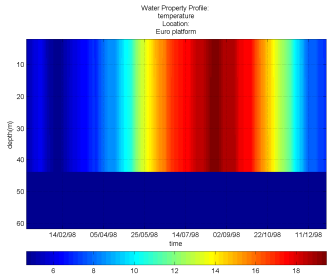

Figure 58: temperature profiles at Euro Platform

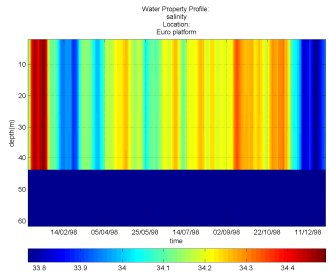

Figure 59: salinity profiles at Euro Platform

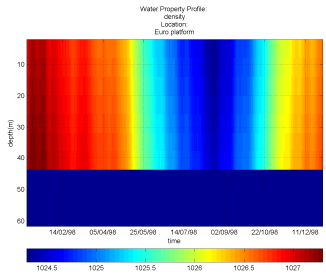

Figure 60: density profiles at Euro Platform

The same graphs are presented for the location that has stratification on the northern boundary, where stratification is present (Figure 57). Temperature and salinity produce a significant vertical gradient in the density in May.

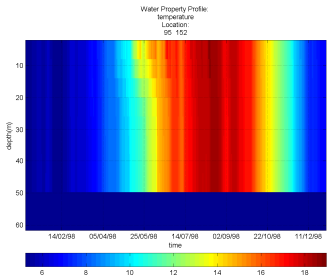

Figure 61: temperature profiles at cell 95,152

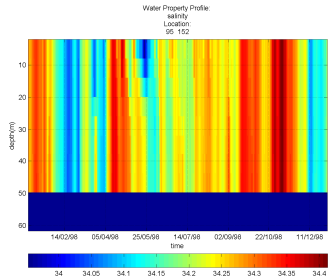

Figure 62: salinity profiles at cell 95,152

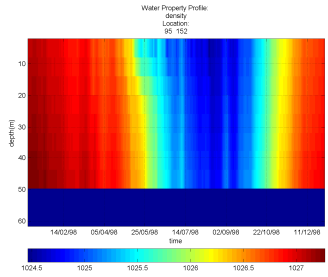

Figure 63: density profiles at cell 95,152

Cohesive Sediment

The cohesive sediment field (Figure 64) during the winter is quite high in ROFI areas. Clearly visible is the plume from the Rhine river.

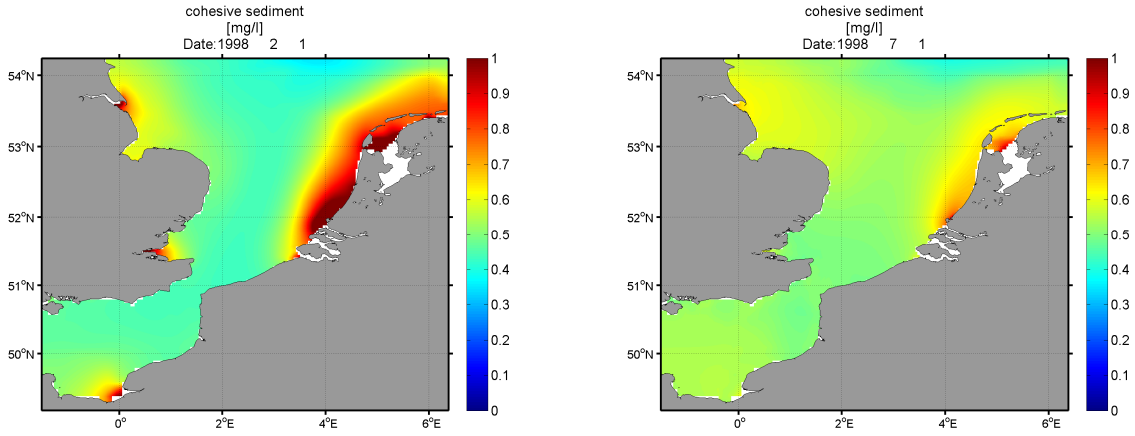

Figure 64: Cohesive Sediment in Winter(1Feb) and Summer(1Jul)

Ammonia

Ammonia levels northeast of the Wadden Sea (upper-right boundary) are relatively high during winter compared with the rest of the domain (Figure 65). It is probably due to the boundary conditions used from WOA 2005. The discharges have a particular impact on the concentration fields in coastal regions.

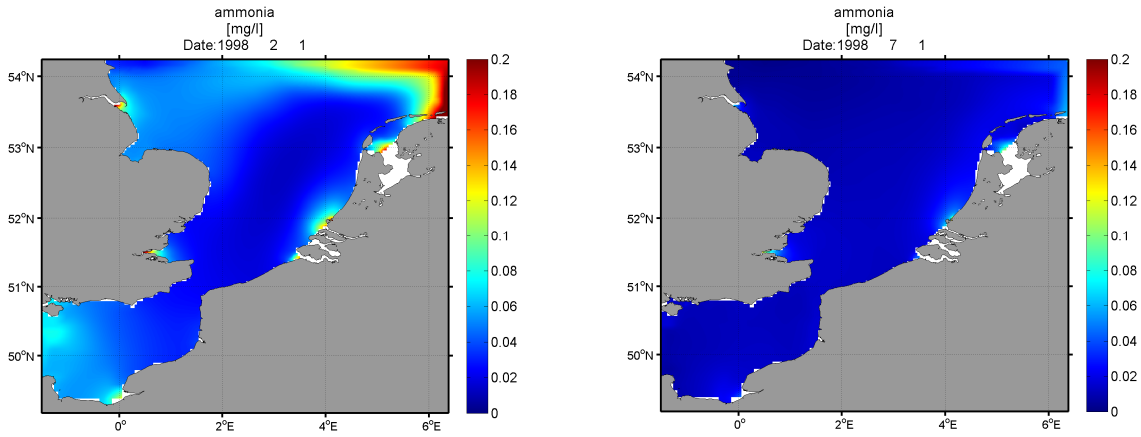

Figure 65: Ammonia in Winter(1Feb) and Summer(1Jul)

Nitrate

Nitrate reduction during summer is visible in the English Channel boundary (left) and English North Sea coast (upper-left) boundaries (Figure 66) due to the ocean influence (boundary conditions). A reduction probably due to primary production is also visible near the coastal areas.

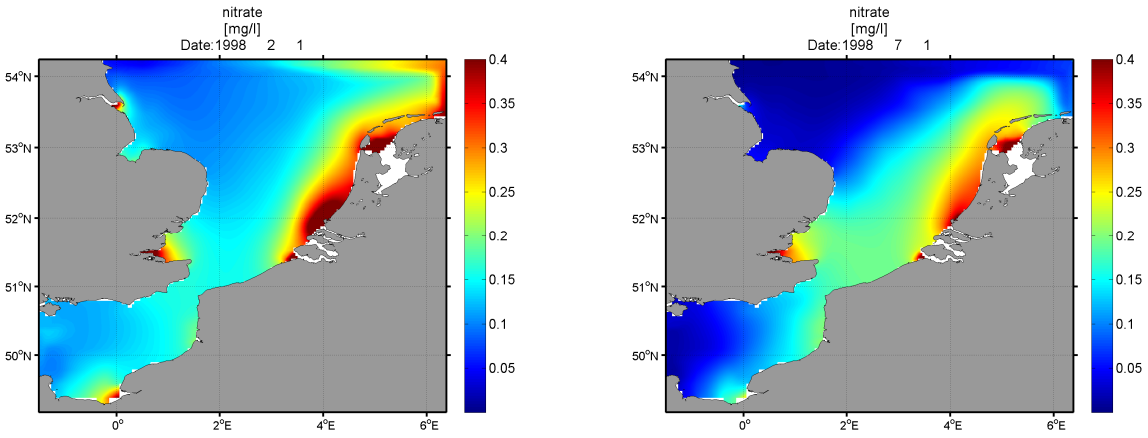

Figure 66: Nitrate in Winter(1Feb) and Summer(1Jul)

Inorganic Phosphorus

As it happens with nitrate, the ocean influence during summer is visible in the left and upper-left boundaries. The plume from the most relevant rivers is also visible (Humber, Thames, Rhine).

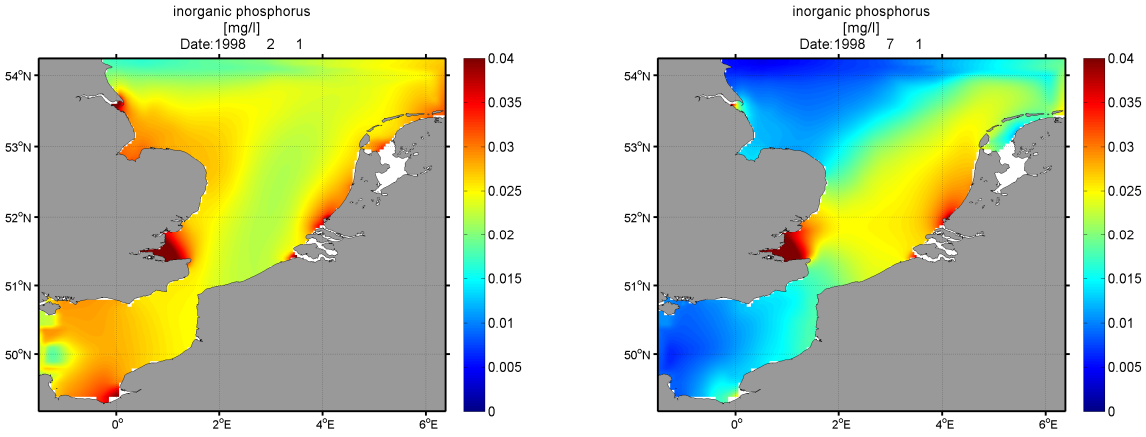

Figure 67: Inorganic phosphorus in Winter(1Feb) and Summer(1Jul)

Phytoplankton

For phytoplankton, the growing season (March – October, from Mills *et al* 2007), the levels reach almost 10 ug chla/l in the ROFI areas, near the Dutch coast, where the nutrient concentrations are higher because of river discharges.

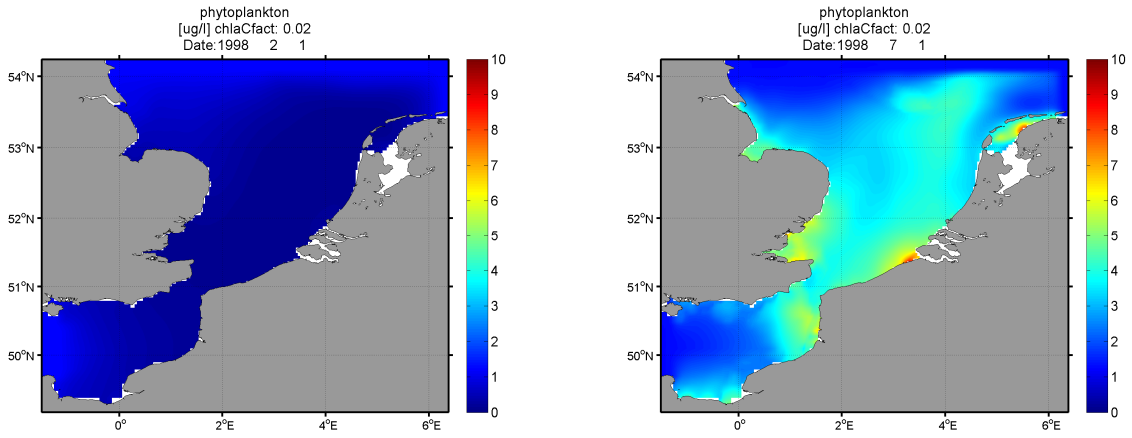

Figure 68: phytoplankton in Winter(1Feb) and Summer(1Jul)

Oxygen

Oxygen depletion is important in assessing eutrophication impacts. The summer oxygen field (Figure 69) demonstrates that in coastal areas the oxygen is reduced to about 7 mg/l, because of organic matter decomposition. The OSPAR threshold level for this region is 6mg/l (Mills *et al* 2007), so we can expect oxygen depletion status in the area.

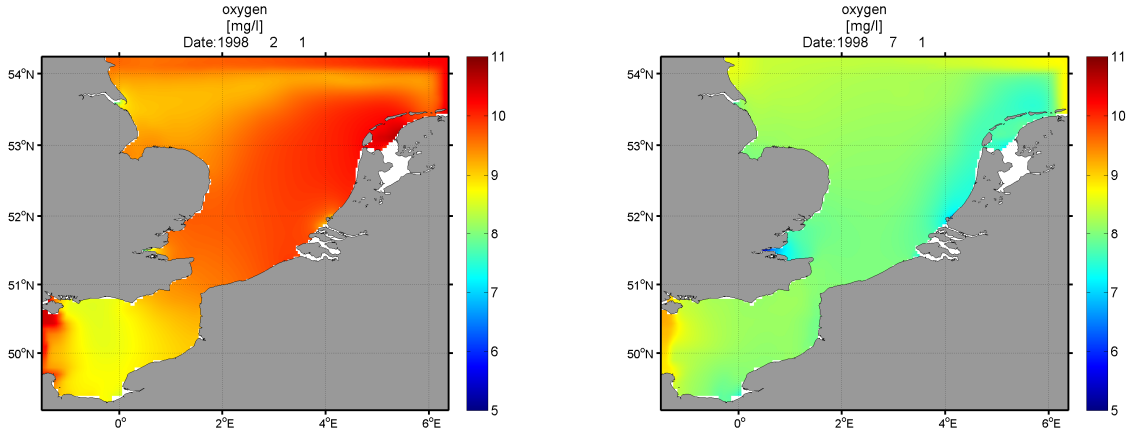

Figure 69: Oxygen in Winter(1Feb) and Summer(1Jul)

Zooplankton

Zooplankton growth is coincident with areas where phytoplankton blooms, but, it is clearly more intense in the Wadden Sea.

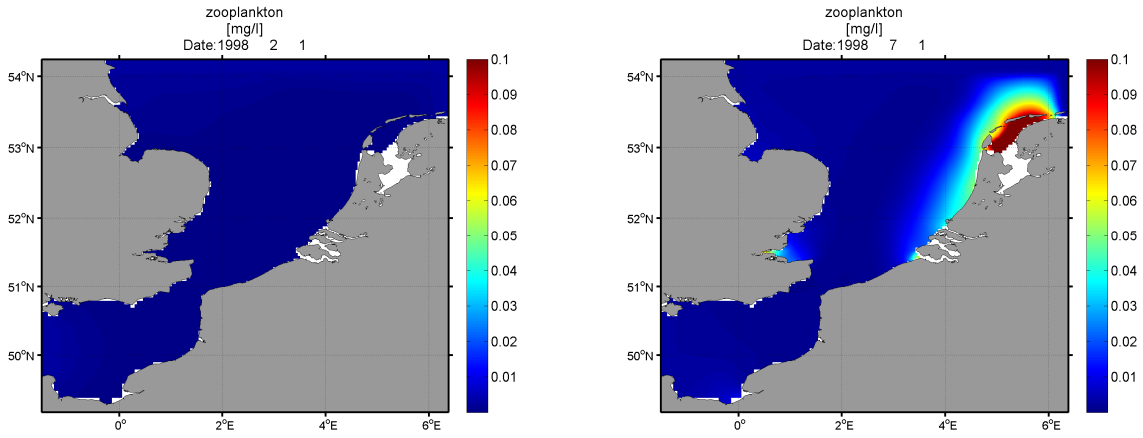

Figure 70: Zooplankton in Winter(1Feb) and Summer(1Jul)

5.2.2. Detailed analysis (Timeseries)

In order to evaluate if the model is correctly simulating the different variables, a comparison with field data has been made. The data was retrieved from the Dutch monitoring system in the North Sea (Rijkswaterstaat). All together, there are at least 20 different stations, monitoring several parameters. The set of parameters recorded by each station is different, so a comparison between two parameters in the same station is sometimes not possible. The location of the stations is represented in the following figure and its coordinates are in annex 1.6.

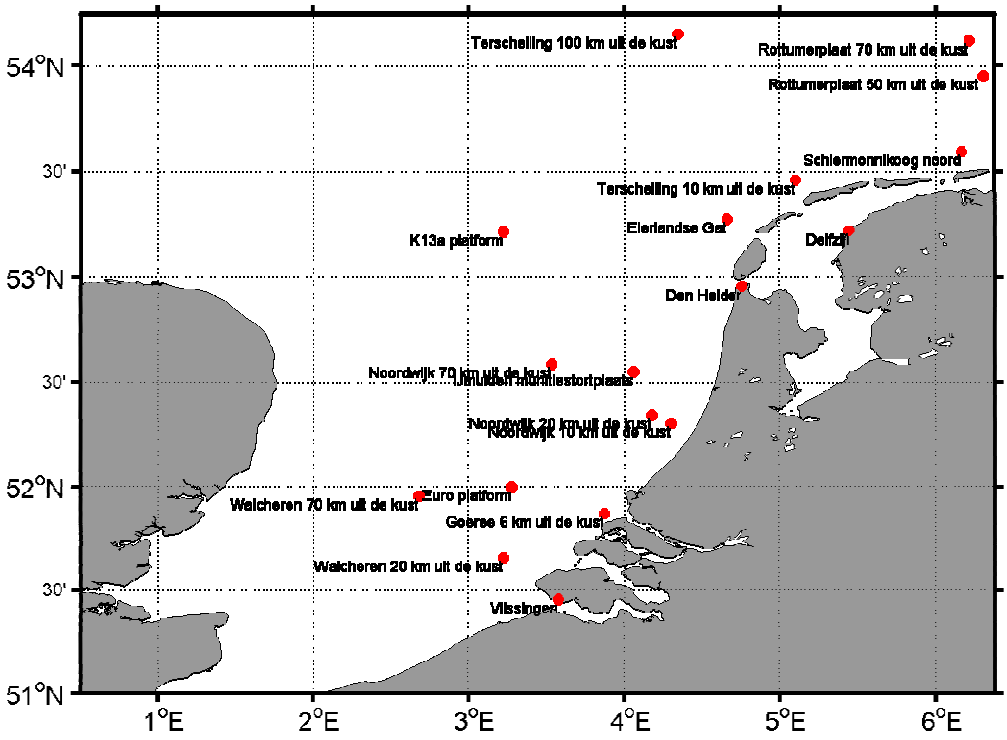

Figure 71: Station locations

Temperature

The model reproduces the temperature evolution correctly over the year. Since many important physical and biological processes are linked to the temperature, the model has to simulate it accurately.

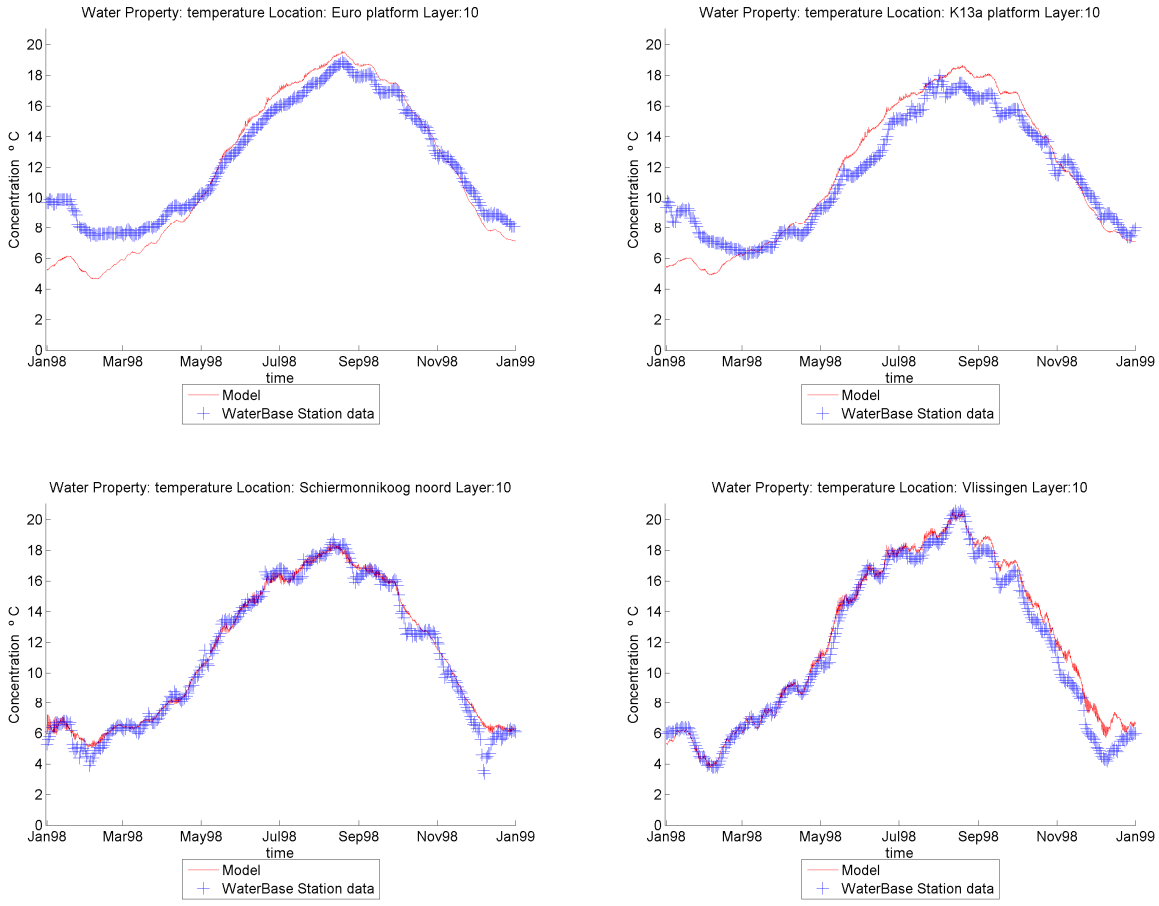

Figure 72: Temperature, model vs field data at stations Euro Platform, K13 Platform, Schiemon. N., and Vlissingen

Salinity

The salinity follows a pattern similar to the station's record. In March-April there is a lower salinity at station Noordwijk 20 which the model does not simulate. But, the model does simulate a lower salinity in November, although the data does not show it. At station Walcheren 20 the record shows a low which the model does not follow. If the results are compared with Figure 46, we can conclude that these fluctuations are probably caused by high riverine flow.

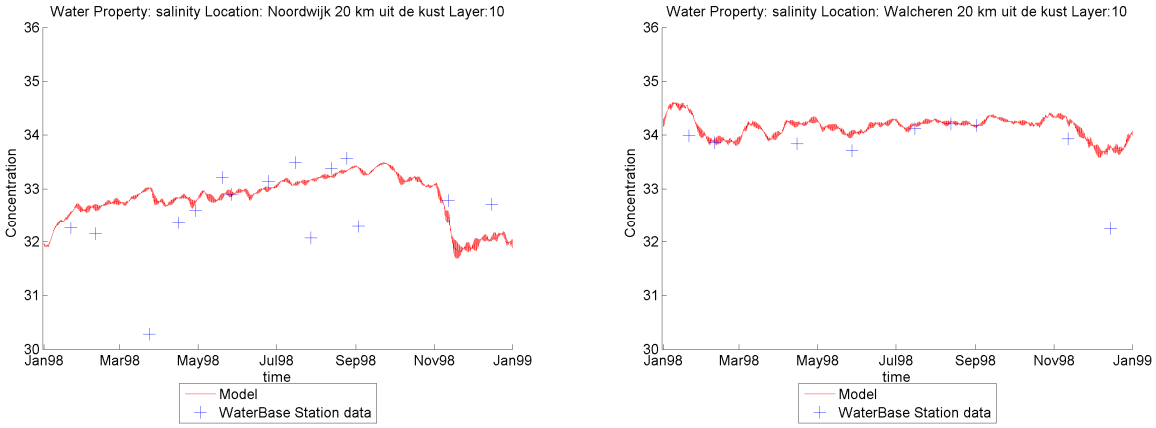

Figure 73: Salinity, model vs field data at stations Noordwijk 20 and Walcheren 20

Ammonia

Ammonia levels reasonably fit the model's curve in all the stations presented (Figure 74). Noordwijk 20 and Goeree 6 show ammonia levels higher than the station. In November, there is an increase in ammonia levels.

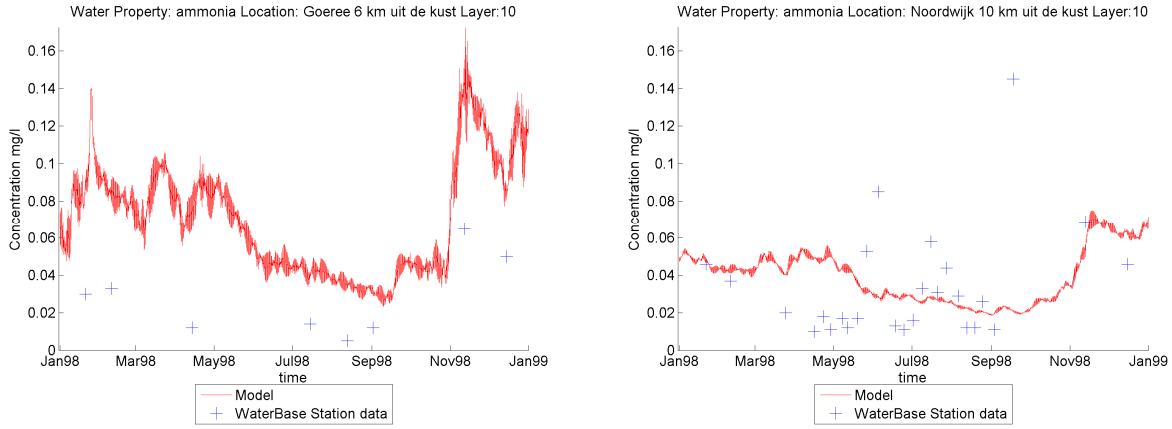

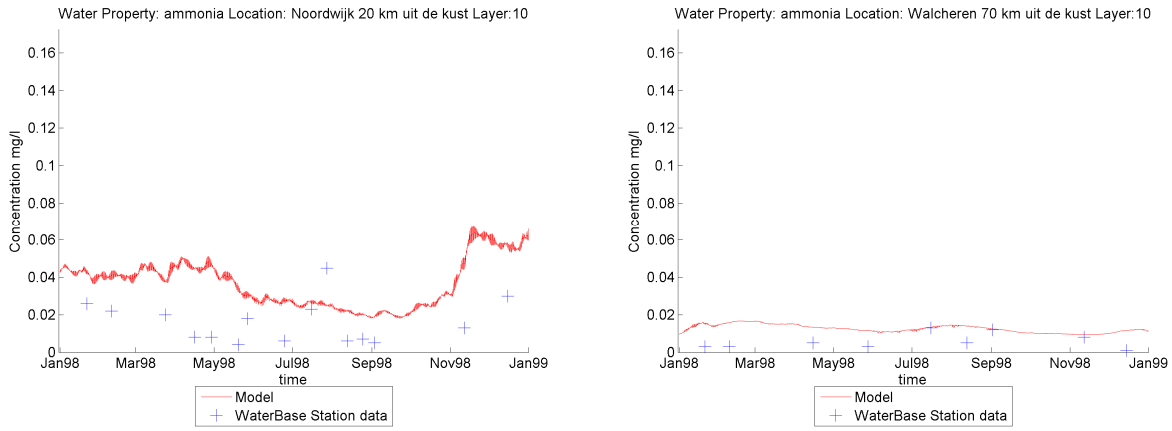

Figure 74: Ammonia, model vs field data at stations Goeree 6, Noordwijk 10, Noordwijk 20 and Walcheren 70

Nitrate

Model nitrate levels are systematically high throughout the year in the four stations represented above. As it happens with ammonia, at stations Noordwijk 20 and Walcheren 20, by November the model is able to reproduce the increase of nitrate in field data.

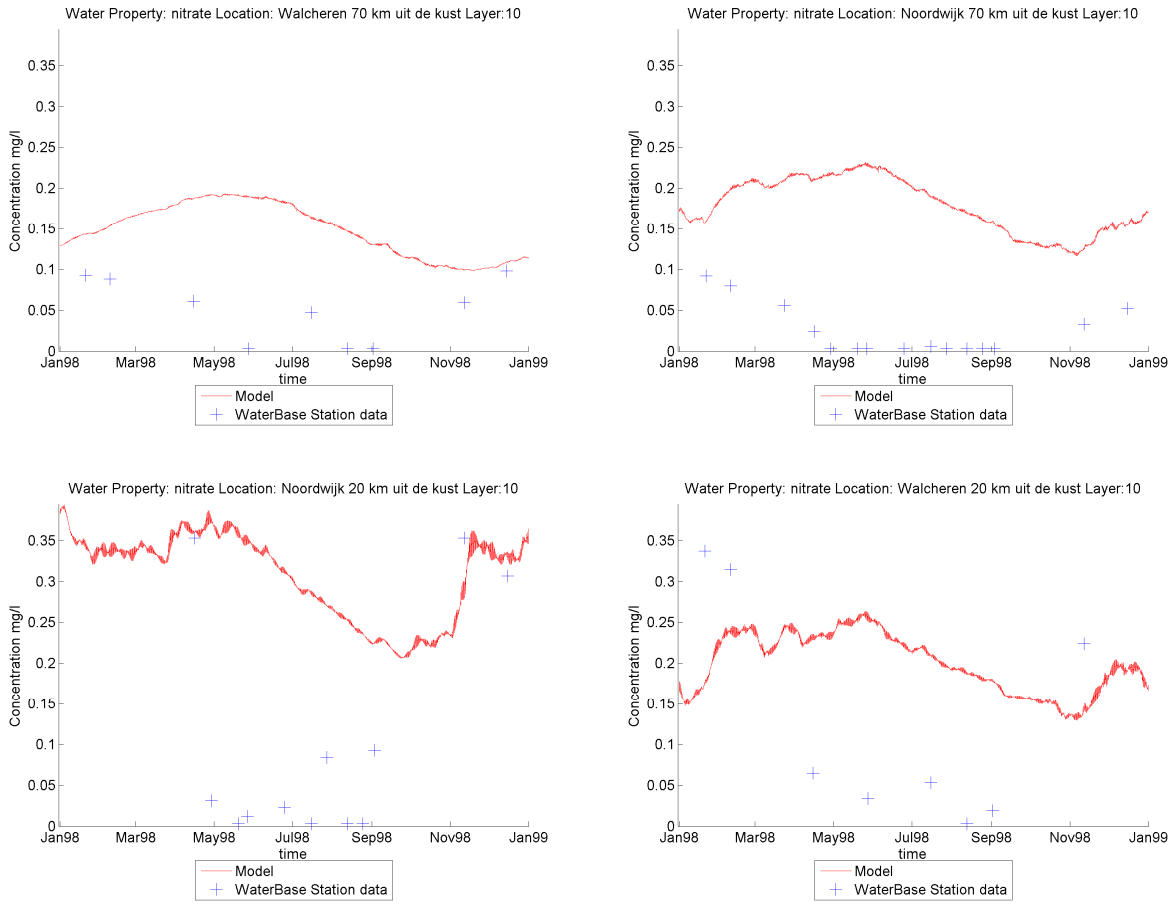

Figure 75: Nitrate, model vs field data at stations Walcheren 70, Noordwijk 70, Noordwijk 20 and Walcheren 20

Inorganic Phosphorus

The inorganic phosphorus timeseries shows high levels during summer growing season, but the model is able to reproduce the winter levels, although the number of record points is not sufficient to allow a solid conclusion.

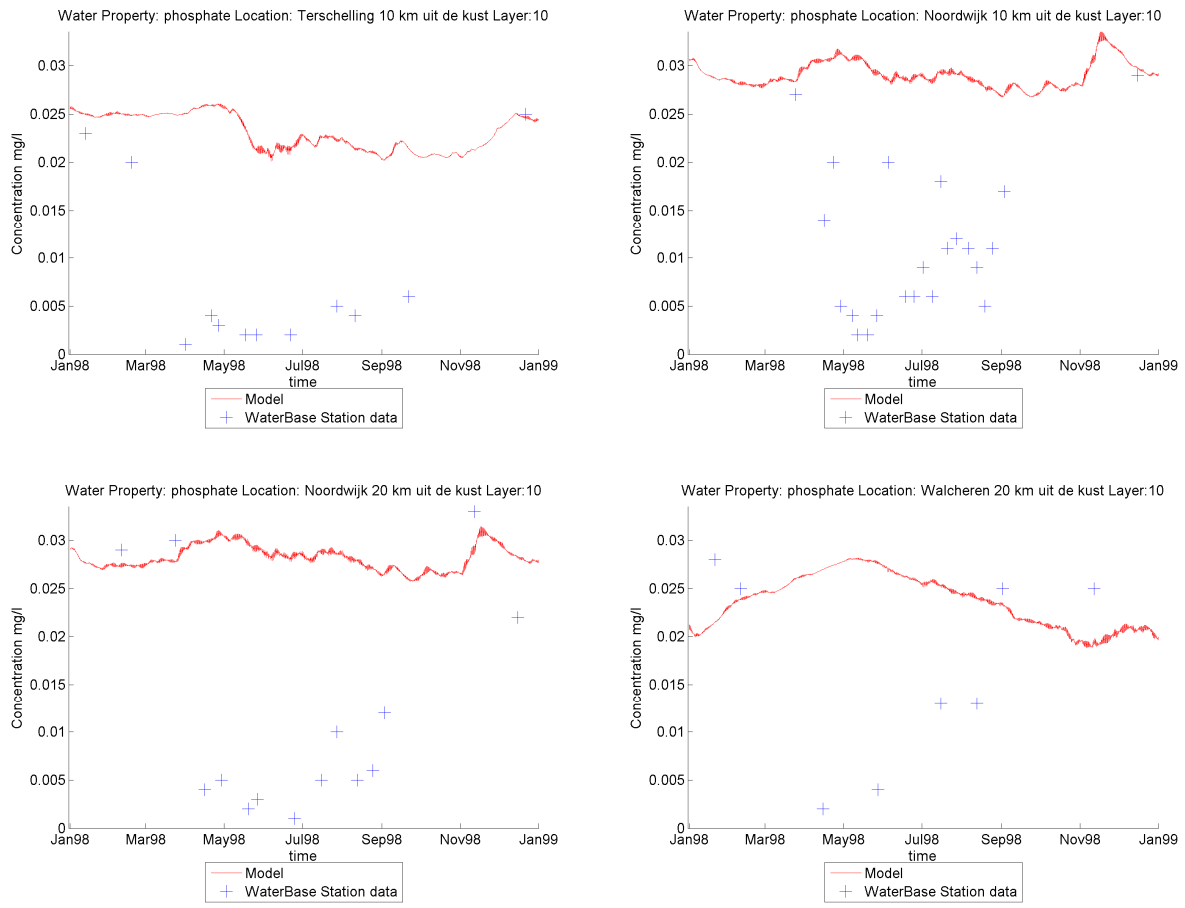

Figure 76: Inorganic phosphorus, model vs field data at stations Terschelling 10, Noordwijk 10, Noordwijk 20 and Walcheren 20

The model overestimates all nutrients. This can be explained by the high values found on the boundary conditions that propagate to the inner domain and due to an underestimation of primary production (presented below). Since the model's riverine nutrient inputs are assumed to be correct (apart from Lake Ijssel), the WOA05 dataset used to ensure nutrient boundary conditions has higher values. These boundary condition imposed had to be interpolated to the model grid. Given that the dataset's grid has a resolution of 1º, it averages the coastal levels (that are typically higher due to discharges) with the offshore levels (lower), giving higher values. The peak in November for all nutrients is probably due to a high riverine discharge (Figure 46), and confirmed also by the salinity evolution analysis (Figure 73).

Phytoplankton

The following figures also include the Satellite imagery value for that specific grid cell at the possible instants (i.e. when there is no clouds/errors), denominated "chla" and pink on the figures. More details on the satellite imagery processing are presented ahead.

As we can see, the model can moderately represent the seasonal pattern of phytoplankton, including the spring bloom, but not the magnitude of the bloom. The model's bloom occurs around June, although the stations data seem to point it around May. Station Noordwijk 20, which has many records in the summer period, shows that the model underestimates the chlorophyll, however, for the satellite does not agree with this data. Satellite data shows that there is always some residual chlorophyll outside of the growing season (March-October).

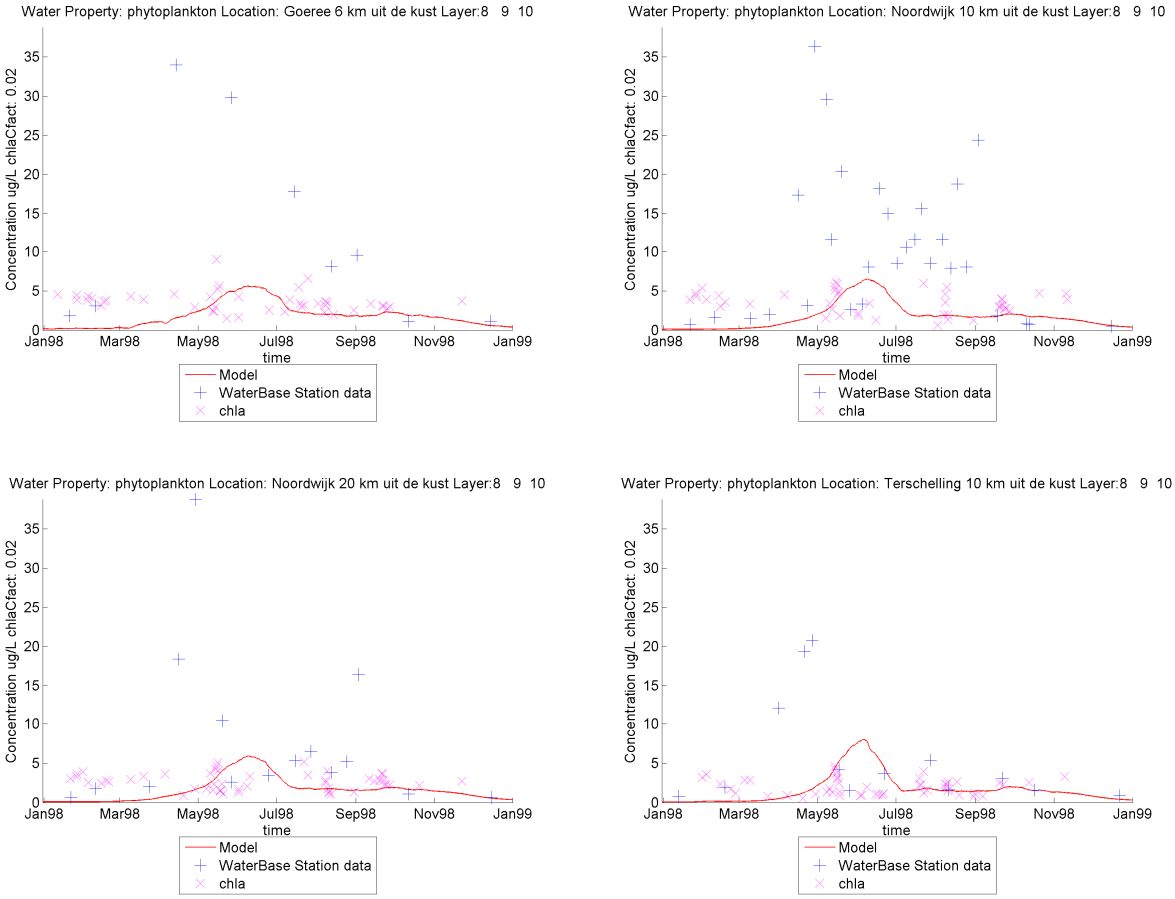

Figure 77: phytoplankton, model vs field data at stations Goeree 6, Noordwijk 10, Noordwijk 20 and Terschelling 10 (red is model, blue is station, purple is satellite)

Chlorophyll comparison with satellite imagery

Phytoplankton comparison with remote sensing data was made using level 1a MLAC chlorophyll data from the SeaWiFS sensor. The images were processed using the MUMM atmospheric correction (Ruddick *et al*, 2000) for the aerosol and water-leaving reflectance due to the turbidity. The following figure (Figure 78) shows the differences between the model and satellite chlorophyll concentration. White areas are areas where there is no satellite data because of cloud cover.

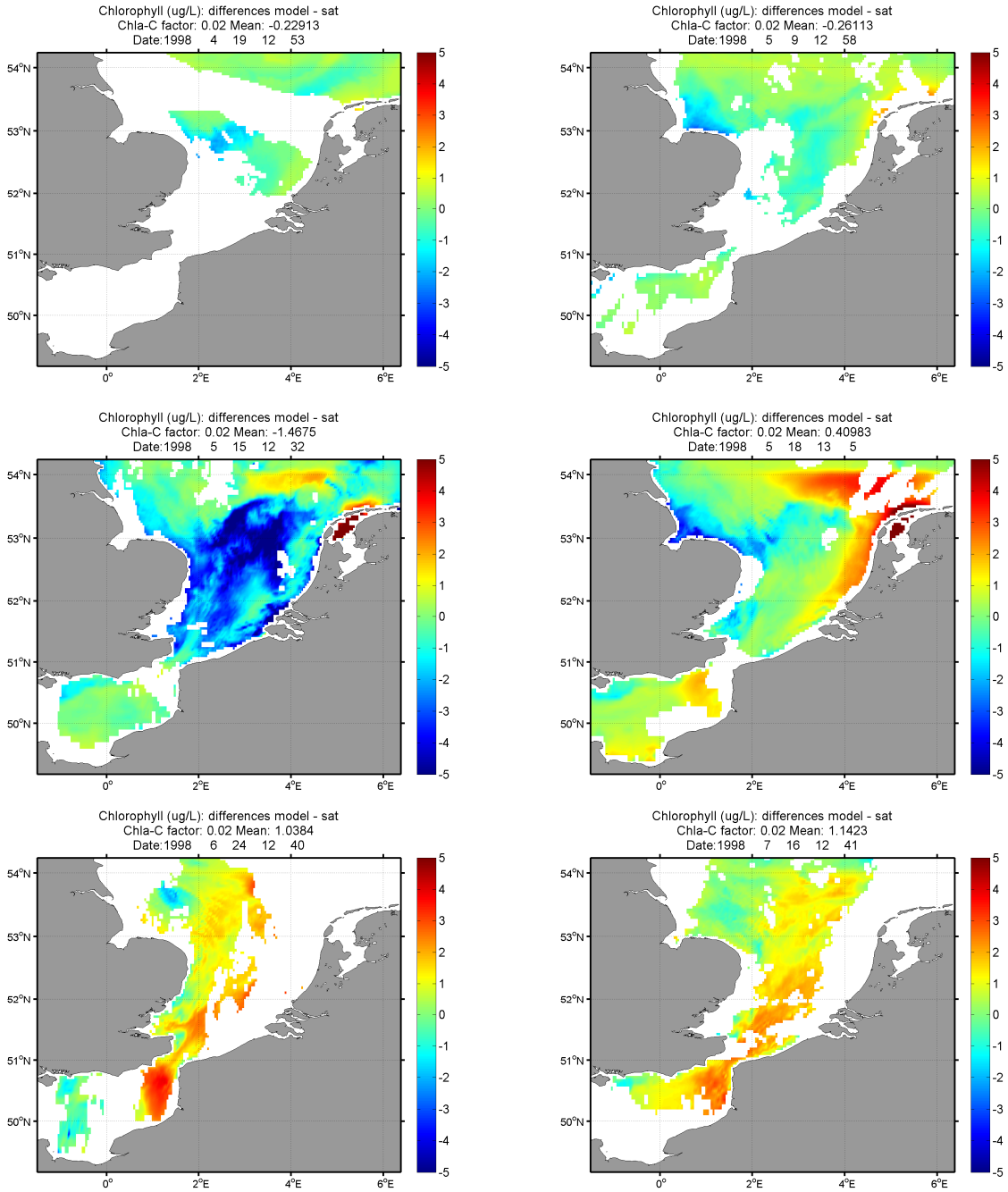

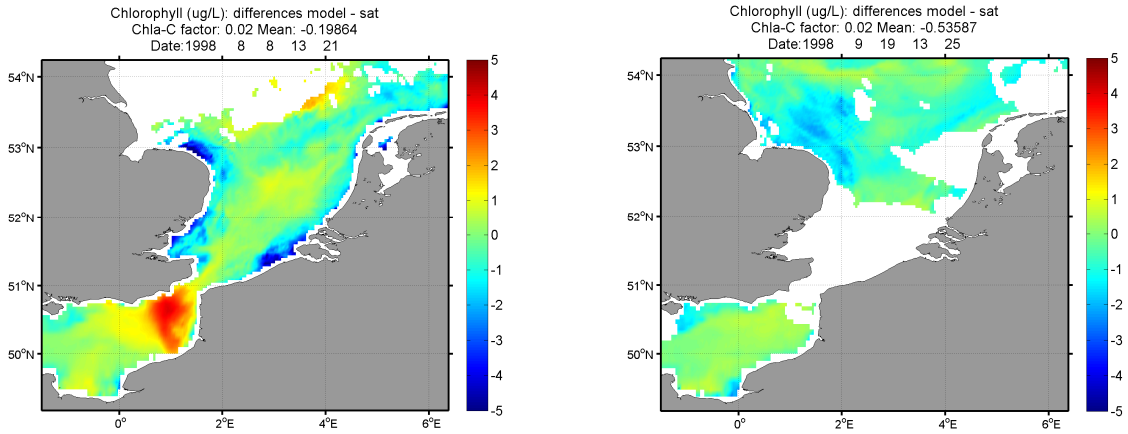

Figure 78: phytoplankton differences(model – satellite) in ug/l, From left to right: a) day 107 – 19 April 1998, b) day 128 – 9 May 1998, c) day 134 – 15 May 1998, d) day 138 – 18 May 1998, e) day 175 – 24 June 1998, f) day 197 – 16 July 1998, g) day 220 – 8 August 1998, h) day 262– 19 September 1998

The preceding figures can only be quality-assessed, since the choice of a chlorophyll-carbon factor is a very influential in these results: they can have 100% variability. Furthermore, the data availability is not good all year round: there are clouds or data errors in almost all images, appearing as white patches.

Analysing the satellite images set (not shown), a big bloom in the centre of the domain can be seen around 15th May that quickly faded away by 18th May. From the preceding images (model-satellite differences), we can asses that the model could not reproduce this bloom at the centre of the domain, but it produces a coastal bloom days after. A time-averaged result could have been made, for example, a 3 day average, but if phytoplankton blooms last for 3 days, this method flattens out the spatial variability and its peaks, so we opted not to do this.

The model generates an immense bloom at the Wadden Sea. This is due to the bad definition of the discharge: the model's Lake Ijssel discharge (Figure 45 and Annex 1.5) should have been defined at two different locations at the Afsluitdijk. By checking the original satellite data, we can conclude that the blooms settle in very quickly and rapidly fade away.

Oxygen

The oxygen levels are important because it is considered an effect of eutrophication. The model's result in this matter is satisfactory: station Noordwijk 70 shows a very good similarity with field data.

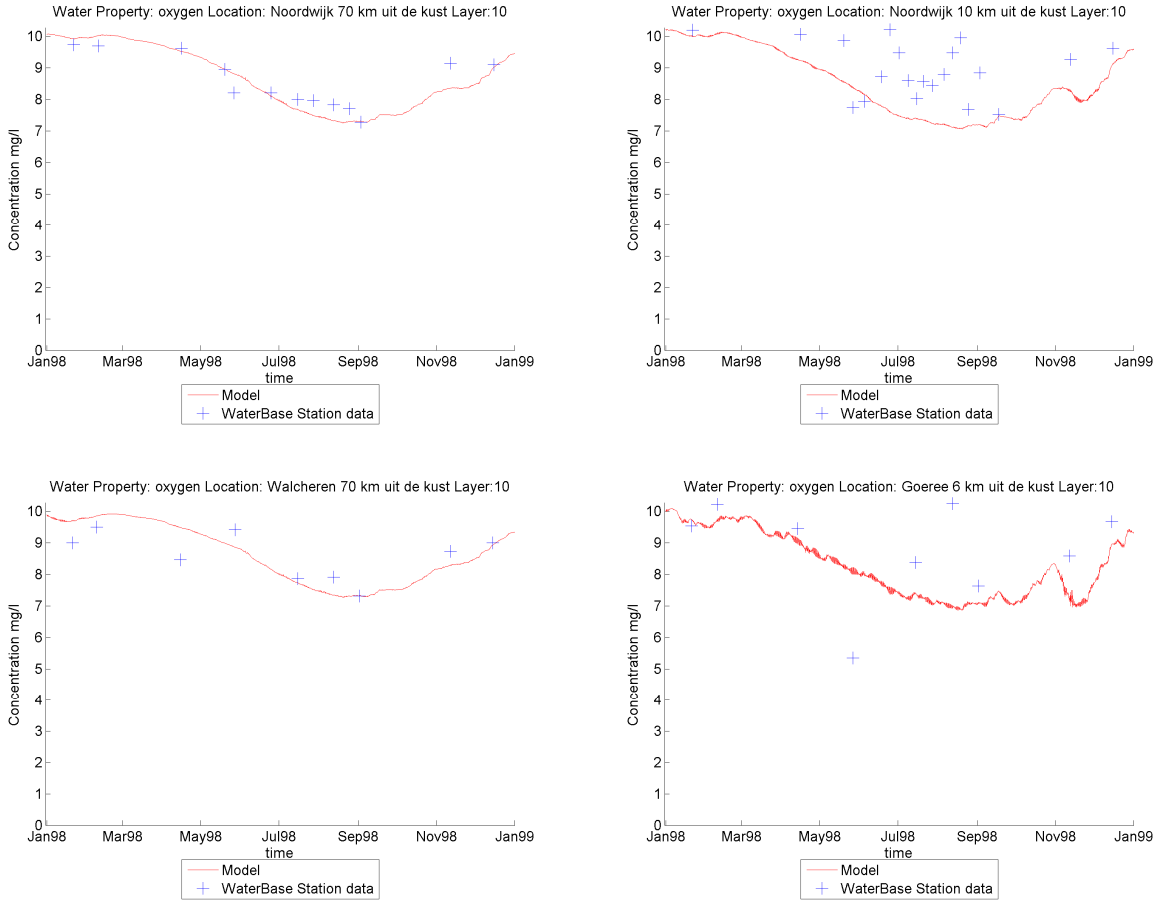

Figure 79: Oxygen, model vs field data at stations Noordwijk 70, Noordwijk 10, Walcheren 70 and Goeree 6

Zooplankton

The zooplankton growing profile is as expected for a grazer: it grows after the phytoplankton bloom and steadily reduces its biomass with time.

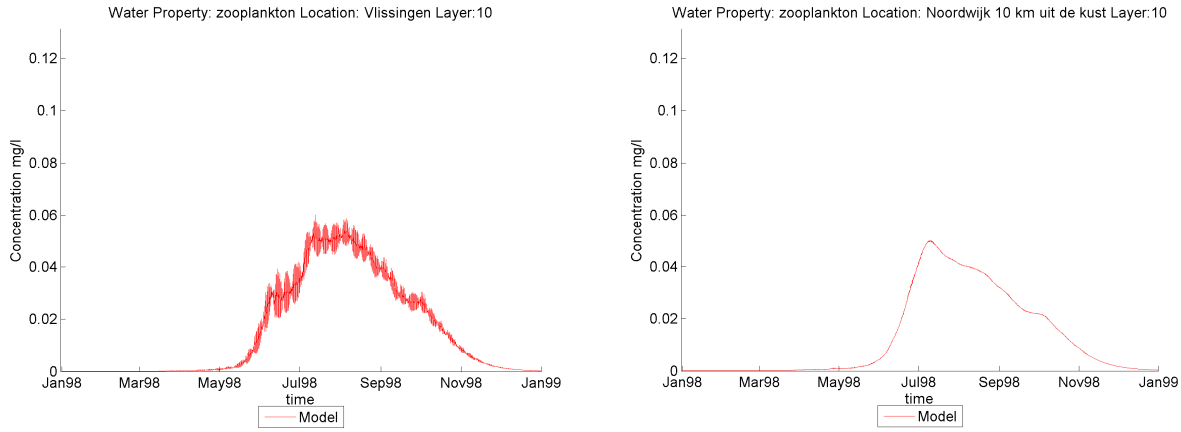

Figure 80: Zooplankton, model vs field data at stations Vlissingen and Noordwijk 10

5.2.3. Integration boxes

To monitor the evolution of each property within the domain, several boxes were defined where the model integrates the cells within each box and outputs the resulting property concentration and fluxes at specific times. The box layout is similar to the countries water boundaries. Box nr 0(zero) represents the boundaries of the domain.

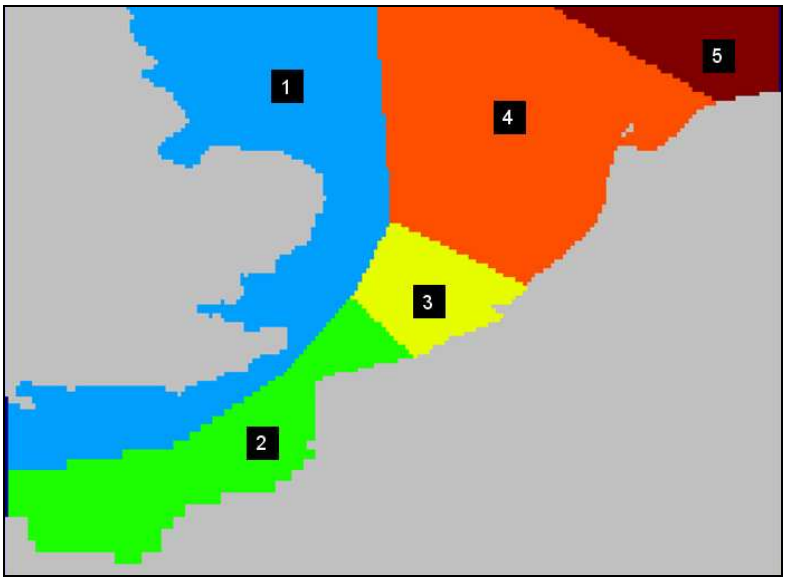

Figure 81: Box model setup showing the 5 boxes.

Timeseries: the box model's view

The following images are plots of a property in all five boxes.

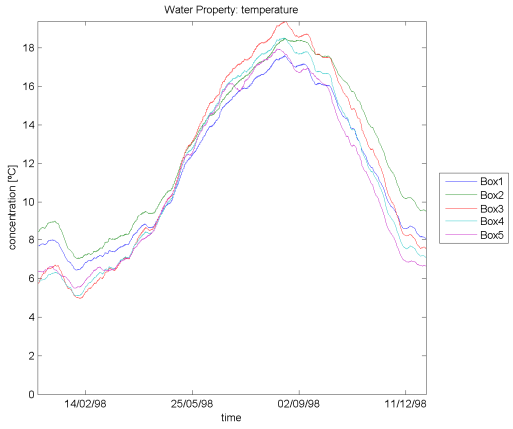

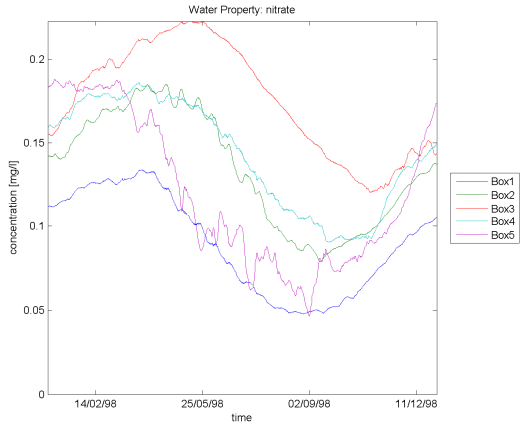

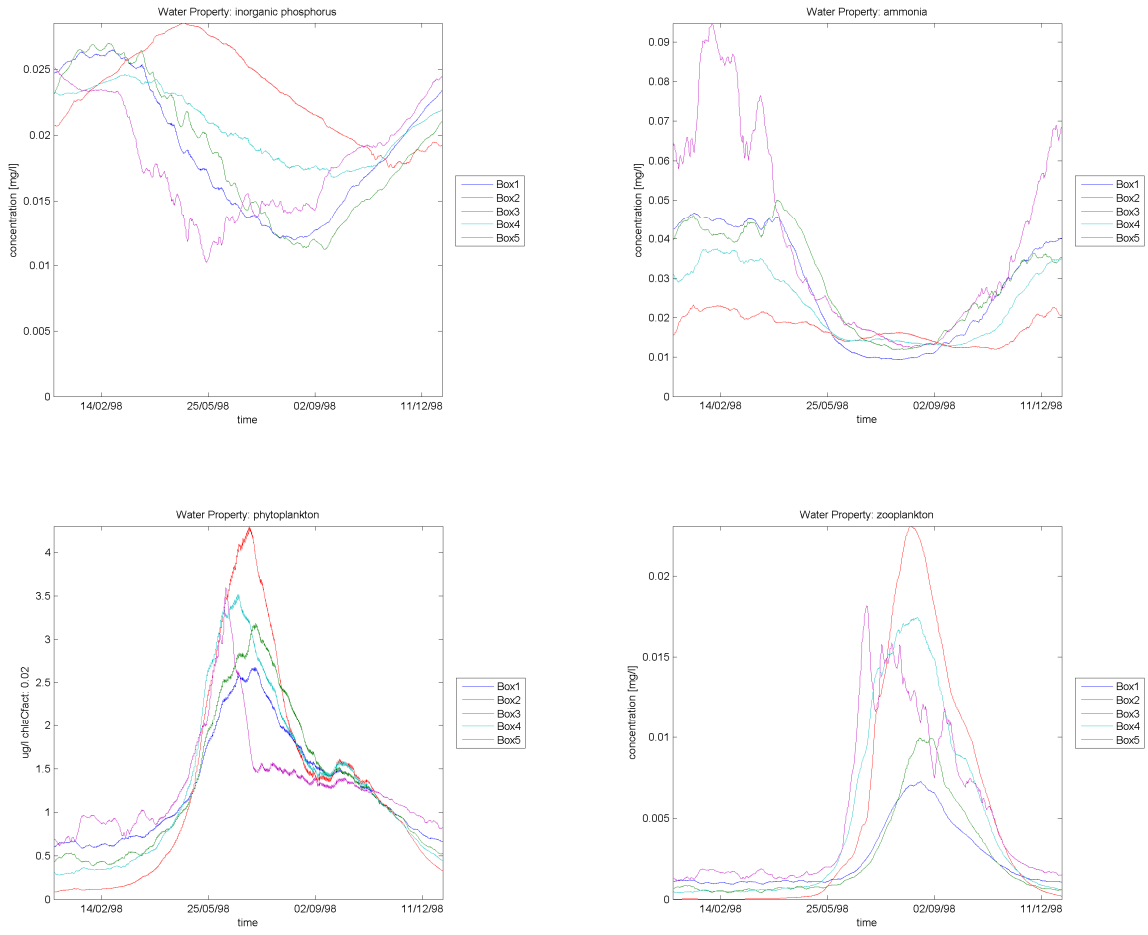

Figure 82: Property variation with time in all boxes for temperature, nitrate, inorganic phosphorus, ammonia, phytoplankton and zooplankton

For each property, the patterns between each box is similar, although some boxes' concentrations differ from each other (e.g. nitrate in box 3). The differences can be explained due to the boundary conditions used.

All variables in a box

The following figure (Figure 83) shows the evolution of the main properties in a specific box. Analysing the plot, we can asses that nitrate and ammonia levels diminish when phytoplankton grows. Zooplankton grows with a slight delay, after the phytoplankton bloom. Nitrate reaches the minimum levels around September-October. Phosphorus, in the other hand, does not have an accentuated decrease of concentration as nitrate or ammonia, due to the boundary conditions and river discharges (Figure 46).

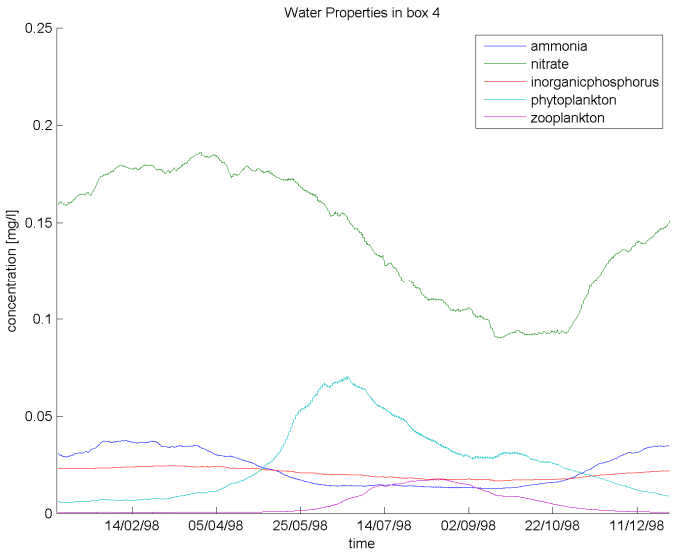

Figure 83: All main variables variation with time in the main box (nr 4)

Nutrient fluxes within boxes

The following images (below) are the calculated fluxes between boxes and, when possible, the riverine inputs aggregated by box. The total calculation time span is one year (1998). Each label has a colour that reflects its relative intensity: red is the highest, blue the lowest.

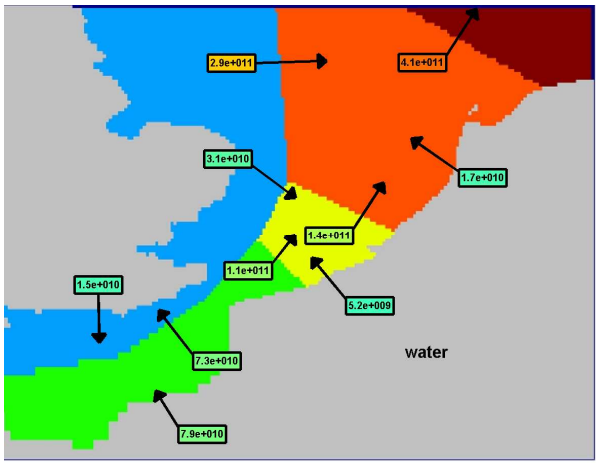

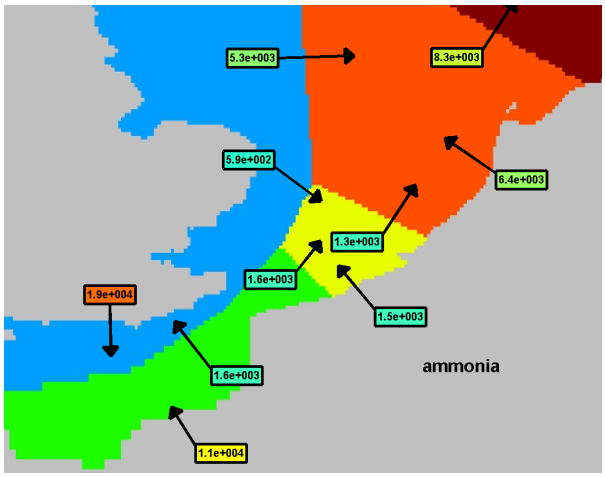

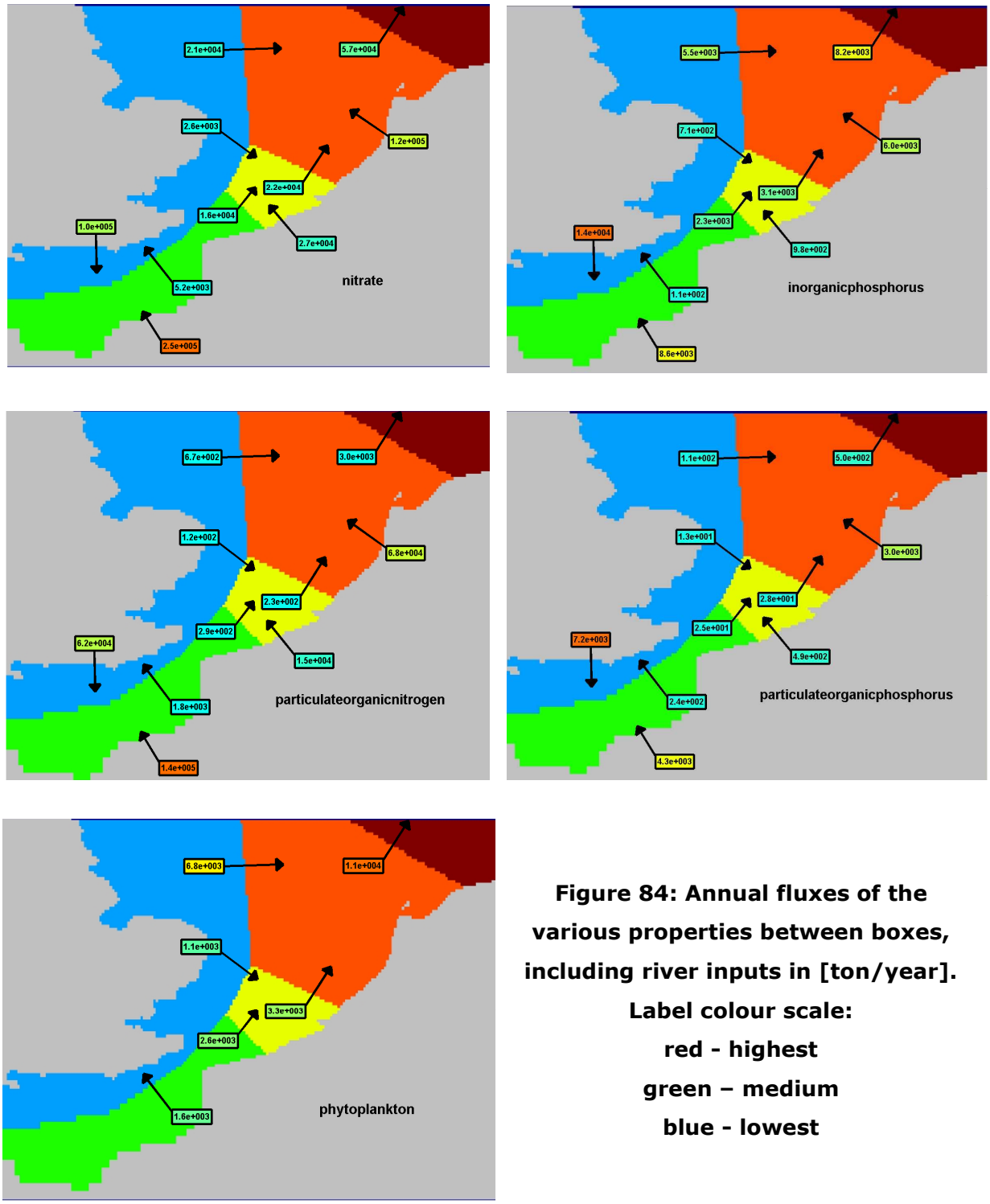

Figure 84: Annual fluxes of the various properties between boxes, including river inputs in [ton/year]. Label colour scale: red - highest green – medium blue - lowest

These results can only be compared with other model's results. The problem is that each model has a different way to define the boxes, giving out unrelated results, and thus, not allowing a comparison. The water fluxes agree with the residual flux and velocity of the domain (Figure 49 and Figure 50), following a counter clockwise pattern in the northern part (from the UK to the Netherlands) and a relatively intense flow from the channel going northerly. For most nutrients, the riverine input is a significant contribution. Box number 4 exports phytoplankton to the northern box 4. UK box exports

nutrients to the Belgium and Dutch boxes. French box (nr 2) exports to the UK box. Details are in annex 1.7.

5.2.4. Nutrient, Light and Temperature Limitation on phytoplankton growth

The box concept is used to monitor the nutrient, light and temperature effect on phytoplankton growth. The concept of limitation within the model is explained in Annex II. There is a strong limitation when the value is 0(zero) and no limitation when the value is 1(one).

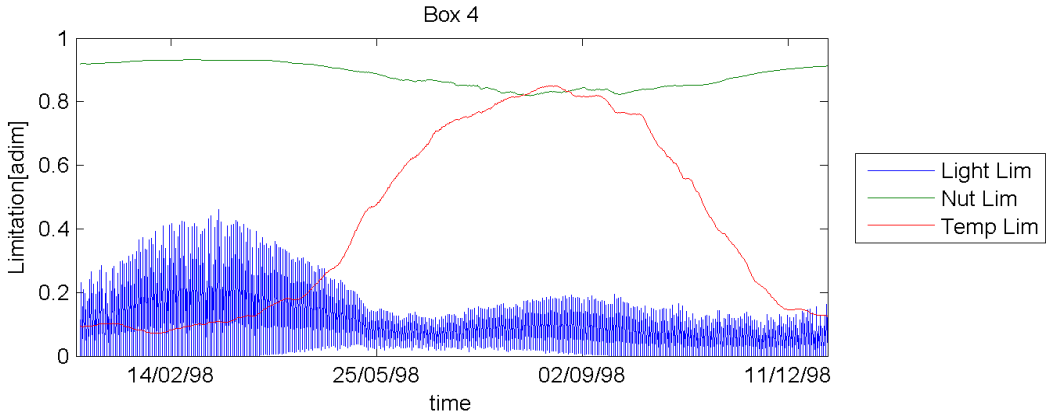

Figure 85: Limitation factor in main box (nr 4)

Evaluating the figure above, we can conclude that the phytoplankton is light limited all year round, with a particular temperature limitation during winter. The light limitation can be caused by reduced solar radiation (during winter), suspended particulate matter (SPM) and the phytoplankton itself causing self shadowing to the lower levels. Since the light extinction scheme is based on Parsons (1984) for the open ocean, which only considers the effect of phytoplankton self-shadowing, SPM has no influence on phytoplankton growth. The previous plot shows that during the summer, the light limitation is due phytoplankton itself, since the solar radiation peak is in this period. This result can also be influenced by the high nutrient concentrations, causing the model to underestimate the nutrient limitation (it is almost irrelevant by analysing Figure 85).

5.3. Conclusion

The models results are moderately good, but some aspects have to be address in order to assess the work done and improve future works. One problem that was faced was modelling which species of plankton: flagellates only, flagellates and diatoms, zooplankton, and bacteria. It was decided to model one of the simplest solutions: flagellates and mesozooplankton. This approach seemed to be correct, since model complexity would not hinder the results interpretations. It turned out to evaluate the phytoplankton quite good, but, diatoms are an important part of the biological cycle in the North Sea, so this process has to be included in the future. The available data used to compare with the model, either from stations or satellite does not have the desired time or spatial resolution. Moreover, only Dutch station data was used because retrieving sufficient and well organized data from other countries/institutions is difficult task.

6. Conclusions

The North Sea is one of the most important shelf seas in Europe as it provides important economical resources to the adjacent countries. The importance of modelling such a used resource is valuable if one is to ensure a sustainable development of the exploitation of such resources. The modelling exercise enables one to measure and predict changes to the system, link cause to effect and enable the stakeholders of such resources to have powerful tools at their hand in order to manage it in the best manner possible.

The knowledge of how the ecological system functions and therefore, all the relevant system variables, made by the modelling exercise, not only at hindcast but also at forecast status, allows the development of a science that is thoroughly connected to the existing management strategies.

The MOHID model has the capability of coupling a hydrodynamical model with an ecological model and this feature is one of the main characteristic that enables a flexible and comprehensive analysis of the model's result, either the ecological or hydrodynamical features. It has been validated in many other applications, so the North Sea application was somewhat a test to its integrity.

The hydrodynamical model performs agreeably with known findings. The general circulation of the wider North Sea is presented in the form of lagrangean tracers, residual circulation and residence times. The tidal harmonic analysis has been made and compared with existing data and it shows that the model performs well, as expected.

As for the ecological model, although the model performs moderately, some difficulties arise from specific options taken during the setup phase. A general comparison of the timeseries and spatial analysis has been made with station data and satellite imagery.

As for the timeseries, the nutrients present a higher level than the field data, but it presents reasonable results for phytoplankton, although it does not simulate the magnitude correctly. The higher nutrients are explained by the use of a climatology that has no sufficient spatial resolution and the underestimation of primary production. Oxygen deficiency is one of the symptoms of eutrophication and regarding this property, the station data fits the model's curve adequately. Satellite imagery is not eligible for a thorough quantitative analysis due to its characteristics, but it reveals that the model is capable of simulating phytoplankton on a wider scale, not specifically in some areas.

Furthermore, a presentation of transboundary nutrient transport has been made, using boxes defining countries maritime areas and that include riverine inputs. The lack of similar data hinders the ability to do a model-model comparison. However, and putting these results at the level of the residual circulation, one can conclude that there is a

transport of nutrients from the UK to the Netherlands and from the French and Belgium boxes to the North, following the circulation pattern.

One of the most challenging tasks is to know which limiting factor on phytoplankton growth. From the model's result, one can conclude that the system is mainly light limited during the growth phase (temperature limited during the winter). Having in mind that the OSPAR strategy requires a member state to reduce 50% of nutrient discharges, this reduction will probably not have an effect on the system because it is light limited(and not nutrient limited as expected). However, the light limitation has to be carefully analysed: the model does not include realistic SPM discharges, neither a field to which it is forced upon, and its light extinction scheme does not include SPM. Nevertheless, other model's results clearly indicated that SPM and therefore light limitation is a question to be seriously addressed. If this conclusion is to be verified, it could have an important effect on water management policies (for e.g. reduction strategies) that would not have an effect on the system.

Moreover, the model's simple trophic level could be more complex, including diatoms, which are an important part of the biogeochemical cycle of the North Sea.

On the many difficulties encountered one has to mention the availability of data to which compare the model's results: at some times, the data does not have enough temporal resolution, impeding the correct validation of results. Furthermore, to use datasets, these have to be carefully processed since they can have particular characteristics that can put the model's results in question, such as the solar radiation problem that was found while developing of the model's setup.

Although a model implementation is not ever finish, on the whole the objectives of the thesis were achieved: the study of a system that is exceptionally well known.

7. Future work

Since the North Sea application was a first tryout of the model in this area, there are many improvements to be made to the model setup. First of all, the implementation of better data has do be done. This data, which is already available, includes nutrient boundary conditions, discharges with more properties (including SPM data) and a full set of high resolution meteorological forcing, all for the year 2002. It also includes nitrogen atmosphere deposition that can be easily implemented in the MOHID model. The model has also to be more complex, i.e., to include diatoms and silica in its setup. This is a crucial step, if the model is to be compared to the other models run in the area.

Moreover, SPM is a relevant parameter on phytoplankton light limitation as it creates a barrier for light to penetrate the water column. This feature has to be enabled, in order to correctly compute phytoplankton growth limitation.

Furthermore, a reduction run, that is, 50% and 70% nutrient discharge has to be made in order to assess the OSPAR guidelines that require a country to reduce its nutrient discharges. This step is important given that the light limitation question has to be addressed and answered. Furthermore, the increase and change of balance of nutrients of the last decades could have an effect on the species composition of the North Sea, which may cause a regime shift in the dominant species that can cause harmful algal blooms more frequently.

The transboundary nutrient transport is a feature that was not fully exploited because of the lack of definitions of transects and box borders. By the time this thesis is finished, OSPAR defined common guidelines for the calculation of such fluxes, which can be used to validate and compare models.

One goal is to use hydrodynamical model in such a way that it can be coupled with other biogeochemical models, such as the BFM.

Many small data analysis applications were made, such as the harmonic analysis package, which can be improved in the future, possibly integrating them on the same data analysis package for MatLab.

The model also shows to be capable of simulating stratification, although its current setup does not allow for it to be reasonably developed because of the temperature boundary conditions used. One work that can be done is to use the 2D hydrodynamical model and a different submodel that includes the stratified area (central North Sea) and study the relation between fronts and primary production/oxygen depletion.

8. References

Allen, C. M., **1982**, "Numerical simulation of contaminant dispersion in estuary flows", Proc. R. Soc. London. A 381, 179-194

Andersen, OB, Egbert GD, Erofeeva SY, Ray RD. **2006**. "Mapping nonlinear shallow-water tides: a look at the past and future", Ocean Dynamics, Volume 56, Numbers 5-6

Backhaus, J. O. and Hainbucher, D., **1987**, "A finite-difference general circulation model for shelf seas and its application to low frequency variability on the North European Shelf", In: J. C. J. Nihoul and B. M. Jamart (eds.), Three-Dimensional Models of Marine and Estuarine Dynamics, Elsevier Oceanography Series, 45: 221- 244

Beusekom, J.E.E. van, Diel-Christiansen, S., **2007.** "Gobal change and the biogeochemistry of the North Sea: the possible role of phytoplankton and phytoplankton grazing", International Journal of Earth Sciences, doi:10.1007/s00531-007-0233-8

Braunschweig, F., Martins, F., Chambel, P., Neves, R., **2003**. "A methodology to estimate renewal time scales in estuaries: the Tagus Estuary case", Ocean Dynamics 53: 137–145

Braunschweig, F., P. Chambel, L. Fernandes, P. Pina, R. Neves, **2004**a, The object-oriented design of the integrated modelling system MOHID, Computational Methods in Water Resources International Conference, Chapel Hill, North Carolina, USA

Braunschweig, F., R. Neves, P. Chambel, L. Fernandes, **2004**b. "Modelação Integrada de Sistemas Hídricos", 7º Congresso da Água, Associação Portuguesa dos Recursos Hídricos, Lisboa, Portugal

Burchard, H., Bolding, K., and Villarreal, M.R., **1999.** "GOTM - a general ocean turbulence model, Theory, applications and test cases". Technical Report EUR 18745 EN, European Commission.

Cancino, L., Neves, R., **1999**. Hydrodynamic and sediment suspension modelling in estuarine systems, Part II: Application to the Western Scheldt and Gironde estuaries , Journal of Marine Systems, 22, 117-131

Chambel-Leitão, P. , Braunschweig, F., Fernandes L., Neves R. . **2007**. "Integration of MOHID model and tools with SWAT model". Accepted for oral presentation in the SWAT WORKSHOP AND CONFERENCE - July 2007, Delft - the Netherlands.

Coelho, H., Neves, R., White, M., P. C. Leitão, Santos, A., **2002**, A Model for Ocean Circulation on the Iberian Coast, Journal of Marine Systems, 32 (1-3), 153-179

Davies, AM. **1986**. "A three-dimensional model of the northwest European shelf with application to the M4 tide". Journal of Physical Oceanography 16:797–813

EC. **1991**. "Urban Wastewater Treatment Directive 91/271/EEC"

EPA, **1985**. "Rates, constants, and kinetics formulations in surface water quality modelling" 2nd. ed. United States Environmental Protection Agency, Report EPA/600/3-85/040

ERA-40 reanalysis provided by the ECMWF data server at http://data.ecmwf.int/data/

Evans B. M., Sheeder S. A., Lehning D. W. **2003**. A spatial technique for estimating streambank erosion based on watershed characteristics. Journal of Spatial Hydrology Vol.3, No.1 Fall.

Fernandes, L. 2005. "MODELLING OF ARSENIC DYNAMICS IN THE TAGUS ESTUARY". Master Thesis, Instituto Superior Técnico.

Fernandes, R., Neves, R., Leitão, P., Santos, M.,Nunes, S., Braunschweig,F., Coelho, H., **2004** "An Operational Model for the Tagus Estuary" Geophysical Research Abstracts, Vol. 6, 07207

Foreman, M.G.G., **1977**. Manual for Tidal Heights Analysis and Prediction. Pacific Marine Science Report 77-10, Institute of Ocean Sciences, Patricia Bay, Sidney, B.C., 58 pp. (2004 revision)

Helleiner J., SINHA B.; PINGREE R.D, **1997**, The principal lunar semidiurnal tide and its harmonics, Continental Shelf Research, Volume 17, Number 11, , pp. **1321**-**1365**(45)

INAG/Maretec, **2003,** "Water Quality in Portuguese Estuaries".

Kalnay, *et al*. **1996.** The NCEP/NCAR 40-year reanalysis project, Bull. Amer. Meteor. Soc., 77, 437-470.

Lacroix, G, Ruddick, J, Gypens, N, Lancelot, C. **2007**. "Modelling the relative impact of rivers (Scheldt/Rhine/Seine) and Western Channel waters on the nutrient and diatoms/Phaeocystis distributions in Belgian waters (Southern North Sea)", Continental Shelf Research, Volume 27, Issues 10-11, Pages 1422-1446

Lee, A.J., **1980**. North Sea: physical oceanography. In: Banner, F.T.,Collins, M.B., Massie, K.S. (Eds.), The North-West European Shelf Seas: The Sea Bed and the Sea in Motion. II. ElsevierScience Publishers B.V., Amsterdam, pp. 467–493.

Leendertse, J. J., Liu, S. K., **1978.** "A Three-dimensional turbulent energy model for non-homogeneous estuaries and coastal sea systems. Hydrodynamics of Estuaries and Fjords", J.C.J. Nihoul Ed., Elsevier Publ. Co., Amsterdam, pp. 387-405.

Leitão, P., **2003**. "Integração de Escalas e Processos na Modelação do Ambiente Marinho", Dissertação para a obtenção do grau de Doutor em Engenharia do Ambiente, Instituto Superior Técnico, Lisboa

Leitão, P.C., **1996**. "Modelo de dispersão lagrangeano tridimensional", Dissertação para a obtenção do grau de Mestre em Ecologia, Gestão e Modelação de Recursos Marinhos, Instituto Superior Técnico, Lisboa

Letellier, T., **2004**, Etude des ondes de mar´ee sur les plateaux continentaux, PhD thesis, pp 109

Luijendijk, A., **2001**, "Validation, calibration and evaluation of a Delft3D-FLOW model with ferry measurements", MsC Thesis, TUDelft

Lyard, F., Lefevre F., Letellier T,Francis O, **2006**, Modelling the global ocean tides: modern insights from FES2004. Ocean Dynamics 56: 394–415

MARETEC/IST, 2003, "MOHID Technical Description", www.mohid.com.

MARETEC/IST, 2006, "MOHID Water Quality module manual", www.mohid.com.

Martins, F. **2000**, "Modelação Matemática Tridimensional de Escoamentos Costeiros e Estuarinos usando uma Abordagem de Coordenada Vertical Genérica", Dissertação para obtenção do grau de Doutor em Engenharia Mecânica, Instituto Superior Técnico, Universidade Técnica de Lisboa

Martins, F, Leitão, P, Silva A, Neves, R. **2001**. "3D modelling in the Sado estuary using a new generic vertical discretization approach". OCEANOLOGICA ACTA VOL. 24 – N° 1

Martinsen, E.A., Engedahl, H., **1987**. Implementation and testing ofa lateral boundary scheme as an open boundary condition in a barotropic ocean model. Coastal Engineering 11, 603– 627

Mellor, G. L. and Yamada, T., **1982**: Development of a turbulence closure model for geophysical fluid problems. Rev. Geophys. Space Phys., 20, 851-875.

Mills D. Baretta-Bekker, H., Lenhart, H., van der Molen, J. **2007**. ICG-EMO 2nd Workshop User Guide.

Miranda, R., **1999**, Nitrogen Biogeochemical Cycle Modeling in the North Atlantic Ocean, Dissertação para a obtenção do grau de Mestre em Ecologia, Gestão e Modelação de Recursos Marinhos, Instituto Superior Técnico, Lisboa

Neves, R., **1985**, Étude Expérimentale et Modélisation des Circulations Transitoire et Résiduelle dans l'Estuaire du Sado. Ph. D. Thesis, Univ. Liège

Neves, R., Coelho,H., Leitão,P., Martins, H., Santos, A.,**1998**. "A numerical investigation of the slope current along the western european margin". In 12th Int. Conf. On Computational Methods in Water Resources XII.

Nihoul, J.C.J., **1984**, A three-dimensional general marine circulation model in a remote sensing perspective, In Annales Geophysicae, 2, 4, 433-442

NOAA OISSTv2 data provided by the NOAA/OAR/ESRL PSD, Boulder, Colorado, USA, from their Web site at http://www.cdc.noaa.gov/

NOAA, Center for Operational Oceanographic Products and Services, **1998**, "Our Restless Tides" from http://co-ops.nos.noaa.gov/restles1.html

Nunneri, C., Windhorst, W., Turner, R.K. and H. Lenhart. **2007**. Nutrient emission reduction scenarios in the North Sea: an abatement cost and ecosystem integrity analysis, Ecological Indicators, 7:776-792

OSPAR Commission, 2000. Quality Status Report 2000. OSPAR Commission, London. 108 + vii pp.

Pacanowski, R. C. and G. H. Philander, **1981**, Parameterization of vertical mixing in numerical models of tropical oceans, J. Phys. Oceanogr., 11, 1443-1451,

Parker, B., **1991**, Tidal Hydrodynamics, Wiley&Sons, 709pp

Parsons, T.R.; Takahashi, M. & Hargrave, B. **1984**. Biological oceanographic processes, 3rd. ed., Pergamon Press, Oxford, 330 pp.

Patsch J.; Radach G., **1997**. "Long-term simulation of the eutrophication of the North Sea: temporal development of nutrients, chlorophyll and primary production in comparison to observations", Journal of Sea Research, Volume 38, Number 3, pp. 275-310(36)

Pawlowicz, P, Beardsley, B., and Lentz S., **2002.** "Classical tidal harmonic analysis including error estimates in MATLAB using T_TIDE", Computers and Geosciences 28, 929-937.

Pina, P., **2001**, Integrated Approach to Study the Tagus Estuary Water Quality, Dissertação para a obtenção do grau de Mestre em Ecologia, Gestão e Modelação de Recursos Marinhos, Instituto Superior Técnico, Lisboa

Pingree, R.D., Griffiths, D.K., **1978**. Tidal fronts on the shelf seas around the British Isles. J. Geophys. Res. 83, 4615– 4622.

Pohlmann, T., **1996**. Calculating the development of the thermal vertical stratification in the North Sea with a three-dimensional baroclinic circulation model, Continental Shelf Research 16 (2), pp. 163–194.

Portela, L., **1996**, Modelação Matemática de Processos Hidrodinâmicos e de Qualidade da Água no Estuário do Tejo, Dissertação para obtenção do grau de Doutor em Engenharia do Ambiente, Instituto Superior Técnico, Universidade Técnica de Lisboa

Proctor, R., Holt, J.T., Allen, J.I., Blackford, J. **2003**. "Nutrient fluxes and budgets for the North West European Shelf from a three-dimensional model". Science of the Total Environment, 314-315: 769-785.

Radach, G., **1992**. Ecosystem functioning in the German Bight under continental nutrient inputs by rivers. Estuaries 15, 477-496.

Reynolds, R.W., N.A. Rayner, T.M. Smith, D.C. Stokes, and W. Wang, **2002**: An improved in situ and satellite SST analysis for climate. J. Climate, 15, 1609-1625.

Riflet, G, Leitão PC, Fernandes R, Neves RJJ, **2007**, A Simple Pre-Operational Model for the Portuguese Coast, CMNE/CILAMCE Porto

Ruddick, K.G., F. Ovidio, and M. Rijkeboer, **2000. "**Atmospheric correction of SeaWiFS imagery for turbid coastal and inland waters", Applied Optics,. 39(6): p. 897-912.

Santos, A. J., **1995**, "Modelo Hidrodinâmico Tridimensional de Circulação Oceânica e Estuarina", Dissertação para obtenção do grau de Doutor em Engenharia Mecânica, Instituto Superior Técnico, Universidade Técnica de Lisboa

Saraiva S, Pina P, Martins, F., Santos, M., Braunschweig, F., Neves, R., **2007**, Modelling the influence of nutrient loads on Portuguese estuaries, Hydrobiologia, Vol. 587, No. 1., pp. 5-18.

SeaWiFS Level 1a data provided by the NASA Goddard Space Flight Centre, from their Web site at http://oceancolor.gsfc.nasa.gov/

Sharples, J. Ross, O. N. Scott, B. E. Greenstreet, S. P. Fraser, H. , **2006**. "Inter-annual variability in the timing of stratification and the spring bloom in the North-western North Sea" Continental Shelf Research, VOL 26; NUMBER 6, pages 733-751

Silva, A., P. C. Leitão, J. C. Leitão, F. Braunschweig, R. Neves, **2002**, Ria Formosa 3D hydrodynamic model. A contribution for the understanding of the Faro-Olhão inlet processes, Littoral 2002, Porto, Portugal

Skogen, M. D., Søiland H., Svendsen E. **2004. "**Effects of changing nutrient loads to the North Sea". Journal of Marine Systems 46:23–38

Skogen, M.D., Moll, A., **2005**, Importance of ocean circulation in ecological modeling: An example from the North Sea, Journal of Marine Systems 57, 289–300

Smagorinsky, J., **1963**, General circulation experiments with the primitive equations, Monthly Weather, Review, 91(3), 99–165.

Sündermann J., Beddig S., Radach G. and Schlünzen K.H. **2002. "**The North Sea - Problems and Research Needs". Zentrum für Meeres- und klimaforschung der Universität Hamburg, 64 pp.

Tchobanoglous, G. *et al*, 2003. "Wastewater Engineering, Treatment and Reuse", Metcalf&Eddy Inc., Fourth edition, McGrawHill, NY

Tett P., Gowen R., Mills D., Fernandes T., Gilpin L., Huxham M., Kennington K., (...), Malcolm S. .**2007**. Defining and detecting undesirable disturbance in the context of marine eutrophication. Marine Pollution Bulletin, 55 (1-6), pp. 282-297.

Tomczak, M., **1996**, "An Introduction to Physical Oceanography". Flinders University, Australia, http://gaea.es.flinders.edu.au/~mattom/IntroOc/lecture11.html

Trancoso A, Saraiva S, Fernandes L, Pina P, Leitão P, Neves R, **2005**, Modelling macroalgae using a 3 D hydrodynamic-ecological model in a shallow, temperate estuary, Ecological Modelling, Vol. 187, No. 2., pp. 232-246.

UNESCO, **1981**, Tenth Report on the joint panel on oceanographic tables and standards, Technical papers in marine science, N. 36, 24 pp

van Haren, H., **2004**. Current spectra under varying stratification conditions in the central North Sea. J. Sea Res. 51(2): 77-91.

Villarreal, M. R., P. Montero, J. J. Tabuada, R. Prego, P. C. Leitão, V. Pérez-Villar, **2002**, Hydrodynamic model study of the Ria de Pontevedra under estuarine conditions, Estuarine, Coastal and Shelf Science, 54, 101-113

WOA05, data provided by the NOAA/OAR/ESRL PSD, Boulder, Colorado, USA, from their Web site at http://www.cdc.noaa.gov/

WOA94, data provided by the NOAA/OAR/ESRL PSD, Boulder, Colorado, USA, from their Web site at http://www.cdc.noaa.gov/

XTIDE, Tide harmonic database: harmonics.txt, v3.2, **2004**/06/14. Available from http://www.flaterco.com/xtide/files.html.

1. Annex I

1.1. River Discharge data sources

Source:	**Rivers:**
Generated from 1997 data from FRV/Copenhagen	Kyroenjoki, Lapuanjoki, Kalajoki, Pyhaejoki, Siikajoki, Oulujoki, Iijoki + Kiiminkijoki, Simojoki, Kemijoki, Tornionjoki Torne a, Kalix aelv, Rane aelv, Lule aelv, Pite aelv, Skellefte aelv, Kokemaeenjoki, Ume aelv, Oere aelv, Gide aelv, Angermanaelven, Indalsaelven, Ljungan, Ljusnan, Dalaelven, Narva, Luga, Neva, Kymijoki, Kasari, Paernu, Salatsa, Gauya, Daugava + Lielupe, Odra Oder, Rega, Parseta, Vistula Weichsel, Pregola Pregel, Neman Memel, Venta, Maelaren, Nykoepingsan, Motala stroem, Eman, Moerrumsan, Helgean, Roenne aelv, Lagan, Nissan, Aetran, Viskan, Randers Fjord, Goeta aelv, Glomma, Oslofjord, Lagen, Nidelv, Otra + Tovdalselv, Ringkobing Fjord, Kvina + Sira, Limfjorden, Isefjord, Arhus, Oresund, Vejle fjord, AAbenraa fjord, Odense Aa, Koge Bugt, Lolland, Lysefjord, Boknafjord
From OSPAR data supplied by Hermann Lennart, 1977-2002	Elbe, Ems (Eems Dollard), Meuse (Maas at Haringvliet), Rhine (Rijn at Nieuwe Waterweg), North Sea Canal (Noordzeekanaal), Scheldt (Schelde), Lake IJssel (at Vrouwenzand), Weser
Nutrients and daily flow rates from http://www.eau-artois-picardie.fr/, 1976-2006	Authie (at Quend), Canche (at Beutin), Somme (canalised at Cambron)
Data obtained from IFREMER, Jean.Francois.Guillaud@ifremer.fr and Pascal.Lazure@ifremer.fr	Seine, Loire, Vilaine
Nutrients and flow from UK Environment Agency, some flow rates from UK National River Flow Archive, 1977-2005	ADUR, AFON GOCH, ALT, ANNAN, ARUN, AVON AT BANTHAM, AVON AT BOURNEMOUTH, AVON AT BRISTOL, AXE, AYR, BEAULY, BLYTH, BRIDLINGTON, CAMEL, CARNON, CARRON, CHELMER, CLEDDAU, CLWYD, CLYDE, COLNE, CONON, CONWY, COQUET, CREE, DART, DEE AT ABERDEEN, DEE AT CHESTER, DEE AT TONGLAND, DENE MOUTH, DERWENT, DEVERON, DIGHTY WATER, DON, DOVER, DYFI, EARN, EAST SOLENT, EDEN AT CARLISLE, EDEN IN SCOTLAND, ESK AT EDINBURGH, ESK AT MONTROSE, ESK AT WHITBY, ESK INTO SOLWAY FIRTH, EXE, EYE, FAL, FINDHORN, FIRTH OF FORTH, FOWEY, FROME, GLASLYN, GREAT STOUR, GWYRFAI, HASTINGS, HUMBER, IRVINE, ITCHEN, KENT, LEVEN, LEVEN IN SCOTLAND, LOCHY, LOSSIE, LOUGHOR, LUNE, MAWDDACH, MEDWAY, MERSEY, NAIRN, NEATH, NENE, NESS, NITH, OGMORE, OTTER, OUSE AT KINGS LYNN, OUSE AT NEWHAVEN, PARRETT, PORLOCK BAY, RED, RHYMNEY, RIBBLE, ROTHER, SCARBOROUGH, SEVERN, SHIN, SPEY, STOUR AT HARWICH, TAF, TAFF, TAMAR, TAW, TAWE, TAY, TEES, TEIFI, TEIGN, TEST, THAMES, THURSO, TWEED, TYNE, TYNE IN SCOTLAND, TYWI, UGIE, URR WATER, USK, WANSBECK, WATER OF LEITH, WATER OF LUCE, WEAR, WEAVER, WELLAND, WEST BAY, WICK, WITHAM, WYE, WYRE, YARE, YSTWYTH, YTHAN
From unknown source, used for POM model at Cefas, 1995/1999-2001	Avonmore, Bandon, Bann, Barrow, Blackwater, Boyne, Lee, Liffey, Foyle, Slaney

1.2. Nutrient Equivalency

The following table represents assumptions in order to have the properties needed for the model. It is the nutrient correspondence between input data and output data for the discharges, based on Tchobanoglous, 2003. In the header row, we have the input nutrient that in this case is Nitrate + Nitrite, Ammonium, and Phosphate. With these three known nutrient (in), we assume all the others (out) by multiplying by a factor and summing up in rows.

For e.g., in the case of PON, the amount is 0.5 * Nitrate + 0.5 * Ammonium + 0.5 * Nitrite.

Units	**[mg_N/L]**	**[mg_N/L]**	**[mg_N/L]**	**[mg_P/L]**	**[mg_N/L]**
out\in	**Nitrate+Nitrite**	**Nitrate**	**Ammonium**	**Phosphate(IP)**	**Nitrite**
Nitrate	0.95	1			
Ammonium			1		0.6
Phosphate(IP)				1	
Nitrite	0.05	0.05			1
PON		0.5	0.5		0.5
DONr		0.25	0.25		0.25
DONnr		0.25	0.25		0.25
POP				0.5	
DOPr				0.25	
DOPnr				0.25	

Table 3: Nutrient Equivalency table for the discharges

The following table represents the nutrient correspondences in the case of initialization fields and border conditions. In this case, only two nutrients are known(Nitrate, Phosphate from the WOA05 dataset). The rest of the nutrients are a factor of the input nutrient. This is done in this way because the model does not handle multiple fractions as is the case of the discharges.

Units	**[mg_N/L]**	**[mg_P/L]**
out\in	**Nitrate**	**Phosphate(IP)**
Nitrate	1	
Ammonium	0.6	
Phosphate(IP)		1
Nitrite	0.05	
PON	0.5	
DONr	0.25	
DONnr	0.25	
POP		0.5
DOPr		0.25
DOPnr		0.25

Table 4 Nutrient Equivalency table for initial and border conditions

1.3. River Discharge reference

Month	Salility	Temp(ºC)	Sed(mg/l)	phyto(mgC/l)	O2(mgO)/l	Zoo(mgC/l)
1	0.01	5.25	24.67	0.03	10.35	0.003
2	0.01	4.63	21.55	0.06	10.40	0.006
3	0.01	6.32	18.48	0.18	10.41	0.018
4	0.01	8.80	11.27	0.50	11.05	0.050
5	0.01	12.53	8.41	0.33	9.27	0.033
6	0.01	15.89	5.32	0.21	8.18	0.021
7	0.01	18.24	6.57	0.15	7.43	0.015
8	0.01	20.16	6.32	0.13	7.18	0.013
9	0.01	17.54	11.82	0.09	7.23	0.009
10	0.01	13.90	11.75	0.08	8.07	0.008
11	0.01	9.78	22.30	0.05	8.82	0.005
12	0.01	6.57	35.30	0.02	9.95	0.002

Table 5 River discharge reference used adapted from Wissenkerke station (Oosterscheld, Netherlands)

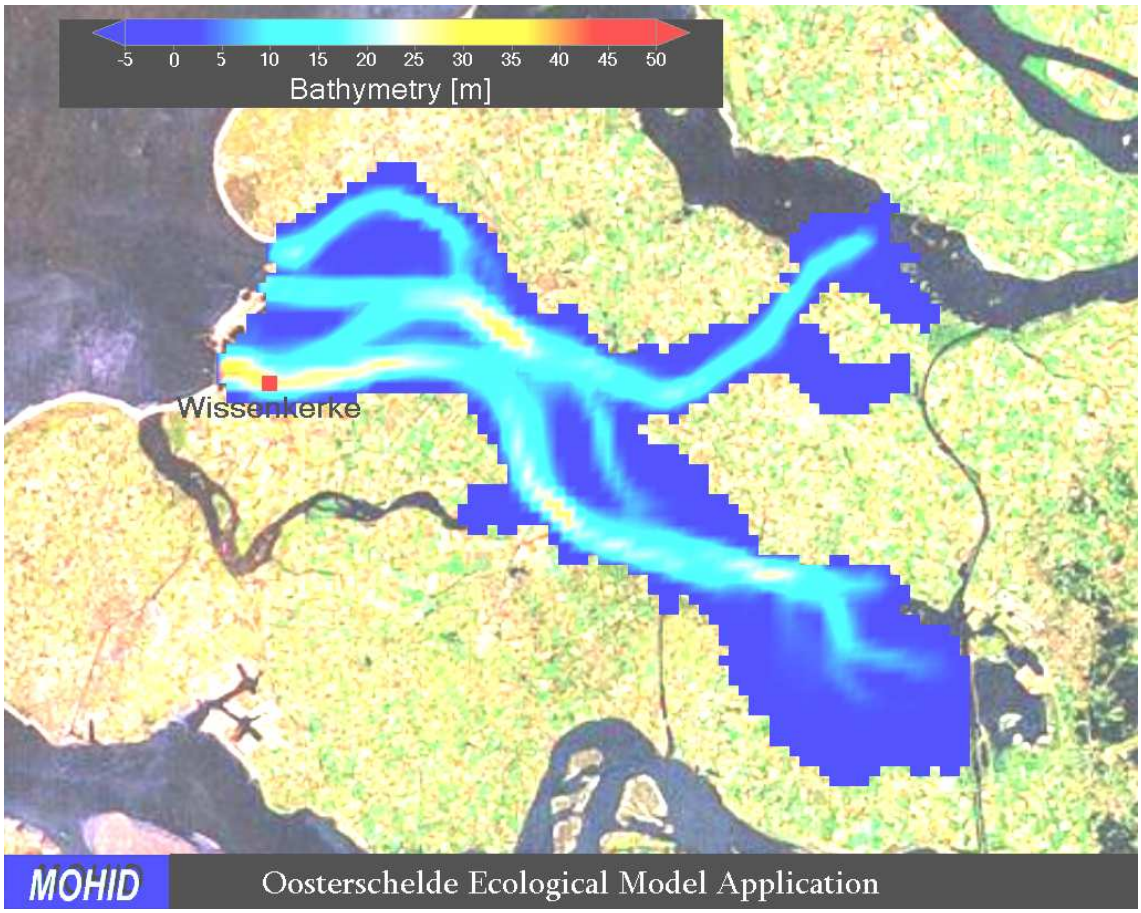

Figure 86: Wissenkerke station location (red dot)

1.4. 3D Model river discharge statistics

The following table represents the statistical mean from 1990 to 2003 of the discharges in the 3D model. It is sorted by flow column.

	Flow [m3/s]	Nitrate [mg_N/L]	Ammonium [mg_N/L]	Phosphate(IP) [mg_P/L]	Silicate [mg_Si/L]	Nitrite [mg_N/L]	PON [mg_N/L]	DONr [mg_N/L]	DONnr [mg_N/L]	POP [mg_P/L]	DOPr [mg_P/L]	DOPnr [mg_P/L]
Rhine (Rijn at Nieuwe	1423.	3.02	0.19	0.14	2.47	0.16	1.68	0.84	0.84	0.07	0.03	0.03
Meuse (Maas at Haringvliet)	733.9	2.84	0.35	0.09	5.73	0.15	1.67	0.83	0.83	0.04	0.02	0.02
Seine	519.3	6.60	0.66	0.55	3.30	0.35	3.80	1.90	1.90	0.28	0.14	0.14
Lake IJssel (at Vrouwenzand)	513.5	1.72	0.10	0.02	1.85	0.09	0.96	0.48	0.48	0.01	0.01	0.01
HUMBER	229.5	7.09	1.22	1.06	7.96	0.37	4.34	2.17	2.17	0.53	0.27	0.27
Scheldt (Schelde)	143.6	4.55	0.67	0.22	4.11	0.24	2.73	1.36	1.36	0.11	0.06	0.06
THAMES	106.1	10.2	2.06	2.36	8.59	0.54	6.43	3.22	3.22	1.18	0.59	0.59
North Sea Canal	94.4	2.30	0.36	0.23	2.95	0.12	1.39	0.70	0.70	0.11	0.06	0.06
Somme (canalised at	36.9	18.5	0.30	0.32	6.74	0.98	9.90	4.95	4.95	0.16	0.08	0.08
YARE	14.6	7.20	0.64	0.51	3.32	0.38	4.11	2.06	2.06	0.25	0.13	0.13
OUSE AT KINGS LYNN	14.0	7.94	0.90	0.88	7.34	0.42	4.63	2.31	2.31	0.44	0.22	0.22
MEDWAY	13.4	8.30	3.27	1.62	10.4	0.44	6.01	3.00	3.00	0.81	0.41	0.41
Canche (at Beutin)	13.0	24.3	0.20	0.41	0.00	1.28	12.8	6.44	6.44	0.21	0.10	0.10
ARUN	12.0	4.66	2.79	0.90	5.79	0.25	3.85	1.93	1.93	0.45	0.22	0.22
Authie (at Quend)	8.6	25.8	0.14	0.29	0.00	1.36	13.6	6.84	6.84	0.14	0.07	0.07
ITCHEN	6.1	5.14	1.96	0.73	10.2	0.27	3.68	1.84	1.84	0.37	0.18	0.18
NENE	5.6	8.85	0.42	1.08	5.74	0.47	4.87	2.43	2.43	0.54	0.27	0.27
OUSE AT NEWHAVEN	5.5	3.36	10.5	2.29	4.20	0.18	7.05	3.53	3.53	1.14	0.57	0.57
STOUR AT HARWICH	5.2	7.30	4.91	1.34	4.83	0.38	6.30	3.15	3.15	0.67	0.33	0.33
WITHAM	4.0	11.0	0.34	0.75	4.21	0.58	6.00	3.00	3.00	0.38	0.19	0.19
WELLAND	3.9	8.55	0.81	0.63	3.40	0.45	4.91	2.45	2.45	0.32	0.16	0.16
GREAT STOUR	3.7	8.62	3.51	1.89	7.91	0.45	6.30	3.15	3.15	0.95	0.47	0.47
EAST SOLENT	2.3	3.51	21.6	4.30	0.00	0.18	12.6	6.33	6.33	2.15	1.07	1.07
ROTHER	1.8	2.53	0.15	0.18	5.58	0.13	1.41	0.70	0.70	0.09	0.05	0.05
COLNE	1.5	12.1	4.99	2.90	6.87	0.64	8.87	4.44	4.44	1.45	0.72	0.72
ADUR	1.1	7.43	0.14	1.54	0.00	0.39	3.98	1.99	1.99	0.77	0.39	0.39
DOVER	0.8	2.56	21.8	2.93	0.00	0.13	12.2	6.12	6.12	1.47	0.73	0.73
HASTINGS	0.4	1.34	21.8	4.79	0.00	0.07	11.6	5.81	5.81	2.39	1.20	1.20
BRIDLINGTON	0.2	3.42	22.5	6.50	0.00	0.18	13.0	6.53	6.53	3.25	1.62	1.62

Table 6: 3D model discharge statistics

1.5. 3D Model River Discharge Locations

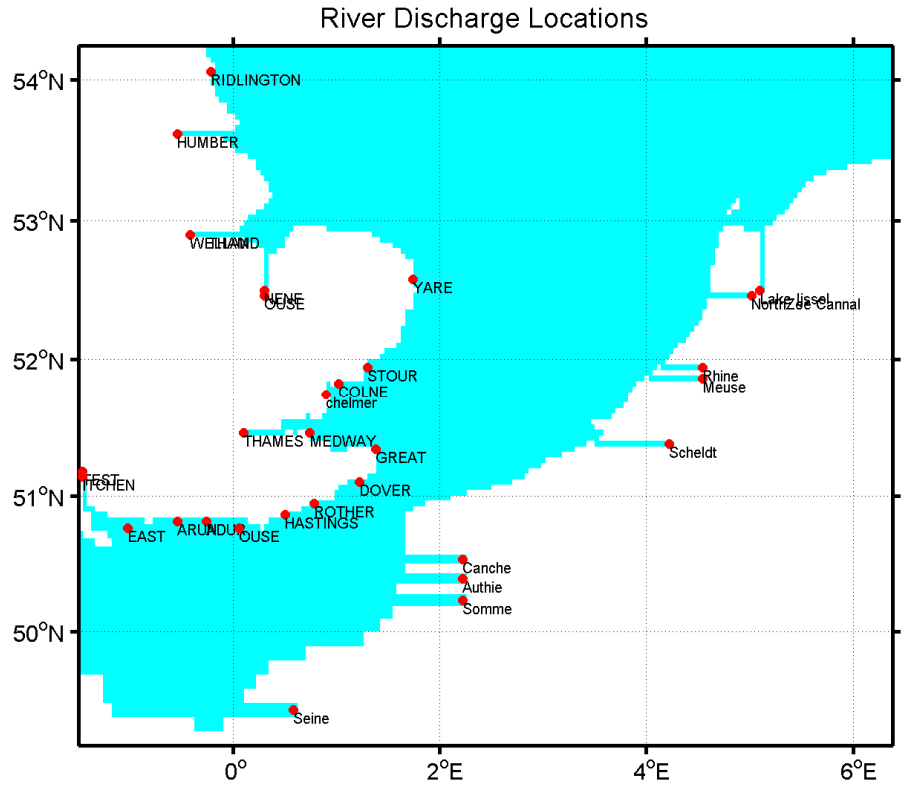

Figure 87: River Discharge locations

1.6. Station locations

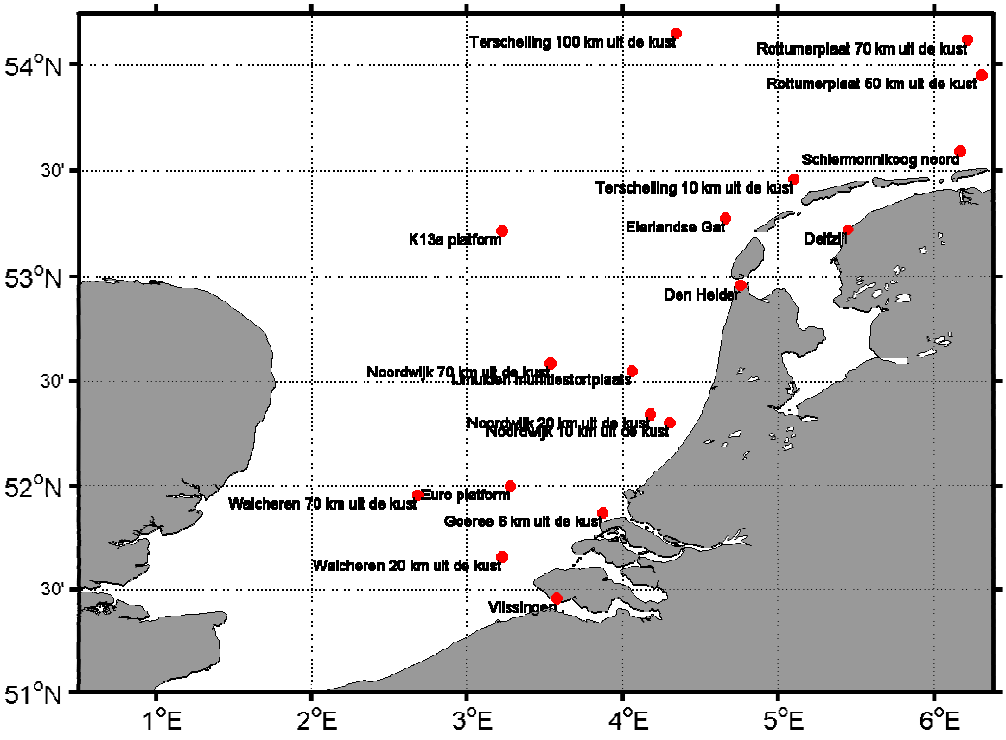

Figure 88: Station locations

Longitude	Latitude	Name
5.1008	53.4611	Terschelling 10 km uit de kust
3.5314	52.5861	Noordwijk 70 km uit de kust
3.8736	51.8697	Goeree 6 km uit de kust
4.3025	52.3022	Noordwijk 10 km uit de kust
4.175	52.3417	Noordwijk 20 km uit de kust
3.2206	51.6586	Walcheren 20 km uit de kust
4.6617	53.2769	Eierlandse Gat
3.2764	51.9986	Euro platform
4.0583	52.55	IJmuiden munitiestortplaats
3.2203	53.2178	K13a platform
2.6792	51.9569	Walcheren 70 km uit de kust
4.7585	52.9574	Den Helder
6.1667	53.5956	Schiermonnikoog noord
3.5765	51.4557	Vlissingen
5.45	53.22	Delfzijl

1.7. Nutrient fluxes between boxes

[ton/year]	Flux_1_2	Flux_1_3	Flux_1_4	Flux_2_3	Flux_3_4	Flux_4_5
water	-7.28E+10	3.08E+10	2.92E+11	7.28E+10	1.07E+11	-3.08E+10
phytoplankton	-1.62E+03	1.11E+03	6.78E+03	1.62E+03	2.61E+03	-1.11E+03
nitrate	-5.22E+03	2.55E+03	2.14E+04	5.22E+03	1.65E+04	-2.55E+03
Inorganic phosphorus	-1.07E+02	7.05E+02	5.47E+03	1.07E+02	2.32E+03	-7.05E+02
Particulate organic nitrogen	-1.84E+03	1.24E+02	6.72E+02	1.84E+03	2.95E+02	-1.24E+02
Particulate Organic phosphorus	-2.44E+02	1.33E+01	1.06E+02	2.44E+02	2.47E+01	-1.33E+01

Table 7: Water and nutrient fluxes between boxes in [ton/year]

river	water	nitrate	inorganic phosphorus	particulate organic nitrogen	particulate organic phosphorus	ammonia
Box1	1.52E+10	9.96E+04	1.43E+04	6.17E+04	7.16E+03	1.86E+04
Box2	1.73E+10	1.23E+05	6.01E+03	6.77E+04	3.01E+03	6.40E+03
Box3	5.17E+09	2.72E+04	9.80E+02	1.51E+04	4.90E+02	1.48E+03
Box4	7.85E+10	2.46E+05	8.55E+03	1.35E+05	4.28E+03	1.13E+04
Box5	0.00E+00	0.00E+00	0.00E+00	0.00E+00	0.00E+00	0.00E+00

Table 8: River discharges fluxes into the boxes in [ton/year]

Annex II

Technical Description of the Ecological Model

Index:

1.1. Introduction

The paradigm behind the MOHID system was inspired by Prof. DiToro's (member of HydroQual) words: "Phytoplankton does not have GPS", meaning that biochemical processes are 0D and do not depend on the referential and dimensions considered to quantify transport. In the MOHID case, the methodology consists in building a biogeochemical module, where the external forcing conditions are given (ex: light, temperature, salinity) and mass fluxes between state variables (ex: nitrate, phytoplankton and zooplankton) are computed for each control volume. This is an efficient way to guarantee a high level of robustness in the code and to maintain it. This approach is also followed by DHI's MIKE system, which like MOHID, has several transport models.

1.2. Coupling hydrodynamic and biogeochemical models

One way to accomplish the coupling of a biogeochemical pelagic module with different eulerian transport models is to build a biochemical module that computes the reactions for one control volume. Consequently, the biochemical subroutines have to be called inside the loops, a method proved to be computational time consuming. The alternative is to build a module that solves the biochemical processes for a 1D array of control volumes. The MOHID system has an interface called ModuleInterface, responsible for transferring information (forcing conditions and state variables) from 1D, 2D or 3D structured grids to a 1D array and for calling the 0D biochemical module subroutines. MOHID system was developed following an object-oriented programming philosophy. This interface is a class (or module) currently used to transfer information from the module responsible for the transport processes in the water column to the module responsible for the biochemical process in the sediment. The same happens between the sediment transport module and sediment biochemical processes modules. In this way, ModuleWaterQuality is a zero-dimensional ecological model, which can be used by the eulerian or lagrangian transport modules. Figure 1 represents the information flux between the water quality module and other modules.

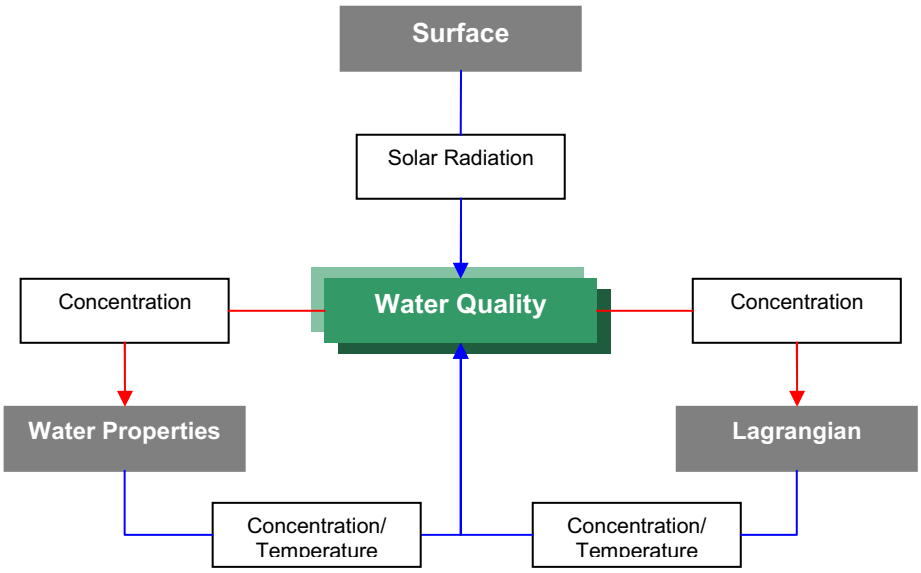

Figure 1: Information flux between Water Quality Module and the other modules.

1.3. Constructing the Interface

The interface construction phase consists on the memory allocation and options consistency to couple the transport model to the biochemical model. Thus, the variables needed to initialize the interface are:

- Name of the biochemical model to be executed;
- An array with the names of the state variables (properties) being modeled by the transport model, which have been defined to have sinks and sources terms using the defined biochemical equations; this is important, so that properties are defined coherently in both models and the properties indexing task can be performed straightforwardly;
- A mapping matrix (WaterPointsxD, being x the number of dimensions) that takes the value of 0 for land points and 1 for water points; this is used to define the size of the 1D arrays where most information will be stored and then given to the biochemical module.
- A size variable (SizexD, being x the number of dimensions), used to translate (loop through) 2D and 3D matrixes to 1D arrays.

1.3.1. Boundary conditions

MOHID assumes that the system that is being modelled is delimited by boundaries that can be in five different situations:

- Open surface: in contact with the atmosphere;
- Bottom: where shear stress and erosion/deposition of sediments are considered;
- Open lateral boundaries: where exchange fluxes with other water bodies are considered;
- Closed lateral boundaries: that can be fixed or movable(such as cells that are influenced by the tidal oscillations); Fluxes in these boundaries are considered always null; Rivers are considered as discharges

1.3.2. Interfacing during the run

ModuleInterface first task is to gather information on state variables needed by the biochemical models. So, the transport model must loop through all properties, sending its concentration as an argument. Optionally, other variables can also be sent, like radiation at the top of the control volume, control volume thickness and the light extinction coefficient field. Mapping arrays (WaterPointsxD and OpenPointsxD) must be given so that biochemical processes can be computed, if desired, for example, only in covered cells. OpenPointsxD is a variable, which takes the value of 0 if the cell is uncovered and 1 if it is covered with water.
State variables information (i.e. concentration of properties which have sinks and sources defined by the biochemical module) is stored in a bi-dimensional array with size equal to the number of

properties versus the number of control volumes, with each property properly indexed in this array. The indexing is done in the constructing phase in agreement with the two models. On the other hand, properties like temperature and salinity as well as light and mapping variables, are stored in specific 1D arrays.
The loop through all the properties continues until all information is gathered. This is achieved by creating a logical array with the indexed properties, defining the ones that have already been added to the state variables array. When everything is ready, the biochemical model is then called, looping through the number of control volumes, changing the state variables values.
The biochemical model time step can be, and often is, different from the transport model time step. The latter needs, due to numerical reasons, smaller time steps than the biochemical models. Thus, in each biochemical time step the state variables values are previously stored in another array, allowing to compute the concentration variation during this time step. This flux is then available to the transport model to actualize the properties concentration in its own time step.

1.4. The ecological Model

The ecological model described in *Module Water Quality* is adapted from EPA (1985) and pertain to the category of ecosystem simulations models i.e. sets of conservation equations describing as adequately as possible the working and the interrelationships of real ecosystem components. The nitrogen, oxygen, phosphorus and silica biogeochemical cycles are included. A brief description of these cycles is presented in the next sections.
Many of the equations are written as dependent on a regulating factor, which contains the functional response of the organism to some environmental parameters such as light, nutrients or temperature. When growth is a function of many resources, there is a large range of functional forms that might express the joint dependence. To control the various possibilities, it is common to think of separate resources as limiting factors reducing some theoretical maximum growth rate - factors that can be determined separately and the combined by a small number of ways.

1.4.1. State Variables

Variable	Description		Unit
Φ^{phy}	**Flagellates Concentration**	Organism	[mg C/l]
Φ^{dia}	Diatoms Concentration		[mg C/l]
Φ^{zoo}	**Mesozooplankton Concentration**		[mg C/l]
Φ^{cil}	Microzooplankton Concentration		[mg C/l]
Φ^{bact}	Bacteria Concentration		[mg C/l]
Φ^{NH_4}	**Ammonia Concentration**	Nitrogen	[mg N/l]
Φ^{NO_2}	**Nitrite Concentration**		[mg N/l]
Φ^{NO_3}	**Nitrate Concentration**		[mg N/l]
Φ^{PON}	**Particulate Organic Nitrogen Concentration**		[mg N/l]
Φ^{DONnr}	**Dissolved Organic Nitrogen Non Refractory Concentration**		[mg N/l]
Φ^{DONre}	**Dissolved Organic Nitrogen Refractory Concentration**		[mg N/l]
Φ^{IP}	**Inorganic Phosphorus Concentration**	Phosphorus	[mg P/l]
Φ^{POP}	**Particulate Organic Phosphorus Concentration**		[mg P/l]

Φ^{DOPnr}	**Dissolved Organic Phosphorus Non Refractory Concentration**		[mg P/l]
Φ^{DOPre}	**Dissolved Organic Phosphorus Refractory Concentration**		[mg P/l]
Φ^{DissSi}	Dissolved Silica Concentration	Silica	[mg Si/l]
Φ^{BioSi}	Biogenic Silica Concentration		[mg Si/l]
Φ^{oxy}	**Dissolved Oxygen Concentration**	Oxygen	[mg O_2/l]

Table 1: Water Quality Module available State Variables.

As mentioned before, in this study the model only simulates phytoplankton (flagellates) and zooplankton (mesozooplankton). The above table describes the state variables available to MOHID and, in bold, the ones used in this study.

1.4.2. Phytoplankton

Phytoplankton is described in terms of carbon concentration (mg C / l). The model assumes three limitations affecting the organisms maximum growth rate, μ_{max}^{X}: Temperature $\Psi(T)^{X}$, light effect $\Psi(E)^{X}$ and nutrient limitation, which is computed as the minimum of $\Psi(N)^{X}$, $\Psi(P)^{X}$. The model is able to consider either one or the two groups of primary producers.

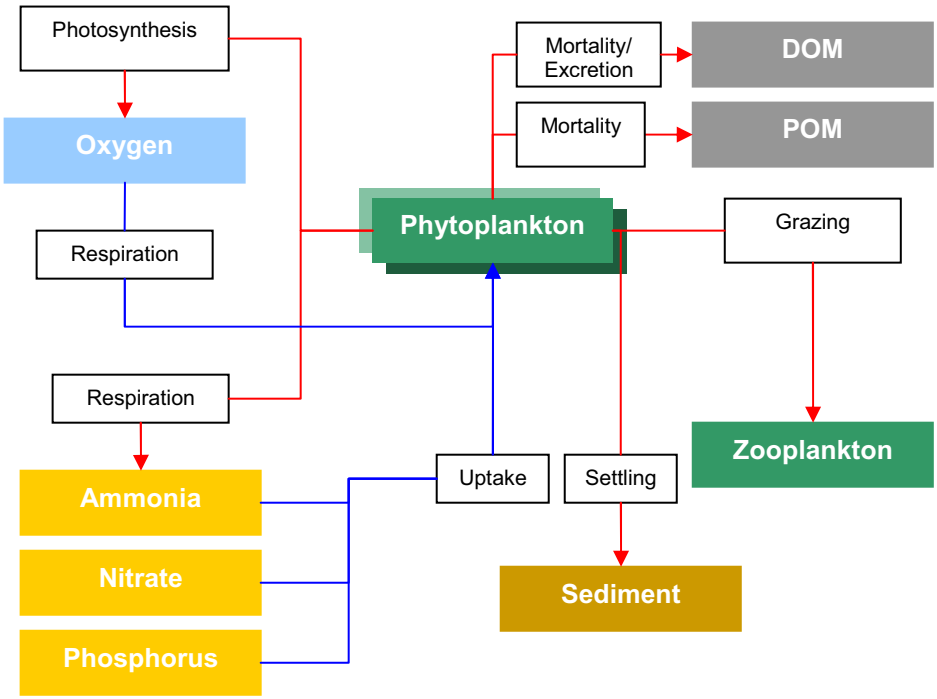

Figure 2: Internal Flux of Phytoplankton

The simulation of the primary producers is developed with the following considerations (Figure 2):

- Organisms consume inorganic nutrients (ammonia and nitrate from the nitrogen cycle and inorganic phosphorus from the phosphorus cycle, and silicate in the case of diatoms) depending on their availability;
- Organisms' growth is also influenced by the temperature and availability of light as a source of energy for photosynthesis;
- Dissolved oxygen is produced during respiration process consumes oxygen and produces ammonia;
- By excretion phytoplankton produces dissolved organic material (DONr, DONnr, DOPr and DOPnr);
- By mortality phytoplankton increases the dissolved organic material and the particulate organic material (PON and POP) in the system;
- By zooplankton grazing, the concentration of flagellates and diatoms decreases.

- By ciliates grazing, the concentration of flagellates decreases;
- Settling process is modeled in the ModuleWaterProperties as for any other particulate property in the model.

$$\frac{\partial \Phi^X}{\partial t} = \left(\mu^X - r^X - ex^X - m^X\right)\Phi^X - G^X \qquad X \equiv phy, dia$$

μ^X	Gross Growth Rate	[d-1]
r^X	Total Respiration Rate	[d-1]
ex^X	Excretion Rate	[d-1]
m^X	Natural Mortality Rate (non-predatory)	[d-1]
G^X	Grazing Rate	[mg C/l.d-1]

Phytoplankton limitation

Each growth limitation factor can range from a value of 0 to 1. A value of 1 means the factor does not limit growth (i.e. is at optimum intensity, nutrients are available in excess, etc) and a value of 0 means the factor is so severely limiting that growth is inhibit entirely.
The model uses:

- A minimum formulation only for nutrients limitation, in which the most severely limiting factor alone is assumed to limit growth. This formulation is based on "Liebig's law of the minimum" which states that the factor in shortest supply will control the growth of algae;
- A multiplicative formulation for the three main limiting factors (light, nutrients and temperature) in which all factors are multiplied together. This approach assumes that several factors in short supply will more severely limit growth than a single factor in short supply. The major criticism of this approach is that the computed growth rates may be excessively low when several factors are limiting. Also, the severity of the reduction increases with the number of limiting nutrients considered in the model, making comparison between models difficult.

The phytoplankton growth rate is computed as:

$$\mu^X = \mu^{\max} * \min(\mu^N, \mu^P) * \mu^L * \mu^T \qquad \textbf{(1)}$$

μ^X	Phytoplankton Growth Rate	[d-1]
$\mu^{\max}$	Maximum Growth Rate	[d-1]
μ^N	Nitrogen limitation factor	[adim]
μ^P	Phosphorus limitation factor	[adim]
μ^L	Light limitation factor	[adim]
μ^T	Temperature limitation factor	[adim]

Specific information about each parameter is presented ahead.

Phytoplankton equations

$$\frac{\partial \Phi^X}{\partial t} = \left(\mu^X - r^X - ex^X - m^X\right)\Phi^X - G^X \qquad X \equiv phy, dia$$

μ^X	Gross Growth Rate	[d-1]

r^X	Total Respiration Rate	[d-1]
ex^X	Excretion Rate	[d-1]
m^X	Natural Mortality Rate (non-predatory)	[d-1]
G^X	Grazing Rate	[mg C/l.d-1]

Symbol	*Description*	*Unit*	*Formulation*
μ^X	Gross Growth Rate	d^{-1}	$\mu^{phy} = \mu_{max}^{phy}.\Psi(T)^{phy}.\Psi(I)^{phy}.Min\left[\Psi(N)^{phy}, \Psi(P)^{phy}\right]$
			$\mu^{dia} = \mu_{max}^{dia}.\Psi(T)^{dia}.\Psi(I)^{dia}.Min\left[\Psi(N)^{dia}, \Psi(P)^{dia}, \Psi(Si)^{dia}\right]$
$\mu_{max}^X(T_{ref})$	Maximum Gross growth Rate at the reference temperature		[d^{-1}]
$\Psi(T)^X$	Temperature Limitation Factor		adim
$\Psi(I)^X$	Light Limitation Factor		adim
$\Psi(N)^X$	Nitrogen Limitation Factor		adim
$\Psi(P)^X$	Phosphorus Limitation Factor		adim
$\Psi(Si)^{dia}$	Silica Limitation Factor		adim

Table 2: Phytoplankton Gross Growth Rate

Symbol	Description	Unit	Formulation
$\Psi(T)^X$	***Temperature Limitation Factor***	***adim***	$\Psi(T)^X = K_A(T)^X K_B(T)^X$
$K_A(T)^X$	**-**	***adim***	$K_A(T)^X = \frac{K_1^X.e^{\gamma_1^X.\left(T-T_{\min}^X\right)}}{1+K_1^X.\left(e^{\gamma_1^X.\left(T-T_{\min}^X\right)}-1\right)}$
$K_B(T)^X$	**-**	***adim***	$K_B(T)^X = \frac{K_4^X.e^{\gamma_2^X.\left(T_{\max}^X-T\right)}}{1+K_4^X.\left(e^{\gamma_2^X.\left(T_{\max}^X-T\right)}-1\right)}$
γ_1^X	**-**	***adim***	$\gamma_1^X = \frac{Ln\frac{K_2^X\left(1-K_1^X\right)}{K_1^X\left(1-K_2^X\right)}}{T_{opt\min}^X - T_{\min}^X}$
γ_2^X	**-**	***adim***	$\gamma_2^X = \frac{Ln\frac{K_3^X\left(1-K_4^X\right)}{K_4^p\left(1-K_3^X\right)}}{T_{opt\max}^X - T_{\max}^X}$
K_1^X	***Constant to control temperature response curve shape***	***adim***	
K_2^X	***Constant to control temperature response curve shape***	***adim***	
K_3^X	***Constant to control temperature response curve shape***	***adim***	
K_4^X	***Constant to control temperature response curve shape***	***adim***	
$T_{\min}^X$	***Minimum tolerable temperature***	***[ºC]***	
$T_{\max}^X$	***Maximum tolerable temperature***	***[ºC]***	
$T_{opt_{\min}}^X$	***Minimum temperature of the optimal interval for organism activity***	***[ºC]***	
$T_{opt_{\max}}^X$	***Maximum temperature of the optimal interval for organism activity***	***[ºC]***	

Table 3: Temperature Limitation Factor

Symbol	Description	Unit	Formulation	
$\Psi(I)^X$	*Light Limitation Factor*	***adim***	$\Psi(I)^X = \frac{e^1}{k^X.z} \times \left(e^{-\frac{I_0}{I_{opt}^X} \times e^{(-k^X.z)}} - e^{-\frac{I_0}{I_{opt}^X}} \right)$	
k	*Light extinction coefficient in the water column*	***[m^{-1}]***	Constant	$k = \text{Constant}$
			Parsons et al. 1984	$k = 0.04+0.0088\text{Chla}+0.54\text{Chla}^{2/3}$
			Portela, 1996 (Tagus Estuary)	$k = 1.24 + 0.036 SPM$
			Combined Parsons and Portela	$k = [0.04 + 0.0088 Chla + 0.54 Chla^{2/3}] \times 0.7 + [0.036 \times 0.5 \times SPM]$
			Multiparameters	$k = \sum k^X \Phi^X$
$Chla$	*Chlorophyll a concentration*	***µgChl a/l***	$Chla = \Phi^X \times \alpha_{Chla:C} \times 1000$	
SPM	*Solid Suspended Matter Concentration*	***adim***	$SPM = \sum \Phi^X \quad X \equiv coesivese\,\text{dim}\,ents, PON, POP, phy, dia, zoo$	

z	***Depth***	***[m]***
$I_{o\ 1}$	***Incident Radiation***	***[W/m^2]***
I_{opt}^X	***Optimum light intensity for photosynthesis***	***[W/m^2]***
$\alpha_{Chloa:C}$	***Chlorophyll_a/C Ratio***	***[µgChla/ µgC]***

Table 4: Light Limitation Factor

Light extinction coefficient used in this study is the one from **Parsons et al. 1984**

SYMBOL	*DESCRIPTION*	*UNIT*	*FORMULATION*
$\Psi(N)^X$	NITROGEN LIMITATION FACTOR	ADIM	$\Psi(N)^X = \frac{\Phi^{NH_4} + \Phi^{NO_3}}{K_N^X + \Phi^{NH_4} + \Phi^{NO_3}}$
$\Psi(P)^X$	PHOSPHORUS LIMITATION FACTOR	ADIM	$\Psi(P)^X = \frac{\Phi^{IP}}{K_P^X + \Phi^{IP}}$
$\Psi(Si)^{dia}$	SILICA LIMITATION FACTOR IN DIATOMS GROWTH	ADIM	$\Psi(Si)^{dia} = \frac{\Phi^{DissSi}}{K_{Si}^{dia} + \Phi^{DissSi}}$

K_N^X	NITROGEN HALF-SATURATION CONSTANT	**[MGN/L]**
K_P^X	PHOSPHORUS HALF-SATURATION CONSTANT	**[MGP/L]**
K_{Si}^{dia}	SILICA HALF-SATURATION CONSTANT	**[MGSI/L]**

Table 5: Nutrients Linitation Factor

Symbol	Description	Unit	***Formulation***
r^X	Total Respiration Rate	d^{-1}	$r^X = k_{re}^X e^{(0.069T)} + k_{rp}^X \mu^X$ [EPA, 1985]

T	Temperature	[ºC]
k_{re}^X	Endogenous respiration constant	[d^{-1}]
k_{rp}^X	Photorespiration fraction	adim
μ^X	Growth Rate	[d^{-1}]

Table 6: Total Respiration Rate

[1] Computed in Light Extinction Module

Symbol	Description	Unit	*Formulation*
ex^X	Excretion Rate	d^{-1}	$ex^X = \varepsilon^X \mu^X (1-\psi(I)^X)$ [EPA, 1985]
ε^X	Excretion constant	adim	
μ^X	Growth Rate	[d^{-1}]	
$\psi(I)^X$	Light Limitation Factor	adim	

Table 7: Excretion Rate.

Symbol	*Description*	*Unit*	*Formulation*
m^X	Natural Mortality Rate	d^{-1}	$m^X = m^X_{\max} \frac{\frac{\Phi^X}{\mu^X}}{K^X_m + \frac{\Phi^X}{\mu^X}}$
$m^X_{\max}$	Maximum mortality rate	[d^{-1}]	
K^X_m	Mortality half-saturation rate	[mgC/l.d^{-1}]	
μ^X	Growth Rate	[d^{-1}]	

Table 8: Natural Mortality (Non-grazing) rate

SYMBOL	*DESCRIPTION*	*UNIT*	*DEFAULT VALUE*	*KEYWORD*
$\mu^{phy}_{\max}$	FLAGELLATES MAXIMUM GROSS GROWTH RATE	D^{-1}	2	GROWMAXF
k^{phy}_{re}	ENDOGENOUS RESPIRATION CONSTANT FOR FLAGELLATES	D^{-1}	0.0175	FENDREPC
k^{phy}_{rp}	FRACTION OF ACTUAL PHOTOSYNTHESIS WHICH IS OXIDIZED BY PHOTORESPIRATION FOR FLAGELLATES	ADIM	0.125	PHOTORES
ε^{phy}	EXCRETION CONSTANT FOR FLAGELLATES	ADIM	0.07	EXCRCONS
$m^{phy}_{\max}$	MAXIMUM MORTALITY RATE FOR FLAGELLATES	D^{-1}	0.02	FMORTMAX
K^{phy}_{m}	MORTALITY HALF-SATURATION RATE FOR FLAGELLATES	MG C $L^{-1}D^{-1}$	0.3	FMORTCON
E^{phy}	ASSIMILATION EFFICIENCY OF THE FLAGELLATES BY ZOOPLANKTON	ADIM	0.8	ASS_EFIC
K^{phy}_N	NITROGEN HALF-SATURATION CONSTANT FOR FLAGELLATES	MG N L^{-1}	0.014	NSATCONS
K^{phy}_P	PHOSPHORUS HALF-SATURATION CONSTANT FOR FLAGELLATES	MG P L^{-1}	0.001	PSATCONS
I^{phy}_{opt}	OPTIMUM LIGHT INTENSITY FOR FLAGELLATES PHOTOSYNTHESIS	WM^{-2}	121	PHOTOIN
$T^{phy}_{opt_{\min}}$	MINIMUM TEMPERATURE OF THE OPTIMAL INTERVAL FOR FLAGELLATES PHOTOSYNTHESIS	ºC	25	TOPTFMIN
$T^{phy}_{opt_{\max}}$	MAXIMUM TEMPERATURE OF THE OPTIMAL INTERVAL FOR FLAGELLATES PHOTOSYNTHESIS	ºC	26.5	TOPTFMAX
$T^{phy}_{\min}$	MINIMUM TOLERABLE TEMPERATURE FOR FLAGELLATES	ºC	4	TFMIN

	PHOTOSYNTHESIS			
$T_{\max}^{phy}$	MAXIMUM TOLERABLE TEMPERATURE FOR FLAGELLATES PHOTOSYNTHESIS	ºC	37	TFMAX
K_1^{phy}	CONSTANT TO CONTROL TEMPERATURE RESPONSE CURVE SHAPE ON FLAGELLATES	ADIM	0.05	TFCONST1
K_2^{phy}	CONSTANT TO CONTROL TEMPERATURE RESPONSE CURVE SHAPE ON FLAGELLATES	ADIM	0.98	TFCONST2
K_3^{phy}	CONSTANT TO CONTROL TEMPERATURE RESPONSE CURVE SHAPE ON FLAGELLATES	ADIM	0.98	TFCONST3
K_4^{phy}	CONSTANT TO CONTROL TEMPERATURE RESPONSE CURVE SHAPE ON FLAGELLATES	ADIM	0.02	TFCONST4
$\alpha_{N:C}^{phy}$	FLAGELLATES NITROGEN/CARBON RATIO	MGN/MG C	0.18	FRATIONC
$\alpha_{P:C}^{phy}$	FLAGELLATES PHOSPHORUS/CARBON RATIO	MGP/MG C	0.024	FRATIOPC
f_{inorg}^{phy}	FRACTION OF SOLUBLE INORGANIC MATERIAL EXCRETED BY FLAGELLATES	ADIM	0.4	FSOLEXCR
f_{orgD}^{phy}	FRACTION OF DISSOLVED ORGANIC MATERIAL EXCRETED BY FLAGELLATES	ADIM	0.5	FDISSDON

Table 9: Phytoplankton (Flagellates) Parameters

1.4.3. Zooplankton

Figure 3 represents the main processes considered by the model for microzooplankton and mesozooplankton simulation and the tables below describe the formulations used to compute the properties concentration evolution in time, described in carbon concentration (mg C/l). Like in primary producers, the two zooplankton groups have similar formulation differing in terms of specific parameters and grazing possibilities. Globally, zooplankton (micro and mesozooplankton) considers:
Organisms' growth is influenced by the temperature and prey concentration;
Respiration process consumes oxygen and produces ammonia;
Excretion represents a source of dissolved and particulate organic material (DONr, DONnr, DOPr and DOPnr) in the system;
By mortality, zooplankton increases the particulate organic material (PON and POP);
Microzooplankton grazing on bacteria and flagellates;
Mesozooplankton grazing on diatoms and flagellates.

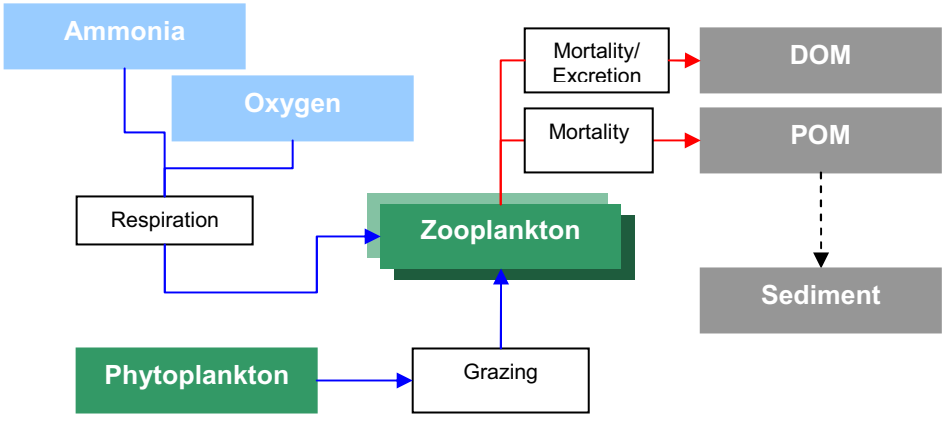

Figure 3: Zooplankton Processes.

Zooplankton equations and parameters

$$\frac{\partial \Phi^X}{\partial t} = \left(\mu^X - r^X - ex^X - m^X\right)\Phi^X - G^X$$

μ^X	Gross Growth Rate	[d^{-1}]
r^X	Total Respiration Rate	[d^{-1}]
ex^X	Excretion Rate	[d^{-1}]
m^X	Natural Mortality Rate (non-predatory)	[d^{-1}]
G^X	Grazing Rate	[mg C/l.d^{-1}]

Symbol	Description	Unit	Formulation	
μ^X	Gross Growth Rate	d^{-1}	1 Flagellates Group 1 Zooplankton Group	$\mu^{zoo} = \mu_{\max}^{zoo}.\Psi(T)^{zoo}.\Psi(F)^{zoo}$
			>1 Flagellates Group >1 Zooplankton Group	$\mu^{zoo} = \sum g_{zoo}^X G_{zoo}^X \qquad X \equiv phy, dia, cil$
				$\mu^{cil} = \sum g_{cil}^X G_{cil}^X \qquad X \equiv phy, bact$
$\Psi(T)^X$	Temperature Limitation Factor	adim	*See Table 2:* Phytoplankton Gross Growth Rate	
$\Psi(F)^{zoo}$	Food Limitation Factor	adim	$\Psi(F)^{zoo} = \begin{cases} 1 - e^{-\Lambda(\Phi^X - \Phi_{\min X}^{zoo})} \\ 0 \quad if \quad \Phi_{phy} < \Phi_{\min X}^{zoo} \end{cases}$	
r^X	Respiration Rate	d^{-1}	$r^X = \rho_{carbon}^X \Psi(T)^{zoo}$	
ex^X	Excretion Rate	d^{-1}	$ex^X = \left(k_{ex}^X b_{ex}^X\right)^T$	
m^X	Natural Mortality Rate (Non-grazing mortality	d^{-1}	$m^X = \begin{cases} \frac{a_m^X}{\Phi^{prey}} + m_{\min}^X & if\ \Phi^{prey} > \Phi_{\min_{prey}}^X \\ m_{\max}^X & if\ \Phi^{prey} \le \Phi_{\min_{prey}}^X \end{cases}$	$\Phi^{prey} = \sum \Phi^Y$ $Y \equiv \begin{cases} phy, dia, cil & if\ X = zoo \\ phy, bact & if\ X = cil \end{cases}$
G^{zoo}	Grazing Rate	d^{-1}	$G^{zoo} = p^{zoo} \Phi^{zoo}$	

Symbol	Description	Unit
$\mu_{\max}^X$	Maximum Gross growth Rate	$[d^{-1}]$
g_Y^X	Assimilation Coefficient of Y by X	adim
Λ	Ivlev grazing constant	[l/mgC]
ρ_{carbon}^X	Carbon consumption Rate in respiration	$[d^{-1}]$
k_{ex}^X	Excretion Rate at 0º	$[d^{-1}]$
b_{ex}^X	Constant for excretion curve	adim
a_m^X	Constant for mortality curve	adim
$m_{\min}^X$	Minimum Natural Mortality Rate	$[d^{-1}]$
$m_{\max}^X$	Maximum Natural Mortality Rate	$[d^{-1}]$
$\Phi_{\min_{prey}}^X$	Minimum prey concentration for grazing	[mgC/l]
p^{zoo}	Zooplankton predatory mortality rate: predation by higher trophic levels	$[d^{-1}]$
G_Y^X	Y Grazing on X	[mg C/l.d^{-1}]

Table 10: Zooplankton(Mesozooplankton) Formulations

Symbol	Description	Unit	Value	Keyword
$\mu_{\max}^{zoo}$	Zooplankton Maximum gross growth rate	d-1	0.15	GROWMAXZ
$\alpha_{N:C}^{zoo}$	Zooplankton Nitrogen/Carbon Ratio	mg N/mgC	0.15	ZRATIONC
$\alpha_{P:C}^{zoo}$	Zooplankton Phosphorus/Carbon Ratio	mg P/mgC	0.024	ZRATIOPC
f_{inorg}^{zoo}	Soluble inorganic fraction on the mesozooplankton excretions	adim	0.4	ZSOLEXCR
f_{orgD}^{zoo}	Fraction of dissolved organic material excreted by mesozooplankton	adim	0.5	ZDISSDON

$T^{zoo}_{opt_{\min}}$	Minimum temperature of the optimal interval for mesozooplankton growth	°C	24.8	TOPTZMIN
$T^{zoo}_{opt_{\max}}$	Maximum temperature of the optimal interval for mesozooplankton growth	°C	25.1	TOPTZMAX
$T^{zoo}_{\min}$	Minimum temperature mesozooplankton growth	°C	5	TZMIN
$T^{zoo}_{\max}$	Minimum temperature of the optimal interval for mesozooplankton growth	°C	35	TZMAX
K^{zoo}_{1}	Constant to control temperature response curve shape on mesozooplankton	adim	0,05	TZCONST1
K^{zoo}_{2}	Constant to control temperature response curve shape on mesozooplankton	adim	0,98	TZCONST2
K^{zoo}_{3}	Constant to control temperature response curve shape on mesozooplankton	adim	0,98	TZCONST3
K^{zoo}_{4}	Constant to control temperature response curve shape on mesozooplankton	adim	0,02	TZCONST4
ρ^{zoo}_{carbon}	Rate of mesozooplankton consumption of Carbon by respiration and non-predatory mortality	d-1	0.036	ZREFRESP
Λ	Ivlev grazing constant	l/mgC	1.6	IVLEVCON
p^{zoo}	Zooplankton predatory mortality rate: predation by higher trophic levels	d-1	0.02	ZPREDMOR
$\Phi^{zoo}_{\min_{prey}}$	Minimum prey concentration for mesozooplankton grazing	mgC/l	0.0045	ZOOPREYMIN
$\Phi^{zoo}_{\min_{cil}}$	Minimum Microzooplankton concentration for mesozooplankton grazing	mgC/l	0.0045	GRAZCILMIN
$\Phi^{zoo}_{\min_{phy}}$	Minimum Flagellates concentration for mesozooplankton grazing	mgC/l	0.0045	GRAZFITOMIN
$\Phi^{zoo}_{\min_{dia}}$	Minimum Diatoms concentration for mesozooplankton grazing	mg C/l	0.0045	DIGRAZMIN
k^{zoo}_{ex}	Zooplankton Excretion Rate	d-1	0.02	ZEXCFAC
b^{zoo}_{ex}	Constant for mesozooplankton excretion curve	adim	1.0305	ZEXCCONS
a^{zoo}_{m}	Constant for mesozooplankton mortality curve	adim	0.0	MORTZCOEF
$m^{zoo}_{\min}$	Minimum Rate for mesozooplankton Natural Mortality	d-1	0.001	MINMORTZ
$m^{zoo}_{\max}$	Maximum Rate for mesozooplankton Natural Mortality	d-1	0.04	MAXMORTZ
K^{zoo}_{graz}	Half-Saturation Constant for Grazing	mgC/l	0.85	INGCONSZ
c^{zoo}_{phy}	Capture Efficiency of flagellates by mesozooplankton	adim	0.8	ZOOEFFCAPHY
c^{zoo}_{cil}	Capture Efficiency of Microzooplankton by mesozooplankton	adim	0.2	ZOOEFFCAPCIL
c^{zoo}_{dia}	Capture efficiency of Diatoms by mesozooplankton	adim	0.8	DIZOOEFFCAP
$I^{zoo}_{\max}$	Zooplankton maximum ingestion rate	d-1	1.0	ZINGMAX
g^{zoo}_{phy}	Assimilation Coefficient of Flagellates by mesozooplankton	adim	0.8	ZOPHYASS
g^{zoo}_{cil}	Assimilation Coefficient of Microzooplankton by mesozooplankton	adim	0.8	ZOCILASS
g^{zoo}_{dia}	Assimilation Coefficient of Diatoms by mesozooplankton	adim	0.8	DIZOASS
ρ^{zoo}_{phy}	Proportion of flagellates in mesozooplankton ingestion	adim	0.3	PHYRATING
ρ^{zoo}_{cil}	Proportion of Microzooplankton in mesozooplankton ingestion	adim	0.3	CILRATINGZOO
ρ^{zoo}_{dia}	Proportion of Diatoms in mesozooplankton ingestion	adim	0.3	DIRATINGZOO

Table 11: Zooplankton Parameters

Grazing

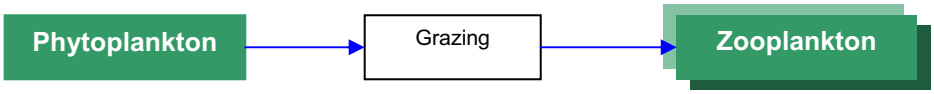

Figure 4: Grazing Processes.

$$G^{phy} = G^{phy}_{zoo} \Phi^{zoo}$$

G^X	Total Grazing Rate on X	mgC(X)/l.d-1
G^X_Y	Y Grazing on X	d^{-1}

Symbol	Description	Unit	***Formulation***
(1) Flagellates and Zooplankton Simulation			$G^{phy}_{zoo} = \frac{\mu^{zoo}}{E^{phy}}$
(2) Diatoms and Zooplankton Simulation			$G^{dia}_{zoo} = \frac{\mu^{zoo}}{E^{dia}}$
(3) Flagellates, Diatoms and Zooplankton Simulation			$G^{dia}_{zoo} = \rho^{dia}_{zoo}.I^{zoo}_{\max}.\Psi^{dia}_{zoo}.\Psi(T)^{zoo}$ $G^{phy}_{zoo} = \rho^{phy}_{zoo}.(I^{zoo}_{\max} - G^{dia}_{zoo}).\Psi^{dia}_{zoo}.\Psi(T)^{zoo}$
(4) Flagellates, Macrozooplankton, Microzooplankton and Bacteria			$\begin{cases} G^{phy}_{zoo} = \rho^{phy}_{zoo}.I^{zoo}_{\max}.\Psi^{phy}_{zoo}.\Psi(T)^{zoo} \\ G^{phy}_{cil} = \rho^{phy}_{cil}.I^{cil}_{\max}.\Psi^{phy}_{cil}.\Psi(T)^{cil} \end{cases}$ $G^{cil}_{zoo} = \rho^{cil}_{zoo}.(I^{zoo}_{\max} - G^{phy}_{zoo}).\Psi^{dia}_{zoo}.\Psi(T)^{zoo}$ $G^{bact}_{cil} = \rho^{bact}_{cil}.I^{cil}_{\max}.\Psi^{bact}_{cil}.\Psi(T)^{cil}$
(5) Diatoms, Macrozooplankton, Microzooplankton and Bacteria			$G^{dia}_{zoo} = \rho^{dia}_{zoo}.(I^{zoo}_{\max}).\Psi^{dia}_{zoo}.\Psi(T)^{zoo}$ $G^{cil}_{zoo} = \rho^{cil}_{zoo}.(I^{zoo}_{\max} - G^{dia}_{zoo}).\Psi^{cil}_{zoo}.\Psi(T)^{zoo}$ $G^{bact}_{cil} = \rho^{bact}_{cil}.I^{cil}_{\max}.\Psi^{bact}_{cil}.\Psi(T)^{cil}$
(6) Diatoms, Flagellates, Macrozooplankton,Microzooplankton and Bacteria Simulation			$G^{dia}_{zoo} = \rho^{dia}_{zoo}.(I^{zoo}_{\max}).\Psi^{dia}_{zoo}.\Psi(T)^{zoo}$ $\begin{cases} G^{phy}_{zoo} = \rho^{phy}_{zoo}.(I^{zoo}_{\max} - G^{dia}_{zoo}).\Psi^{phy}_{zoo}.\Psi(T)^{zoo} \\ G^{phy}_{cil} = \rho^{phy}_{cil}.I^{cil}_{\max}.\Psi^{phy}_{cil}.\Psi(T)^{cil} \end{cases}$ $G^{cil}_{zoo} = \rho^{cil}_{zoo}.(I^{zoo}_{\max} - G^{dia}_{zoo} - G^{phy}_{zoo}).\Psi^{cil}_{zoo}.\Psi(T)^{zoo}$ $G^{bact}_{cil} = \rho^{bact}_{cil}.I^{cil}_{\max}.\Psi^{bact}_{cil}.\Psi(T)^{cil}$
Ψ^X_Y	Y Grazing Limitation by X concentration	adim	$\Psi^X_Y = \begin{cases} \frac{c^X_Y.\Phi^X - \Phi^{\min X}_Y}{K^Y_{graz} + (c^X_Y.\Phi^X - \Phi^{\min X}_Y)} & if\ (c^X_Y.\Phi^X - \Phi^{\min X}_Y) > 0 \\ 0 & c.c \end{cases}$	
X	Predated organism		
Y	Predator organism		

μ^X	Growth rate	d^{-1}
$\Psi(T)^X$	Temperature Limitation Factor	adim
K^Y_{graz}	Half-saturation constant for predation	[mg C/l]
c^X_Y	Y capture efficiency on X	adim
ρ^X_Y	Proportion of X in Y ingestion	adim
$\Phi^{\min X}_Y$	Minimum X concentration for Y grazing	[mgC/l]
E^X	Assimilation efficiency of X by zooplankton $(X \equiv phy, dia)$	adim
$I^Y_{\max}$	Y maximum ingestion rate	d^{-1}

Table 12: Grazing Formulation

1.4.4. Nitrogen Cycle

In the Mohid water quality module, the nitrogen appears as organic and inorganic nitrogen.
The inorganic nitrogen is divided into ammonia (NH_4), nitrite (NO_2) and nitrate (NO_3).
The organic nitrogen is divided into particulate organic nitrogen (PON), dissolved organic nitrogen non refractory (DONnr) and dissolved organic nitrogen refractory (DONre). DONnr includes small molecular substrates, assumed to be degraded in the day of production and DONre with a longer turn over.

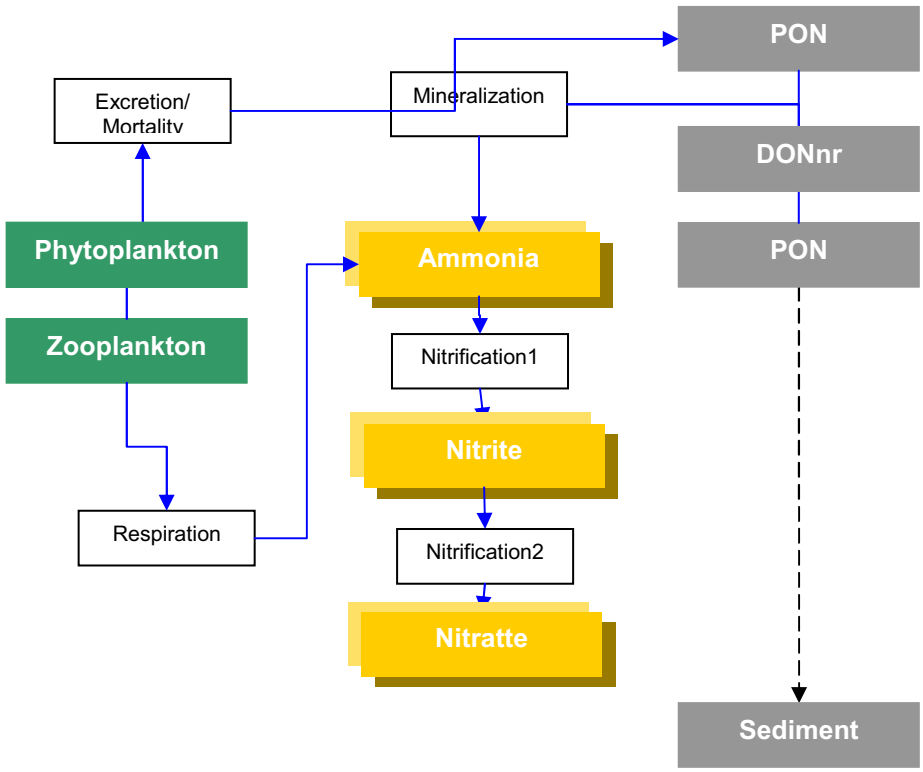

Figure 5: Nitrogen Biogeochemical Cycle.

Ammonia

The sources of ammonia are the organic forms of nitrogen (PON, DONnr and DONre) due to decay and phytoplankton due to the dark respiration process. The sinks of ammonia are nitrite (nitrification) and phytoplankton (uptake).

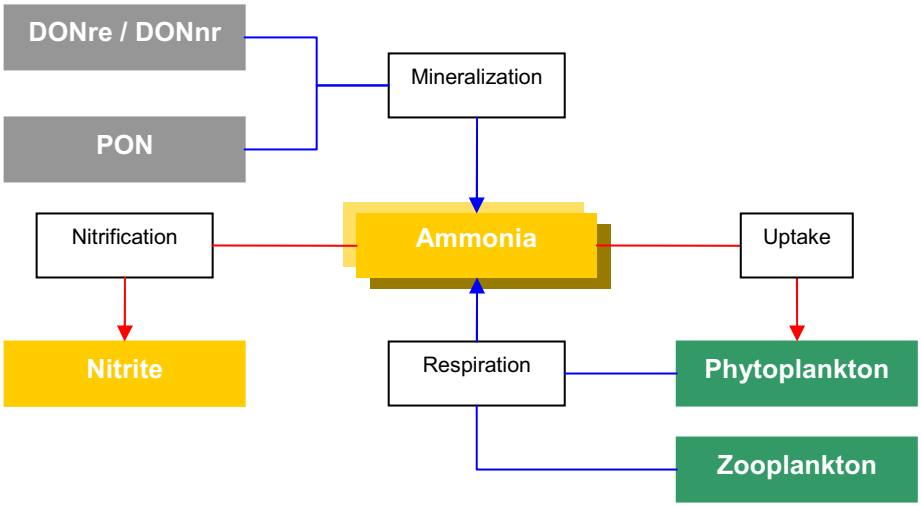

Figure 6: Internal Flux ammonia

The rate equation of ammonia is given by:

$$\frac{\partial \Phi_{NH4}}{\partial t} = \left(f_{in/Phy} ex_{Phy} - \mu_{NH4}\right)\Phi_{Phy} + f_{in/Z} ex_z \Phi_z + \varphi_{Nre}\Phi_{DONre} + \varphi_{Nnr}\Phi_{DONnr} + f_{orgP/Phy}\varphi_{det}\Phi_{PON}$$

The assimilation rate of NH_4, μ_{NH4}, is given by:

$$\mu_{NH4} = \beta_{NH4}\alpha_{N:C}\mu_{Phy}$$

where β_{NH4} is the ammonia preference factor given by:

$$\beta_{NH4} = \frac{\Phi_{NH_4} \cdot \Phi_{NO_3}}{\left(K_N + \Phi_{NH_4}\right)\left(K_N + \Phi_{NO_3}\right)} \cdot \frac{\Phi_{NH_4} \cdot K_N}{\left(K_N + \Phi_{NH_4}\right)\left(K_N + \Phi_{NO_3}\right)}$$

and $\alpha_{N:C}$ represents the Redfield ratio between N:C.
The mineralization rate of DONre, φ_{Nre} is given by:

$$\varphi_{Nre} = M_{DONre}\theta_{DONre}(T - T_{ref})\frac{\Phi_{Phy}}{K_{PhyNut\,\mathrm{Re}\,ge} + \Phi_{Phy}}$$

where

M_{DONre} – reference rate for the mineralization of DONre
θ_{DONre} – temperature coefficient for the mineralization of DONre
T_{ref} – reference temperature
$K_{PhyNutRege}$ – half saturation constant for the regeneration of phytoplankton

The mineralization rate of DONnr, φ_{Nnr} is given by:

$$\varphi_{Nnr} = M_{DONnr}\theta_{DONnr}(T - T_{ref})$$

where

M_{DONnr} – reference rate for the mineralization of DONnr
θ_{DONnr} – temperature coefficient for the mineralization of DONnr

The dissolution rate of PON, φ_{det}, is given by:

$$\varphi_{det} = M_{det}\theta_{det}(T - T_{ref})$$

where

M_{det} – reference rate for the dissolution of PON
θ_{det} – temperature coefficient for the dissolution

Nitrite

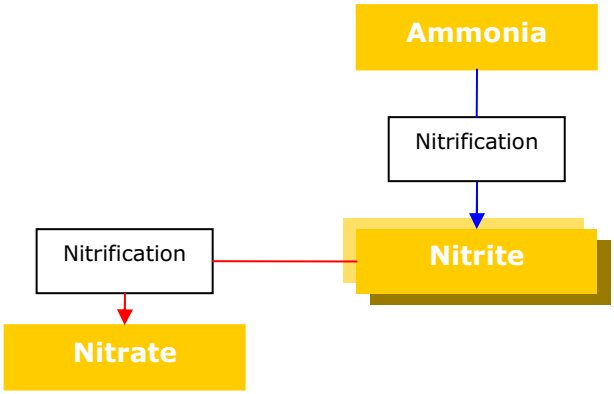

Figure 7: Internal Flux Nitrite

The rate equation of nitrite is given by:

$$\frac{\partial \Phi_{NO2}}{\partial t} = \varphi_{2N}\Phi_{NH4} - \varphi_{2N}\phi_{NO2}$$

with the rate of nitrification, φ_{2N} is given by:

$$\varphi_{2N} = M_{nit}\theta_{nit}\left(T - T_{ref}\right)\frac{\Phi_{O2}}{K_{nit} + \Phi_{O2}}$$

where

M_{nit} – reference rate of nitrification
θ_{nit} – temperature coefficient for nitrification
K_{nit} – half saturation constant for nitrification

Nitrate

The source of nitrate, modeled by Mohid, is nitrite and the sink the uptake by phytoplankton.

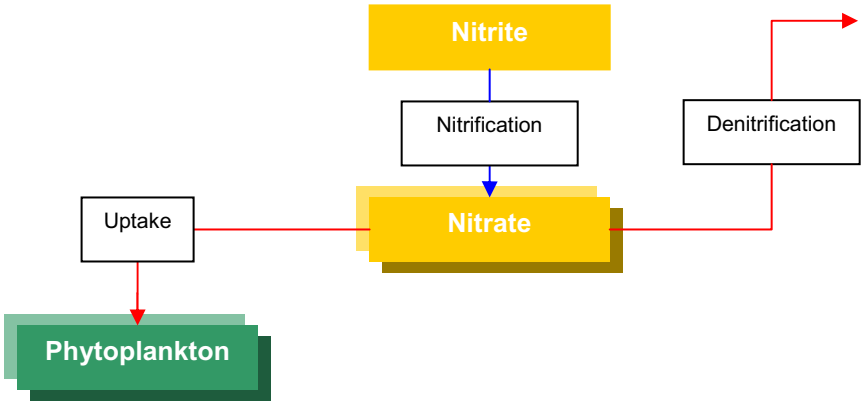

Figure 8: Internal Flux Nitrate

The rate equation of nitrate is given by:

$$\frac{\partial \Phi_{NO3}}{\partial t} = \varphi_{2N}\Phi_{No2} - \varphi_{2N}\phi_{NO3} - \mu_{NO3}$$

The assimilation rate of NO_3, μ_{NO3}, is given by:

$$\mu_{NO3} = (1 - \beta_{NH4})\alpha_{N:C}\mu_{Phy}$$

Particulate Organic Nitrogen

The sources of PON are the mortality of phytoplankton and zooplankton and the sinks are the mineralization to ammonia and the decomposition to DONre.

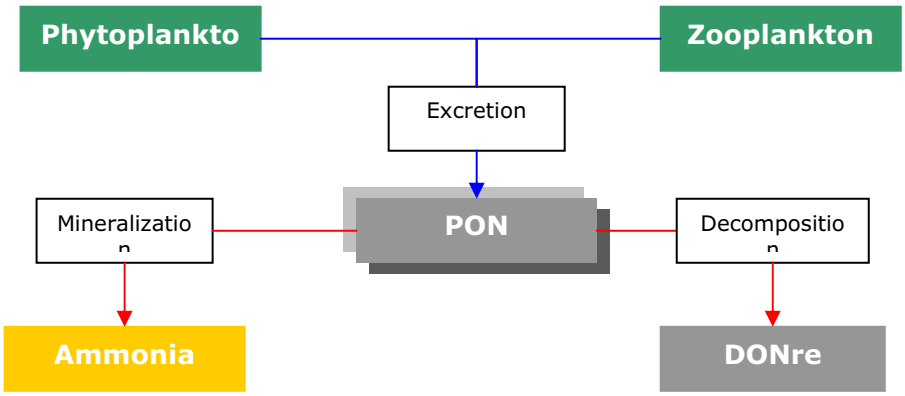

Figure 9: Internal Flux of PON

The rate equation of the PON is given by:

$$\frac{\partial \Phi_{PON}}{\partial t} = \left[\left(1 - f_{orgD/Phy}\right)\left(1 - f_{in/Phy}\right)ex_{Phy} + m_{Phy}\right]\Phi_{Phy} +$$

$$\left[\left(1 - f_{orgD/Z}\right)\left(1 - f_{in/Z}\right)ex_{Z} + m_{Z}\right]\Phi_{Z} - \varphi_{\det}\Phi_{PON}$$

All variables have the same meaning as in the previous paragraphs.

Non Refractory Dissolved Organic Nitrogen (DONnr)

The sources of DONnr are the mortality and the excretions of phytoplankton and zooplankton and the sinks are the mineralization to ammonia.

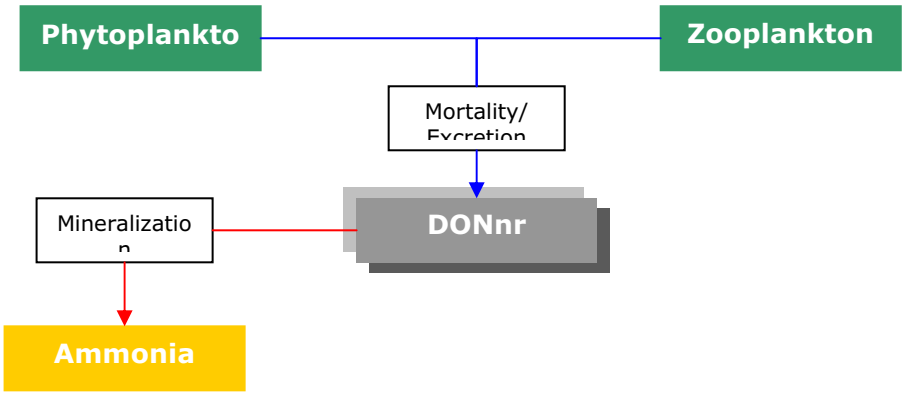

Figure 10: Internal Flux of DONnr

The rate equation of the DONnr is given by:

$$\frac{\partial \Phi_{DONnr}}{\partial t} = f_{orgD/Phy}\left(1 - f_{in/Phy}\right)ex_{Phy}\Phi_{Phy}$$

$$+ f_{orgD/Z}\left(1 - f_{in/Z}\right)ex_{Z}\Phi_{Z} - \varphi_{Nnr}\Phi_{DONnr}$$

All variables have the same meaning as in the previous paragraphs.

Refractory Dissolved Organic Nitrogen

The source of DONre is the decomposition of the PON and the sink is the mineralization to ammonia.

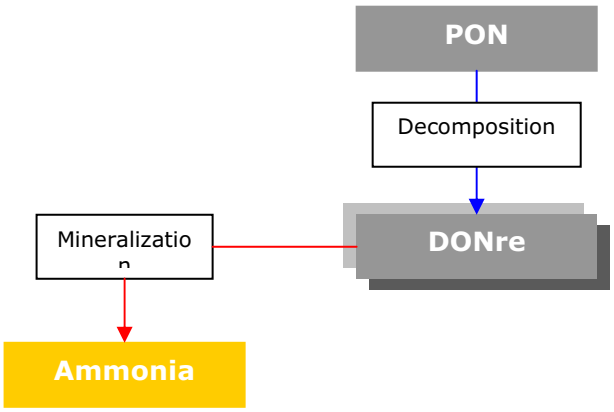

Figure 11: Internal Flux of DONr

The rate equation of the DONre is given by:

$$\frac{\partial \Phi_{DONre}}{\partial t} = \varphi_{\det} \Phi_{PON} (1 - f_{orgP/Phy}) - \varphi_{Nr} \Phi_{DONre}$$

All variables have the same meaning as in the previous paragraphs.

Symbol	*Description*	*Unit*	*Formulation*	
$\beta_{NH_4}^X$	X ammonia preference factor	adim	$\beta_{NH4}^X = \left(\frac{\Phi^{NH4}}{K_N^X + \Phi^{NH4}}\right)\left(\frac{\Phi_{NO3}}{K_N^X + \Phi^{NO3}}\right) + \left(\frac{\Phi^{NH4}}{\Phi_{NO3} + \Phi^{NH4}}\right)\left(\frac{K_N^X}{K_N^X + \Phi^{NO3}}\right) \quad X \equiv phy, dia$	
K_{dec}^{PON}	PON decomposition Rate	d^{-1}	$K_{dec}^{PON} = K_{dec}^{PON}(T_{ref}).\theta_{dec}^{(T-T_{ref})}$	
$K_{\min}^{DONre}$	DONre mineralization Rate	d^{-1}	$K_{dec}^{DONre} = K_{\min}^{DONre}(T_{ref}).(\theta_{\min}^{DONre})^{(T-T_{ref})} \frac{\sum \Phi^X}{K_r^{phy} + \sum \Phi^X} \quad X \equiv phy, dia$	
$K_{\min}^{DONnr}$	DONnr mineralization Rate	d^{-1}	$K_{\min}^{DONnr} = K_{\min}^{DONnr}(T_{ref}).\theta_{\min}^{DONnr(T-T_{ref})} \frac{\sum \Phi^X}{K_r^{phy} + \sum \Phi^X} \quad X \equiv phy, dia$	
K_{nit}	Nitrification Rate	d^{-1}	$K_{nit} = K_{nit}^{ref}(T_{ref})\theta_{nit}^{(T-T_{ref})} \frac{\Phi^{oxy}}{K_{nit}^{sat} + \Phi^{oxy}}$	
K_{dnit}	Denitrification Rate	d^{-1}	$K_{dnit} = K_{dnit}^{ref}(T_{ref})\theta_{dnit}^{(T-T_{ref})} \frac{K_{dnit}^{sat}}{K_{dnit}^{sat} + \Phi^{oxy}}$	
δ_N^Y	Non-assimilated material by Y	d^{-1}	1 Phytoplankton Group 1 Zooplankton Group	$\delta_N^{zoo} = (1 - E^X)\frac{\mu^{zoo}}{E^X}\alpha_{N:C}^X \quad Y \equiv phy, dia$
			>1 Phytoplankton Group >1 Zooplankton Group	$\delta_N^{zoo} = \sum[(1 - g_{zoo}^X)G_{zoo}^X \alpha_{N:C}^X] \quad Y \equiv phy, dia, cil$ $\delta_N^{cil} = \sum[(1 - g_{cil}^X)G_{cil}^X \alpha_{N:C}^X] \quad Y \equiv phy, bact$
φ_N^Y	Stoichiometric food web losses	d^{-1}	1 Phytoplankton Group 1 Zooplankton Group	$\varphi_N^{zoo} = \mu^{zoo}(\alpha_{N:C}^{phy} - \alpha_{N:C}^{zoo})$
			>1 Phytoplankton Group >1 Zooplankton Group	$\varphi_N^{zoo} = \sum(\alpha_{N:C}^X - \alpha_{N:C}^{zoo})g_{zoo}^X G_{zoo}^X \quad X \equiv phy, dia, cil$ $\varphi_N^{cil} = \sum(\alpha_{N:C}^X - \alpha_{N:C}^{cil})g_{cil}^X G_{cil}^X \quad X \equiv phy, bact$

T	Water Temperature	°C
T_{ref}	Reference Temperature	20 °C
K_N^X	Nitrogen half-saturation constant	mg N l^{-1}
E^X	Assimilation efficiency of X by zooplankton	adim
g_Y^X	Assimilation Coefficient of X by Y	adim
G_Y^X	Y grazing on X	[d^{-1}]
$\alpha_{N:C}^X$	Nitrogen/Carbon Ratio	mg N/mgC
μ^X	Growth rate	[d^{-1}]
ex^X	Excretion Rate	[d^{-1}]
r^X	Respiration Rate	[d^{-1}]

m^X	Natural Mortality Rate	[d^{-1}]
p^{zoo}	Zooplankton predatory mortality rate: predation by higher trophic levels	[d^{-1}]
$K_{dec}^{PON}(T_{ref})$	PON decomposition rate at reference temperature	d^{-1}
θ_{dec}	PON decomposition temperature coefficient	adim
$K_{\min}^{DONre}(T_{ref})$	DONre mineralization rate at reference temperature	d^{-1}
$\theta_{\min}^{DONre}$	DONre mineralization temperature coefficient	adim
K_r^{phy}	Nutrient Regeneration Half-Saturation Constant	mgC/ l
$K_{\min}^{DONnr}(T_{ref})$	DONnr mineralization Rate at reference temperature	d^{-1}
$\theta_{\min}^{DONr}$	DONre minreralization temperature coefficient	adim
$K_{nit}^{ref}(T_{ref})$	Nitrification rate at reference temperature	adim
θ_{nit}	Nitrification temperature coefficient	adim
K_{nit}^{sat}	Nitrification half-saturation constant	mg O_2/l
$K_{dnit}(T_{ref})$	Denitrification Rate at reference temperature	d^{-1}
θ_{dnit}	Denitrification temperature coefficient	adim
f_{inorg}^X	Fraction of inorganic material excreted by X	adim
f_{orgD}^X	Dissolved organic fraction excreted by X	adim
f_{orgP}	Fraction of PON available for mineralization	adim

Table 13: Nitrogen Formulations

Symbol	*Description*	*Unit*	*Value*	Keyword
$K_{dec}^{PON}(T_{ref})$	PON decomposition Rate at reference temperature	d^{-1}	0.1	NOPREF
θ_{dec}	PON decomposition temperature coefficient	adim	1.02	NOPCOEF
$K_{\min}^{DONre}(T_{ref})$	DONre mineralization Rate at reference temperature	d^{-1}	0.01	NMINR
$\theta_{\min}^{DONre}$	DONre minreralization temperature coefficient	adim	1.02	TMINR
K_r^{phy}	Nutrient Regeneration Half-Saturation Constant	mgC/ l	1	FREGSATC
$K_{nit}(T_{ref})$	Nitrification Rate at reference temperature	d^{-1}	0.06	NITRIREF
K_{nit}^{sat}	Nitrification half-saturation constant	mg O_2/l	2.0	NITSATCO
K_{dnit}^{sat}	Denitrification half-saturation constant	mg $O_{2/l}$	0.1	DENSATCO
θ_{nit}	Nitrification temperature coefficient	adim	1.08	TNITCOEF
$K_{dnit}(T_{ref})$	Denitrification Rate at reference temperature	d^{-1}	0.125	DENITREF
θ_{dnit}	Denitrification temperature coefficient	adim	1.045	TDENCOEF
$K_{\min}^{DONnr}(T_{ref})$	DONnr mineralization Rate at reference temperature	d^{-1}	0.1	NMINENR
$\theta_{\min}^{DONr}$	DONre minreralization temperature coefficient	adim	1.02	TMINNR
f_{orgP}	Fraction of PON available for mineralization	adim	0.7	PHDECOMP

Table 14: Nitrogen Parameters

1.4.5. Phosphorus Cycle

In the Mohid water quality module, phosphorus appears, like nitrogen, in an organic and an inorganic form.
The inorganic phosphorus is assumed to be available as orthophosphate (PO_4) for uptake by phytoplankton.
The organic phosphorus is divided into particulate organic phosphorus (POP), dissolved organic phosphorus non refractory (DOPnr) and dissolved organic phosphorus refractory (DOPre). The rate equations of phosphorus are implemented in the same way as the nitrogen cycle, except that there is just one compartment of inorganic phosphorus.

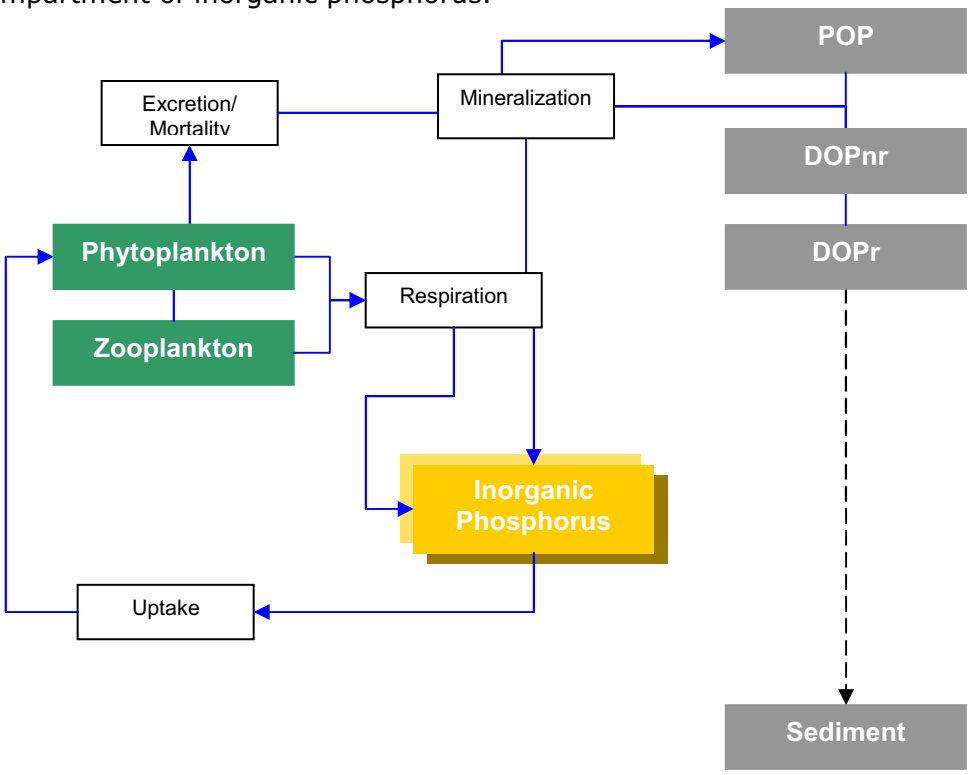

Figure 12: Phosphorus biogeochemical cycle

Inorganic Phosphorus

$$\frac{\partial \Phi^{IP}}{\partial t} = \underbrace{\left[f_{inorg}^{phy}(ex^{phy} + r^{phy})\alpha_{P:C}^{phy} - \mu^{phy}\alpha_{P:C}^{phy} \right]\Phi^{phy}}_{flagellates}$$
$$+ \underbrace{\left[f_{inorg}^{dia}(ex^{dia} + r^{dia})\alpha_{P:C}^{dia} - \mu^{dia}\alpha_{P:C}^{dia} \right]\Phi^{dia}}_{diatoms}$$
$$+ \underbrace{[(f_{inorg}^{zoo} ex^{cil} + r^{cil})\alpha_{P:C}^{cil}]\Phi^{cil}}_{microzooplankton}$$
$$+ \underbrace{\left[(f_{inorg}^{zoo} ex^{zoo} + r^{zoo})\alpha_{P:C}^{zoo} \right]\Phi^{zoo}}_{mesozooplankton}$$
$$+ \underbrace{K_{\min}^{DOPre}\Phi^{DOPre}}_{DOPre} + \underbrace{K_{\min}^{DOPnr}\Phi^{DOPnr}}_{DOPnr} + \underbrace{f_{orgP}K_{dec}^{POP}\Phi^{POP}}_{POP}$$

Particulate Organic Phosphorus

$$\frac{\partial \Phi^{POP}}{\partial t} = \underbrace{\left[(1-f_{inorg}^{phy})(1-f_{orgD}^{phy})(ex^{phy} + r^{phy}) + m^{phy} \right]\alpha_{P:C}^{phy}\Phi^{phy}}_{flagellates}$$
$$+ \underbrace{\left[(1-f_{inorg}^{dia})(1-f_{orgD}^{dia})(ex^{dia} + r^{dia}) + m^{dia} \right]\alpha_{P:C}^{dia}\Phi^{dia}}_{diatoms}$$
$$+ \underbrace{\left[(1-f_{inorg}^{zoo})(1-f_{orgD}^{zoo})ex^{cil} + m^{cil} \right]\alpha_{P:C}^{cil}\Phi^{cil} + (\delta_P^{cil} + \varphi_P^{cil})\Phi^{cil}}_{microzooplankton}$$
$$+ \underbrace{\left[(1-f_{inorg}^{zoo})(1-f_{orgD}^{zoo})ex^{zoo} + m^{zoo} + p^{zoo} \right]\alpha_{P:C}^{zoo}\Phi^{zoo} + (\delta_P^{zoo} + \varphi_P^{zoo})\Phi^{zoo}}_{mesozooplankton}$$
$$- \underbrace{(1-f_{orgP})K_{dec}^{POP}\Phi^{POP}}_{DONre}$$
$$- \underbrace{f_{orgP}K_{dec}^{POP}\Phi^{POP}}_{IP}$$

Non Refractory Dissolved Organic Phosphorus

$$\frac{\partial \Phi^{DOPnr}}{\partial t} = \underbrace{(1-f_{inorg}^{phy})f_{orgD}^{phy}(ex^{phy} + r^{phy})\alpha_{P:C}^{phy}\Phi^{phy}}_{flagellates} +$$
$$+ \underbrace{(1-f_{inorg}^{dia})f_{orgD}^{dia}(ex^{dia} + r^{dia})\alpha_{P:C}^{dia}\Phi^{dia}}_{diatoms}$$
$$+ \underbrace{(1-f_{inorg}^{zoo})f_{orgD}^{zoo}ex^{cil}\alpha_{P:C}^{cil}\Phi^{cil}}_{microzooplankton}$$
$$+ \underbrace{(1-f_{inorg}^{zoo})f_{orgD}^{zoo}ex^{zoo}\alpha_{P:C}^{zoo}\Phi^{zoo}}_{mesozooplankton}$$
$$- \underbrace{K_{\min}^{DOPnr}\Phi^{DOPnr}}_{IP}$$

Refractory Dissolved Organic Phosphorus

$$\frac{\partial \Phi^{DOPre}}{\partial t} = \underbrace{(1-f_{orgP})K_{dec}^{POP}\Phi^{POP}}_{POP} - \underbrace{K_{\min}^{DOPre}\Phi^{DOPre}}_{IP}$$

Symbol	*Description*	*Unit*	*Formulation*

K_{dec}^{POP}	POP decomposition Rate	d^{-1}	$K_{dec}^{POP} = K_{dec}^{POP}(T_{ref}).\theta_{dec}^{(T-T_{ref})}$	
$K_{\min}^{DOPre}$	DONre mineralization Rate	d^{-1}	$K_{dec}^{DOPre} = K_{\min}^{DOPre}(T_{ref}).(\theta_{\min}^{DOPre})^{(T-T_{ref})} \frac{\sum \Phi^X}{K_r^{phy} + \sum \Phi^X}$ $X \equiv phy, dia$	
$K_{\min}^{DOPnr}$	DONre mineralization Rate	d^{-1}	$K_{\min}^{DOPnr} = K_{\min}^{DOPnr}(T_{ref}).\theta_{\min}^{DOPnr(T-T_{ref})} \frac{\sum \Phi^X}{K_r^{phy} + \sum \Phi^X}$ $X \equiv phy, dia$	
δ_P^Y	Non-assimilated material by Y	d^{-1}	1 Phytoplankton Group 1 Zooplankton Group	$\delta_P^{zoo} = (1-E^X)\frac{\mu^{zoo}}{E^X}\alpha_{P:C}^X$ $Y \equiv phy, dia$
			>1 Phytoplankton Group >1 Zooplankton Group	$\delta_P^{zoo} = \sum[(1-g_{zoo}^X)G_{zoo}^X \alpha_{P:C}^X]$ $Y \equiv phy, dia, cil$
φ_P^Y	Stoichiometric food web losses	d^{-1}	1 Phytoplankton Group 1 Zooplankton Group	$\varphi_P^{zoo} = \mu^{zoo}(\alpha_{P:C}^{phy} - \alpha_{P:C}^{zoo})$
			>1 Phytoplankton Group >1 Zooplankton Group	$\varphi_P^{zoo} = \sum(\alpha_{P:C}^X - \alpha_{P:C}^{zoo})g_{zoo}^X G_{zoo}^X$ $X \equiv phy, dia, cil$

T	Water Temperature	ºC
T_{ref}	Reference Temperature	20 ºC
K_N^X	Nitrogen half-saturation constant	mg N l^{-1}
E^X	Assimilation efficiency of X by zooplankton	adim
g_Y^X	Assimilation Coefficient of X by Y	adim
G_Y^X	Y grazing on X	[d^{-1}]
$\alpha_{P:C}^X$	Phosphorus/Carbon Ratio	mg N/mgC
p^{zoo}	Zooplankton predatory mortality rate: predation by higher trophic levels	[d^{-1}]
μ^X	Growth rate	[d^{-1}]
ex^X	Excretion Rate	[d^{-1}]
r^X	Respiration Rate	[d^{-1}]
m^X	Natural Mortality Rate	[d^{-1}]
$K_{dec}^{POP}(T_{ref})$	POP decomposition rate at reference temperature	d^{-1}
θ_{dec}	POP decomposition temperature coefficient	adim
$K_{\min}^{DOPre}(T_{ref})$	DOPre mineralization rate at reference temperature	d^{-1}
$\theta_{\min}^{DOPre}$	DOPre mineralization temperature coefficient	adim
K_r^{phy}	Nutrient Regeneration Half-Saturation Constant	mgC/ l
$K_{\min}^{DOPnr}(T_{ref})$	DOPnr mineralization Rate at reference temperature	d^{-1}
$\theta_{\min}^{DOPr}$	DOPnr minreralization temperature coefficient	adim
f_{inorg}^X	Fraction of inorganic material excreted by X	adim
f_{orgD}^X	Dissolved organic fraction excreted by X	adim
f_{orgP}	Fraction of PON available for mineralization	adim

Table 15: Phosphorus Formulations

Symbol	*Description*	*Unit*	*Value*	**Keyword**
$K_{dec}^{POP}(T_{ref})$	POP decomposition Rate at reference temperature	d^{-1}	0.2	PPARTMIN
θ_{dec}	POP decomposition temperature coefficient	adim	**1.08**	**TPPARTMINCOEF**
$K_{\min}^{DOPre}(T_{ref})$	DOPre mineralization Rate at reference temperature	d^{-1}	**0.03**	**PMINR**
$\theta_{\min}^{DOPre}$	DOPre minreralization temperature coefficient	adim	**1.064**	**PMINRCOEF**
$K_{\min}^{DOPnr}(T_{ref})$	DOPnr mineralization Rate at reference temperature	d^{-1}	**0.1**	**PMINNR**
$\theta_{\min}^{DOPr}$	DOPre minreralization temperature coefficient	adim	1.064	PMINNRCOEF

Table 16: Phosphorus Parameters

1.4.6. Oxygen Cycle

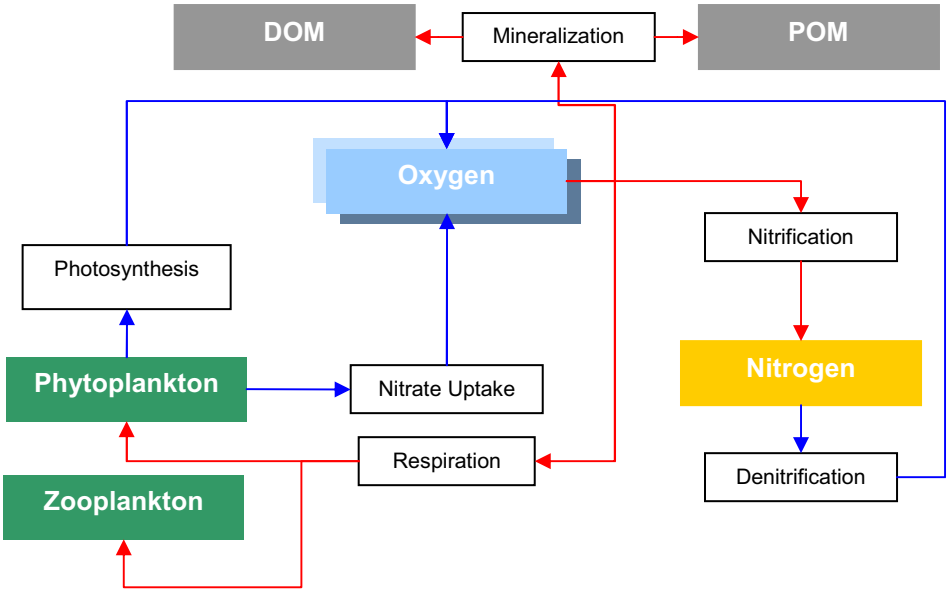

Figure 13: Oxygen Processes

$$\frac{\partial \Phi^{oxy}}{\partial t} = \underbrace{\left(\underbrace{\mu^{phy}\alpha_{O:C}^{photo}}_{photosynthesis} + \underbrace{\left(1-\beta_{NH4}^{phy}\right)\mu^{phy}\alpha_{O:N}^{NO3}\alpha_{N:C}^{phy}}_{nitrate\ uptake} + \underbrace{\mu^{phy}\alpha_{O:P}^{IP}\alpha_{P:C}^{phy}}_{IP\ uptake} - \underbrace{r^{phy}\alpha_{O:C}^{plankton}}_{respiration} \right)\Phi^{phy}}_{flagellates}$$
$$+\underbrace{r^{zoo}\alpha_{O:C}^{zoo}\Phi^{zoo}}_{mesozooplankton} - \underbrace{K_{\min}^{DONre}\alpha_{O:N}^{\min}\Phi^{DONre}}_{refractory\ organic\ nitrogen} - \underbrace{K_{nit}^{oxy}\Phi^{NH4}}_{nitrification} + \underbrace{K_{dnit}^{oxy}\Phi^{NO3}}_{denitrification}$$
$$\underbrace{-K_{dec}^{POP}\alpha_{O:P}^{\min}\Phi^{POP} - K_{\min}^{DOPre}\alpha_{O:P}^{\min}\Phi^{DOPre} - K_{\min}^{DOPnr}\alpha_{O:P}^{\min}\Phi^{DONnr}}_{organic\ phosphorus}$$

Symbol	*Description*	*Unit*	*Formulation*
$\alpha_{O:N}^{\min}$	Oxygen Consumption in Nitrogen Mineralization	mg O/mg $N.d^{-1}$	$\alpha_{O:N}^{\min} = \frac{1}{\alpha_{N:C}^{OM}} \times \alpha_{O:C}^{CO2} \times \frac{\Phi^{oxy}}{0.5+\Phi^{oxy}}$

$\alpha_{O:P}^{\min}$	Oxygen Consumption in Phosphorus Mineralization	mg O/mg P.d-	$\alpha_{O:P}^{\min} = \frac{1}{\alpha_{P:C}^{OM}} \times \alpha_{O:C}^{CO2} \times \frac{\Phi^{oxy}}{0.5 + \Phi^{oxy}}$
K_{nit}^{oxy}	Oxygen Consumption Rate in Nitrification	d^{-1}	$K_{nit}^{oxy} = K_{nit}.\alpha_{O:N}^{NO_3}$
K_{dnit}^{oxy}	Oxygen Consumption Rate in Denitrification	d^{-1}	$K_{dnit}^{oxy} = K_{dnit}.\alpha_{O:N}^{NO_3}$
μ^X	Growth rate	[d^{-1}]	
r^X	Respiration Rate	[d^{-1}]	
$\beta_{NH_4}^X$	Ammonia preference factor	adim	
K_{dnit}	Denitrification Rate	[d^{-1}]	
K_{nit}	Nitrification Rate	[d^{-1}]	
$\alpha_{O:C}^{CO2}$	Oxygen/Carbon Ratio in CO_2	mgO/mgC	
$\alpha_{N:C}^{OM}$	Nitrogen/Carbon ratio in Organic Matter	mgN/mgC	
$\alpha_{P:C}^{OM}$	Phosphorus/Carbon ratio in Organic Matter	mgP/mgC	
$\alpha_{O:N}^{NO3}$	Oxygen/Nitrogen Ratio in Nitrate	mgO_2/mgN	
$\alpha_{O:P}^{IP}$	Oxygen/Nitrogen Ratio in Phosphate	mgO_2/mgP	
$\alpha_{O:C}^{photo}$	Photosynthesis Oxygen:Carbon ratio	mgO_2/mgC	
$\alpha_{O:C}^{X}$	Oxygen/Carbon Ratio in respiration	mgO/mgC	

Table 17: Oxygen Formulation

Symbol	*Description*	*Unit*	*Value*	Keyword
$\alpha_{O:C}^{CO2}$	Oxygen/Carbon Ratio in CO_2	mgO/mgC	32/12	OCRATIO
$\alpha_{O:C}^{photo}$	Photosynthesis Oxygen/Carbon ratio	mgO/mgC	32/12	PHOTOSOC
$\alpha_{O:N}^{NO3}$	Oxygen/Nitrogen Ratio in Nitrate	mgO/mgN	48/14	NITONRAT
$\alpha_{O:P}^{IP}$	Oxygen/Nitrogen Ratio in Phosphate	mgO/mgP	64/31	PHOSOPRAT
$\alpha_{O:C}^{plankton}$	Oxygen/Carbon Ratio in plankton respiration	mgO/mgC	32/12	PLANK_OC_RAT
$\alpha_{O:C}^{zoo}$	Oxygen:Carbon ratioin mesozooplankton respiration	mgO_2/mgC	32/12	ZOCRATIO
$\alpha_{O:C}^{cil}$	Oxygen:Carbon ratio in microzooplankton	mgO_2/mgC	32/12	CILOCRATIO
$\alpha_{O:C}^{bact}$	Bacteria Oxygen:Carbon Ratio	mgO_2/mgC	1.4	BACTRATIOOC
$\alpha_{N:C}^{OM}$	Organic Matter Nitrogen:Carbon Ratio	mgN/mgC	0.18	OMRATIONC
$\alpha_{P:C}^{OM}$	Organic Matter Phosphorus:Carbon Ratio	mgP/mgC	0.024	OMRATIOPC
$\Phi_{\min}^{O_2}$	Minimum oxygen concentration for growth	mgO_2/l	10e-5	MINOXYGEN

Table 18: Oxygen Parameters